

IN SITU RAMAN SPECTROELECTROCHEMICAL TECHNIQUE AS TOOL FOR INVESTIGATING THE PROPERTIES OF ELECTROACTIVE SYSTEMS

Materials Chemistry Research Group, Laboratory of Materials Chemistry and
Chemical Analysis, Department of Chemistry, University of Turku

This is a master thesis work

Felix Osei Sarpong

19.01.2018

Abstract

The electrochemical polymerization of 3,4-ethylenedioxythiophene (EDOT) monomer as conducting polymer was synthesized on various working electrodes (WE) which includes gold (Au), platinum (Pt), glassy carbon (GC) and Fluorinated Tin Oxide (FTO) in different electrolytic solvent medium. The solutes used in the aqueous medium (H_2O) was Potassium Chloride (KCl) salt and Sodium Polystyrene Sulfonate (NaPSS) and the solute used in the organic solvent medium which is acetonitrile (ACN) was tetrabutylammonium hexafluorophosphate (TBAPF₆).

A thin film of poly(3,4-ethylenedioxythiophene) (PEDOT) was electrochemically polymerized on the FTO, Au, Pt and GC three different electrolytes. The cyclic voltammograms (CVs) of the PEDOT films were studied to elucidate the electrochemical properties of the electrolytes.

An in situ Raman spectroscopy measurements were carried out for the polymerized PEDOT films on the different WE (Au, Pt, GC, FTO) and the spectra and its corresponding images were obtained and compared accordingly to explain the doping process of the PEDOT film.

A UV-Vis spectroscopy measurement was also performed on the films on the FTO to present a study on the p and n doping of the PEDOT films which was in tandem with the characterization of Raman spectra measurements.

Key words: 3,4-ethylenedioxythiophene (EDOT), tetrabutylammonium hexafluorophosphate (TBAPF₆), Fluorinated Tin Oxide (FTO), In situ Raman spectroscopy, UV-Vis spectroscopy.

Table of Contents

Table of Contents	i
1. INTRODUCTION.....	1
1.1 Conducting polymers.....	1
1.2 Synthetic routes of PEDOT:PSS.....	3
2. PROPERTIES OF CPs.....	5
2.1 Conductivity of CPs	5
2.2 Electrical properties of CPs	5
2.2.1 Molecular Structure.....	6
2.2.2 Doping of CPs.....	6
2.2.3 Electrochemical properties of doped CPs	8
2.3 Graphene	9
2.3.1 Composite of PEDOT:PSS/graphene.....	10
2.4 Characterization	11
2.4.1 Characterization techniques	11
2.5 Spectroelectrochemistry	12
2.5.1 Raman Spectroscopy.....	12
2.5.2 Raman Spectroelectrochemistry Cell Design	13
2.5.3 Surface – Enhanced Raman Spectroscopy (SERS).....	16
2.5.4 Characterization of PEDOT:PSS/ Graphene	17
3. METHODOLOGY	21
3.1 Materials and Equipment.....	21
3.1.1 Materials	21
3.1.2 Equipment	21
3.1.3 Preparation of electrolyte solutions.....	23
3.1.4 Electrode polishing.....	24
3.2 Experimental Procedures.....	24
3.2.1 Ag/AgCl Fabrication.....	24
3.2.2 Calibration of Ag/AgCl.....	25
3.2.3 Electrochemical polymerization of EDOT monomer on Fluorinated Tin Oxide (FTO)	25
3.2.4 Electrochemical polymerization of PEDOT films using 3-neck cell.....	26

3.2.5 Electrochemical polymerization of PEDOT film using the laboratory fabricated Raman cell	27
3.3 Spectroelectrochemistry	27
4. RESULTS AND DISCUSSIONS	28
4.1 Electrochemical Polymerization of PEDOT film on FTO substrate.	28
4.1.1 Electrochemical Characterization of FTO polymer films.	32
4.2 Electrochemical Polymerization of PEDOT film using 3-neck cell.	34
4.3 Electrochemical Polymerization for laboratory fabricated Raman cell	36
4.4 In situ UV-Vis Spectroscopy	37
4.5 Raman spectroscopy	42
4.5.1 In situ Raman Spectroscopy.....	52
4.5.2 Comparison of various in situ Raman spectra	60
4.5.3 Raman Images	72
5. CONCLUSION AND RECOMMENDATION	74
References.....	75

Table of Figures

Figure 1.1 Examples of ICPs: polypyrrole, polyaniline, trans-polyacetylene and polythiophene [35].	1
Figure 1.2 Chemical structure of PEDOT:PSS made up of a PSS backbone (top) and a PEDOT chain (bottom) ionically bonded [16].	3
Figure 1.3 The two most used synthetic pathways for the synthesis of EDOT and ProDOT monomers [3].	4
Figure 2.1 Conductivity of conducting polymers [35].	5
Figure 2.2 The electronic band and chemical structures of polythiophene (PT) with (a) p-type doping and (b) n-type doping [2].	7
Figure 2.3 Illustration of two electrode electrolytic cell and its components [32].	8
Figure 2.4 Typical cell designs for in situ/operando Raman spectroscopy. (A) Beaker (pyrex) cell design used e.g., by Inaba et al. (1995). (B) Pouch cell from Ghanty et al. [reprinted from reference (Ghanty et al., 2015) with permission of John Wiley and Sons]. (C) Custom-made coin-cell type design developed in our group [37].	14
Figure 2.5 (a) XRD patterns of graphene, PEDOT, PS/PEDOT and PS/G/PEDOT; Inset represents the XRD spectrum of PEDOT:PSS and (b) Raman spectra of a PEDOT, b PS/PEDOT, c PS/G/ PEDOT nanocomposites; Inset represents the Raman spectra of graphene, PEDOT:PSS and PEDOT:PSS/graphene hybrid films [9].	18
Figure 2.6 XPS spectra (a) and Raman shift spectra (b) of PEDOT:P(SS-co-VTMS) [25].	20
Figure 3.1 (a) Picture of Raman cell setup and (b) Schematic diagram of Raman cell showing all parts.	23
Figure 3.2 images of Electrochemical setup of (a) 3-neck cell and (b) quartz cuvette.	25
Figure 3.3 Image of (a) Raman spectrometer from Renishaw and (b) UV-vis spectrometer from Agilent Cary 60. [61].	28
Figure 4.1 Cyclic voltammogram for an electrochemical polymerization of PEDOT film in KCl electrolyte solution. The insert shows characterization CV of the PEDOT film in monomer free 0.1M KCl solution at potential range -1.0V to 1.0V for 5 cycles.	29
Figure 4.2 Cyclic voltammogram for an electrochemical polymerization of PEDOT film in NaPSS solution. The insert shows characterization CV of the PEDOT film in monomer free 0.1M NaPSS solution at potential range -1.0V to 1.0V for 5 cycles.	30
Figure 4.3 Cyclic voltammogram for an electrochemical polymerization of PEDOT film in TBAPF6-ACN solution. The insert shows characterization CV of the PEDOT film in monomer free 0.1M TBAPF6-ACN solution at potential range -1.0V to 1.0V for 5 cycles.	31
Figure 4.4 Cyclic voltammogram of PEDOT film in KCl monomer free solution showing different scan rates.	32
Figure 4.5 Cyclic voltammogram of PEDOT film in NaPSS monomer free solution showing different scan rates.	33
Figure 4.6 Cyclic voltammogram of PEDOT film in TBAPF6-ACN monomer free solution showing different scan rates.	34
Figure 4.7 Electrochemical polymerization of PEDOT film and the corresponding CV in monomer free KCl electrolyte solution. (a-b) for Au electrode, (c-d) for Pt electrode, (e-f) for GC electrode, at different scan rates for 3-neck cell.	35
Figure 4.8 Electrochemical polymerization of PEDOT film and the corresponding CV in monomer free KCl electrolyte solution. (a-b) for Au electrode, (c-d) for Pt electrode, (e-f) for GC electrode, at different scan rates for Raman cell.	37
Figure 4.9 (a) CV for film growth of electrochemically polymerized PEDOT film on FTO in 0.1M KCl solution and UV-VIS absorption spectra measurement of the film (b) spectra of complete cycle for p-doping (c) forward cycle (d) reverse cycle. The cycling potential employed was between 0.6nV and -0.9 V for 31 scans in monomer-free solution of 0.1M KCl.	39
Figure 4.10 (a) CV for film growth of electrochemically polymerized PEDOT film on FTO in 0.1M NaPSS solution and UV-VIS absorption spectra measurement of the film (b) spectra of complete cycle for p-doping (c) forward cycle (d) reverse cycle. The cycling potential employed was between 0.6nV and -0.9 V for 31 scans in monomer-free solution of 0.1M NaPSS.	40
Figure 4.11 (a) CV for film growth of electrochemically polymerized PEDOT film on FTO in 0.1M TBAPF6-ACN solution and UV-VIS absorption spectra measurement of the film (b) spectra of complete cycle for p-doping (c) forward cycle (d) reverse cycle. The cycling potential employed was between 0.6nV and -0.9 V for 31 scans in monomer-free solution of 0.1M TBAPF6-ACN.	41

Figure 4.12 Raman spectra for PEDOT film on Au electrode in KCl solution using 532 nm excitation wavelength.	44
Figure 4.13 Raman spectra for PEDOT film on Au electrode in TBAPF6-ACN solution using 532 nm excitation wavelength.	45
Figure 4.14 Raman spectra for PEDOT film on Au electrode in KCl solution using 785 nm excitation wavelength.	46
Figure 4.15 Raman spectra for PEDOT film on Au electrode in TBAPF6-ACN solution using 785 nm excitation wavelength.	47
Figure 4.16 Raman spectra for PEDOT film on GC electrode in KCl solution using 532 nm excitation wavelength.	48
Figure 4.17 Raman spectra for PEDOT film on GC electrode in TBAPF6-ACN solution using 532 nm excitation wavelength.	49
Figure 4.18 Raman spectra for PEDOT film on GC electrode in KCl solution using 785 nm excitation wavelength.	50
Figure 4.19 Raman spectra for PEDOT film on GC electrode in TBAPF6-ACN solution using 785 nm excitation wavelength.	51
Figure 4.20 In situ Raman spectra recorded for electrochemically polymerized PEDOT film on Au electrode in 0.1M KCl solution using 532 nm excitation wavelength at -0.8 V to 0.7 V scanning potential for p- and n-doping.	52
Figure 4.21 In situ Raman spectra recorded for electrochemically polymerized PEDOT film on Au electrode in 0.1M TBAPF6-ACN solution using 532 nm excitation wavelength at -0.8 V to 0.7 V scanning potential for p- and n-doping.	53
Figure 4.22 In situ Raman spectra recorded for electrochemically polymerized PEDOT film on Au electrode in 0.1M KCl solution using 785 nm excitation wavelength at -0.8 V to 0.7 V scanning potential for p- and n-doping.	54
Figure 4.23 In situ Raman spectra recorded for electrochemically polymerized PEDOT film on Au electrode in 0.1M TBAPF6-ACN solution using 785 nm excitation wavelength at -0.8 V to 0.7 V scanning potential for p- and n-doping.	55
Figure 4.24 In situ Raman spectra recorded for electrochemically polymerized PEDOT film on GC electrode in 0.1M KCl solution using 532 nm excitation wavelength at -0.8 V to 0.7 V scanning potential for p- and n-doping.	56
Figure 4.25 In situ Raman spectra recorded for electrochemically polymerized PEDOT film on GC electrode in 0.1M TBAPF6-ACN solution using 532 nm excitation wavelength at -0.8 V to 0.7 V scanning potential for p- and n-doping.	57
Figure 4.26 In situ Raman spectra recorded for electrochemically polymerized PEDOT film on GC electrode in 0.1M KCl solution using 785 nm excitation wavelength at -0.8 V to 0.7 V scanning potential for p- and n-doping.	58
Figure 4.27 In situ Raman spectra recorded for electrochemically polymerized PEDOT film on GC electrode in 0.1M TBAPF6-ACN solution using 785 nm excitation wavelength at -0.8 V to 0.7 V scanning potential for p- and n-doping.	59
Figure 4.28 Comparison of in situ Raman spectra of PEDOT film polymerized on (a) Au electrode and (b) GC electrode both in 0.1 M KCl using 532 nm excitation wavelength ($\lambda_L=532$ nm).	60
Figure 4.29 Comparison of PEDOT film on (a) Au electrode in 0.1 M TBAPF6-ACN and (b) GC electrode in 0.1 M KCl both in using 532 nm excitation wavelength ($\lambda_L=532$ nm).	61
Figure 4.30 Comparison of PEDOT film on Au electrode in both (a) 0.1 M KCl and (b) 0.1 M TBAPF6-ACN solvents using 532 nm excitation wavelength ($\lambda_L=532$ nm).	62
Figure 4.31 Comparison of PEDOT film on GC electrode in both (a) KCl and (b) TBAPF6-ACN solvents using 532 nm excitation wavelength ($\lambda_L=532$ nm).	63
Figure 4.32 Comparison of the Raman spectra of PEDOT films using (a) 532 nm on Au electrode and (b) 785 nm Au electrode both in 0.1 M KCl solvent.	64
Figure 4.33 Comparison of the Raman spectra of PEDOT films using (a) 532 nm on Au electrode and (b) 785 nm Au electrode both in 0.1 M TBAPF6-ACN solvent.	65

Figure 4.34 Comparison of the Raman spectra of PEDOT films using (a) 532 nm on GC electrode and (b) 785 nm GC electrode both in 0.1 M KCl solvent.	66
Figure 4.35 Comparison of the Raman spectra of PEDOT films using (a) 532 nm on GC electrode and (b) 785 nm GC electrode both in 0.1 M TBAPF6-ACN solvent.	67
Figure 4.36 Comparison of Raman spectra of the PEDOT films polymerized on (a) Au electrode and (b) GC electrode in 0.1 M KCl using 785 nm excitation wavelength ($\lambda_L = 785$ nm).	68
Figure 4.37 Comparison of Raman spectra of PEDOT films polymerized on (a) Au electrode and (b) GC electrode in 0.1 M TBAPF6-ACN using 785 nm excitation wavelength ($\lambda_L = 785$ nm).	69
Figure 4.38 Comparison of in situ Raman spectra of PEDOT film polymerized on Au electrode in (a) 0.1 M KCl and (b) 0.1 M TBAPF6-ACN using 785 nm excitation wavelength ($\lambda_L = 785$ nm).	70
Figure 4.39 Comparison of in situ Raman spectra of PEDOT film polymerized on GC electrode in (a) 0.1 M TBAPF6-ACN and (b) 0.1 M KCl using 785 nm excitation wavelength ($\lambda_L = 785$ nm).	71
Figure 4.40. Different Raman images showing the morphologies of electropolymerized PEDOT film in (a) 0.1M KCl solution (b) 0.1M NaPSS solution (c) 0.1M TBAPF6-ACN solution.	73

1. INTRODUCTION

1.1 Conducting polymers

Polymers in time past, could be classified as insulators based on its properties. Nevertheless, extensive studies have revealed that there are some polymers which have conducting properties as an exception. These polymers that conduct the electrical current are classified as conducting polymers or conjugated polymers [35] [2][3].

The classification of conducting polymers are in two main forms which includes

Intrinsic Conducting Polymer: Polymers like polypyrrole, polyaniline, polyacetylene and polythiophene form the intrinsic conducting polymer group. The π bond electrons which conjugates along the polymer chain is the main cause for the conductivity of these type of polymers. These conducting polymers with the π conjugated electrons also exhibit an alternating single and double bond along their polymer chains.

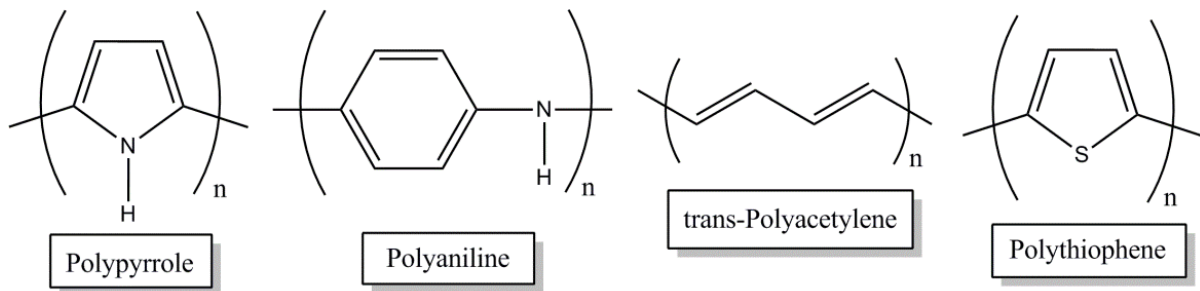


Figure 1.1 Examples of ICPs: polypyrrole, polyaniline, trans-polyacetylene and polythiophene [35].

Extrinsic Conducting Polymer: These type of conducting polymers employs materials like metals, graphite, or transfer complex in the polymer matrix. The inclusion of these conductive materials determines the conductivity for extrinsic conducting polymers [35][3].

Areas of application: Some notable areas of application for CPs can be found in the list below,

- Photovoltaic devices,
- Electrochromic devices,
- Light emitting diodes,
- Sensors,
- Optical devices,
- Batteries,
- Electronic devices,

- Mechanical and electromechanical (actuators in rotary convertors) devices,
- Corrosion protection,
- Catalysis,
- Drug and chemical delivery,
- Membranes.[3][5][35]

Poly(3,4-ethylenedioxythiophene) PEDOT: PSS

Conducting polymers (CPs), with poly(3,4-ethylenedioxythiophene) that has been doped with poly(styrenesulfonate) (PEDOT:PSS) as an example, has been into existence for more than twenty years as a stable, solution-processable hole conductor. They are the basis or the underlying factor for charge transport studies in conducting polymers [3][9][35]. CPs can be grouped as electronic, ionic or mixed type (electronic and ionic) CPs. However mixed type (electronic/ionic) transport in CPs is attracting a great deal of attention due to a host of new devices and some examples are the organic electrochemical transistor (OECT) which consists of a CP layer in which ions injected from an electrolyte modify hole conductivity. Based on their high transconductance, CPs extends its application range from neural interfacing to biosensing which includes bioelectronics (with the emergence of printed electronics and neuroinspired electronics) [3] [9].

PEDOT:PSS CP is widely used in the field of organic electronics as transparent conductive oxides (TCO), and as a hole-conducting layer or electrochromic layer in a wide array of devices moving from organic light-emitting diodes (OLEDs) and organic photovoltaic devices (OPVs) to electrochromics [3].

CPs has been known also to have influence in energy applications which includes batteries/supercapacitors, electrochromic windows and in electromechanical actuators for soft robotics [5].

PEDOT:PSS which is a composite CPs has found its utilization in many devices because the material has high hole conductivity ($>10^3$ S/cm), high stability and commercially available as a dispersion for solution processing [1].

PEDOT:PSS dispersions are typically described as being composed of gel-like particles consisting of a polyanion (PSS^-)-rich shell or backbone which helps to stabilize the PEDOT-enriched chain particles in aqueous solvents. PEDOT oligomers are believed to polymerize onto the PSS template, see Figure 1.2 [16][3].

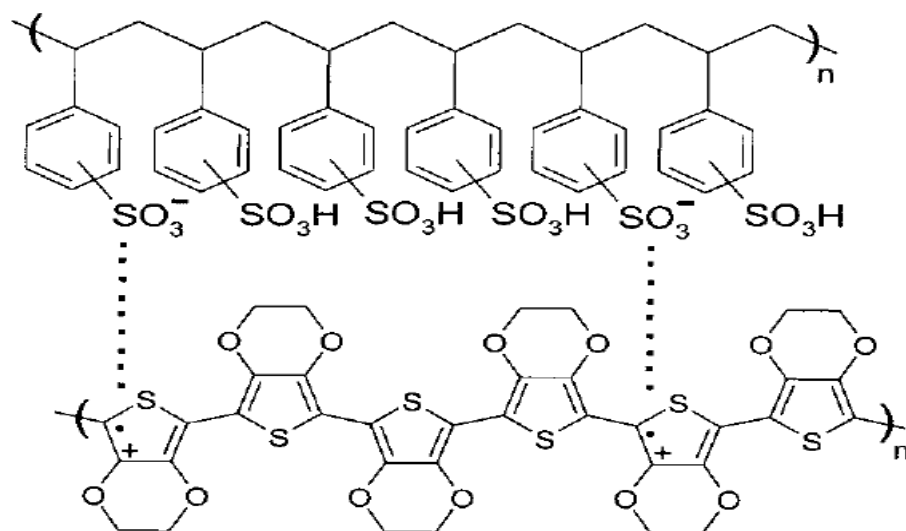


Figure 1.2 Chemical structure of PEDOT:PSS made up of a PSS backbone (top) and a PEDOT chain (bottom) ionically bonded [16].

PEDOT:PSS presents some limitations regardless of how promising it is, and some of the challenges or limitations includes PEDOT chain degradation and possible release of acidic PSS degradation products and lack of functionality of PEDOT and low biocompatibility of PSS [1][9].

1.2 Synthetic routes of PEDOT:PSS

The synthetic routes of PEDOT:PSS can be performed in two different lines or pathways for the synthesizing of functional 3,4-ethylenedioxythiophene monomers EDOT and ProDOT. One synthetic route involves the creation of the thiophene and dioxolane derivatives (pathway #1) and for the second synthetic route, the preliminary material was 3,4-substituted thiophene ring, for example 3,4-dimethoxythiophene or 3,4-dibromothiophene (pathway #2), see Figure 1.3.

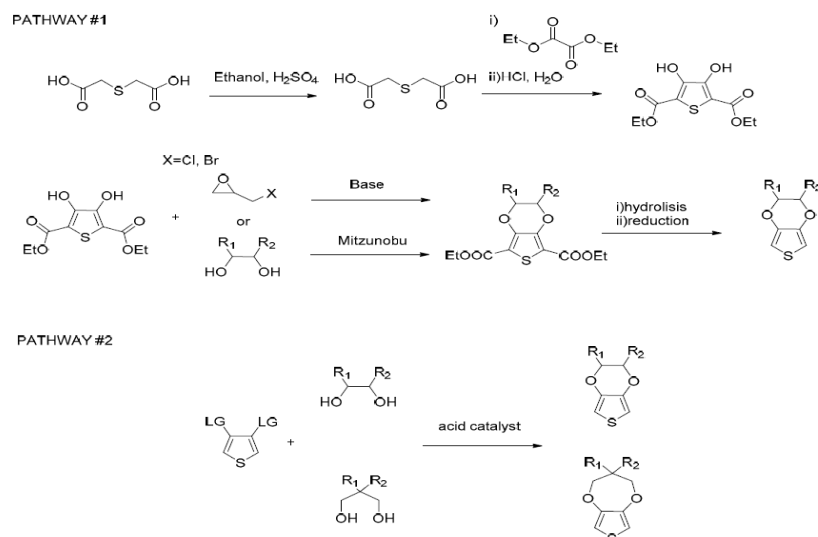


Figure 1.3 The two most used synthetic pathways for the synthesis of EDOT and ProDOT monomers [3].

The macroscopic difference between these two synthetic routes was the number of steps to get to the final product: in the case of pathway #1, more steps are needed, but the price of the starting material for pathway #2 is about 10 to 100 times more expensive than for pathway #1. Pathway #1 is known to be the oldest synthetic route and it is limited to the synthesis of 2-hydroxymethyl-EDOT (EDOT-CH₂OH) and carboxy-EDOT (EDOT-COOH) [17].

In the instance of EDOT-CH₂OH following pathway #2, the reaction with glycerol tends to yield a mixture of EDOT and ProDOT that is difficult to separate. For the situation of EDOT-COOH, PCC (pyridinium chlorochromate) was employed through an oxidative step and hence the groups in position 2 and 5 on the thiophene ring protect the molecule from further polymerization when pathway #1 is used [17][32].

For the ProDOT derivatives, pathway #2 is the only route used in the literature, whereby 1,3-diol derivatives are used to create the dioxepane ring.

ProDOT which is the closest ally EDOT molecule has a propylenedioxy ring rather ethylenedioxy ring attached to the thiophene in the 3,4-position. ProDOT was originally considered a side product in the synthesis [1].

It can be stated clearly that ProDOT can be simply obtained and has a better stability than EDOT. It also has useful applications in organic photovoltaic (OPV), organic electrochemical transistor (OECT), tissue engineering and more, after doping or coupling with EDOT irrespective of its low electrical conductivity compared to EDOT [1].

Currently, EDOT/ProDOT monomers are usually polymerized using different methods like electrochemical polymerization, vapor phase polymerization (VPP) or chemical oxidative polymerization. Electrochemical and VPP polymerization methods usually give polymer films with outstanding properties like surface quality, high conductivity and stable redox chemistry. However, it can be noted that for large-scale applications, chemical polymerization is the preferred route due to its easy scale-up. For instance, this is the method used to produce industrially the PEDOT:PSS dispersions that are commercially available.

2. PROPERTIES OF CPs

2.1 Conductivity of CPs

Conductivity of CPs can either have electrical properties which is determined by the electronic structure of the molecules or electrochemical properties which is determined by the various doping techniques of the polymer. The range of values for the conductivity of CPs are mostly between 10^{-13} and 10^6 S/cm [18][2][5][19].

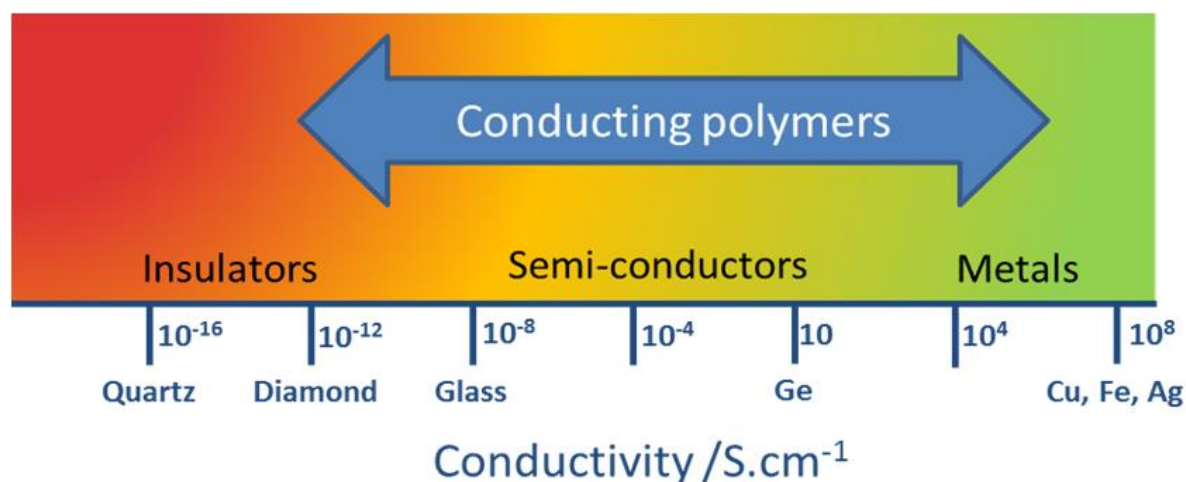


Figure 2.1 Conductivity of conducting polymers [35].

2.2 Electrical properties of CPs

Effective formulations of CP composites that comes with flexibilities, great stabilities, and conductivities have demonstrated that CPs can operate as key material components in light emitting diodes (LEDs), transistors, electrochromic devices, actuators, electrochemical capacitors, photovoltaic cells, and sensors. The critical element of development in these fields is achieving control of the electrical or electrochemical properties of CPs. Consequently, this

work presents a discussion of the electrical and electrochemical properties of CPs, and the latest trends in research on the applications of CPs have been summarized. The flow of electrons in CPs results from the movement of π -bonds between the carbon backbone of the CP structure which causes the movement of electrons in the conjugated double bonds along the carbon chain. Electrical conductivity of CPs can be determined by either the electronic structure of molecules or doping.

2.2.1 Molecular Structure

The electrical conductivity of a material is generally determined by its electronic structure. The energy band theory is a useful way to visualize the differences among conductors, insulators, and semiconductors [2]. The band gap is the energy difference between the valence and conduction bands of a material. When the valence band overlaps the conduction band, the valence electrons are free to move and propagate in the conduction band [17]. This is an intrinsic characteristic of conductors. Semiconductors possess small energy gaps that electrons can cross upon excitation to move to the conduction band, creating a hole in the material. This permit both hole and electron charge transport thereby creating the conduction of current. In the case of insulators, the band gap is too large to be crossed by electrons, and therefore they do not conduct electricity [2][22].

However, the energy band theory may not clearly explain why CPs, being organic materials, conduct electricity.

2.2.2 Doping of CPs

CPs have been doped using different methods to achieve high conductivities. The various types of doping include electrochemical doping, chemical doping, photodoping, non-redox doping, and charge-injection doping [2][17][22].

Un-doped polymers have been reported as insulators (non-conducting) but changes from insulating to metallic when doped and hence becomes conductive. The doping mechanism for CPs is completely different to that for their inorganic counterparts since it possesses a distinct chemical structure. However, dopants employed in the polymer undergo redox processes in which charges are transferred with subsequent formation of charge carriers [2].

This doping reaction can be carried out chemically or electrochemically [4].

The role of the dopant is not only to withdraw electrons from the CP but also to add electrons to the CP backbone and thus representing p-type and n-type doping, respectively. The effect of

doping can be elucidated as that electrons are extracted from the highest occupied molecular orbital (HOMO) of the valence band (oxidation) or transferred to the lowest unoccupied molecular orbital (LUMO) of the conduction band (reduction). This oxidation/reduction process creates charge carriers in the form of polarons (radical ions), bipolarons (dications or dianions), or solitons in the polymer [2]. Conduction by polarons and bipolarons in particular are thought to be the prominent mechanism of charge transport used in conducting polymers with nondegenerate ground state such as in PPV for example [4].

Solitons are known to be the charge carriers in degenerate systems such as polyacetylene. The movement of these charge carriers along polymer chains produces conductivity [2].

Moreover, the oxidation and reduction processes are in conformity to p-type and n-type doping, respectively. In p-type doping, the electron moves directly from the HOMO of the polymer to the dopant species and creates a hole in the polymer backbone unlike in n-type doping, where electrons from the dopant species move to the LUMO of the polymer, resulting in increased electron density. Hence, the density and mobility of charge carriers can be tuned by doping.

The p-doping is widely used in academic research as well as for practical applications because of its stability as compared to the charge carriers in n-doping, see figure 2.2 [2][22].

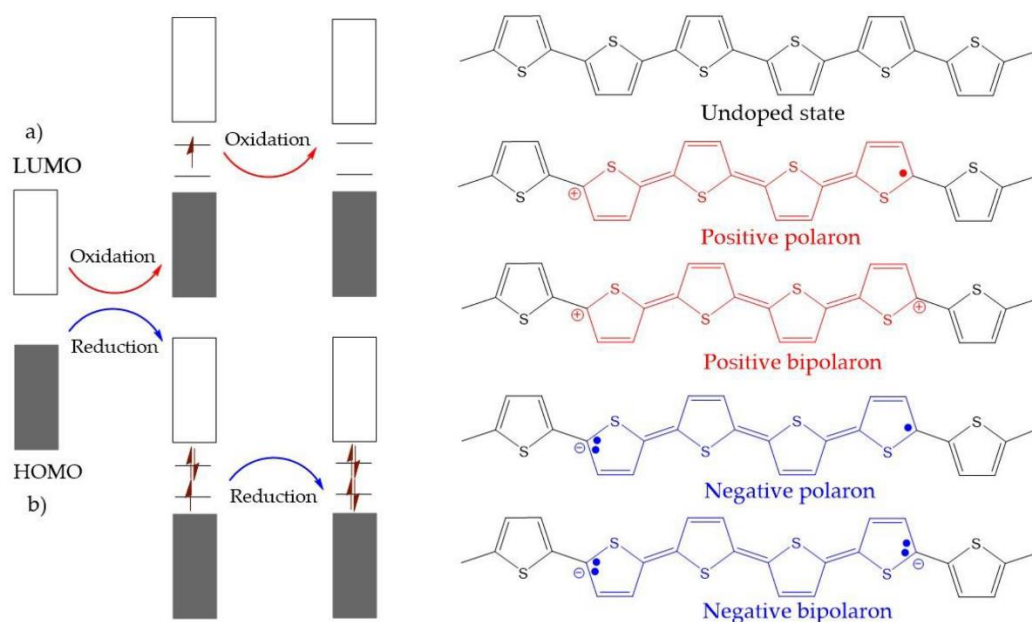


Figure 2.2 The electronic band and chemical structures of polythiophene (PT) with (a) p-type doping and (b) n-type doping [2].

However, there are factors which affect the electrical conductivity of the CPs and these includes:

- *Tunable conductivity*: which talks about how the π conjugated electrons of the polymer matrix can be manipulated to increase the electrical conductivity of the CPs by reducing the structural and the morphological disorder.
- *Charge carrier transport models*: this can be attributed to the disorder nature of the sp^2 defects in the polymer chains and chain ends, chain entanglement, voids and doping defects.
- *Temperature dependence*: In general, the conductivity of doped CPs decreases with decreasing temperature, in contrast to the conductivity of conventional metals which increases with decreasing temperature [2].

2.2.3 Electrochemical properties of doped CPs

Electrochemical doping of CPs can be performed by using an electrolytic cell made from two-electrodes and by using a three-electrode setup whereby there is control on the applied potential because of the use of reference electrode connected by a liquid or solid electrolyte as shown in figure 2.3 below.

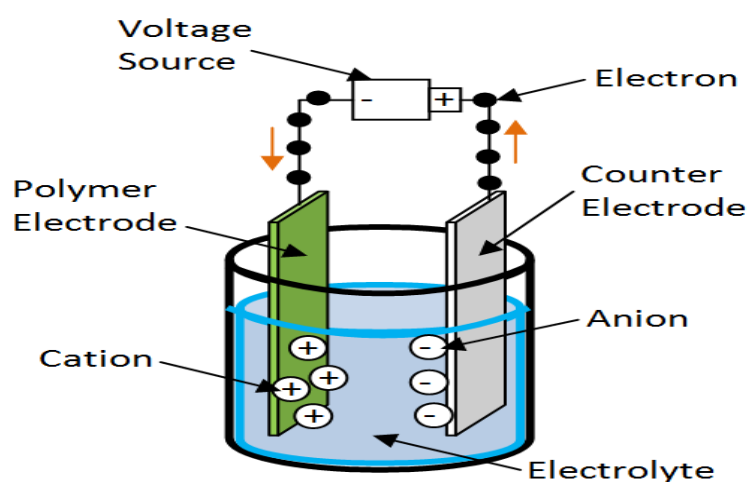


Figure 2.3 Illustration of two electrode electrolytic cell and its components [32].

The electrochemical method for the doping of CPs can be achieved through different processes and this include reversible oxidation/reduction, electrochemical double layer capacitors (EDLCs)/pseudocapacitors, swelling and de-swelling, electrochromism [2]. Doping of CPs typically leads to the formation of charge carriers, which is accompanied by changes (e.g., from benzenoid to quinoid) in the geometric structure of the CP.

The original geometric structure can be recovered by reducing the polymer back to its pristine (undoped) state. The reversibility of doping and de-doping of the polymer corresponds to charge and discharge, which forms the basis of the principles behind polymer-based sensors and capacitors. The p-doping or electro-oxidation of CPs can be rationalized as electrons in the π -bond being extracted and moving along the polymer skeleton while counter-anions from the electrolyte insert into the polymer chain to balance the electronic charge. The mechanism of n-doping or electro-reduction of CPs involves electrons being transported to the polymer backbone and counter-cations inserted into the polymer backbone from the electrolyte solution to balance the overall charge [2][15].

The dominant electrochemical method used to analyse redox processes in CPs is cyclic voltammetry (CV). CV measures the current resulting from an applied potential with fixed scan rate. During redox reactions, reduction makes polymer chains negatively charged while oxidation produces positively charged polymer chains. When doping and de-doping are performed, ions move in and out of the polymer matrix.

2.3 Graphene

Graphene is a single layer of carbon atoms packed into a two-dimensional (2D) honeycomb lattice. The sp^2 hybridized carbon bonds contain in-plane sigma bonds and out-of-plane pi bonds. The π bonds contribute to the electron conduction of graphene and provide weak interaction between graphene layers or graphene and the substrate [6].

Graphene is considered a promising material candidate for electrochemical energy-storage devices because of its high accessible surface area, good mechanical strength, and high electrical conductivity, and it has also been used in composites with ECPs.

Graphene sheets can be obtained by mechanical exfoliation of small mesas of highly oriented pyrolytic graphite [7].

Single- and few-layer single crystalline graphene can also be grown epitaxially on single crystal metal substrates via thermal decomposition of hydrocarbons, or on single crystalline or polycrystalline SiC via segregation of carbon atoms during high temperature annealing [8].

In addition, because of its extremely high surface-to-volume ratio, the conductivity of graphene is highly sensitive to local electrical and chemical perturbations as every atom of graphene is exposed to the ambient environment [6].

Graphene can be used directly as electrode or to modify the glassy electrode (GC) which greatly raises the conductivity of the glassy electrode (GC) in an electrochemical setup. This however results in an improvement in the electron transfer between the target analyte and the electrode surface that has been modified with graphene [6].

Graphene can conduct effectively, however, it has poor solubility and this solubility issue can be enhanced using non – covalent molecular functionalization. Non – covalent molecular functionalization is a process used to manipulate the electronic and chemical properties of graphene. There is less perturbation of the π – conjugated structure of graphene and its derivatives which emanates from the relatively weak van der Waals interaction or loosely-defined π – π interactions between aromatic molecules and graphene. Graphene oxide (GO) has become the most common starting material for graphene-based applications because separated GO sheets can be produced in large quantities [5]. For many applications, the reduction of GO, using chemical or electrochemical reduction or thermal annealing, is desired to restore the graphitic structure [5].

2.3.1 Composite of PEDOT:PSS/graphene

PEDOT:PSS/graphene/PEDOT film is synthesized by a process which involves two stages and these stages are, PEDOT:PSS/graphene hybrid film was spin coated on the substrate as the initial step and then proceeds on to the step of vapor phase polymerization (VPP) of PEDOT film on the PEDOT:PSS/graphene film. Each component in the hybrid film provides exceptional and crucial function to achieve improved electrochemical properties [9].

Other routes that can be used to synthesize composite of PEDOT:PSS/graphene includes electropolymerization of PEDOT and electrical deposition of graphene systematically, spin-coating alternating PEDOT and graphene layers and electrochemical polymerization of PEDOT with functionalized graphene as counterion [5].

A combination of CPs and graphene can effectively reinforce the capacitive performance of nanocomposites.

(Lehtimäki et al., 2015) [5] demonstrated how PEDOT composite doped with graphene oxide (GO) can be electrochemically deposited onto graphite electrode on flexible poly (ethylene terephthalate) (PET) substrates to prevent dispersibility in solvent and to increase capacitance in the supercapacitor's application.

2.4 Characterization

Characterization in materials chemistry refers to the investigation or probing and of the structure and properties of materials and their measurements. There are various techniques that can be employed in the characterization of these materials to determine for example the structure or morphology and chemical species. The physical and chemical properties of the materials are accurately measured and not only that but the structural determination either at the atomic or microscopic level must also be determined accurately. Properties like mechanical, electrical, magnetic, thermal and optical are mostly related to the structure of the material.

2.4.1 Characterization techniques

The different types of characterization used to perform analysis on materials microscopic properties are spectroscopic analysis which includes,

- InfraRed (IR)
- Near InfraRed (NIR)
- Auger Electron Spectroscopy (AES)
- X-ray Photoionization Spectroscopy (XPS)
- Fourier Transform InfraRed (FTIR)
- Raman Spectroscopy
- X-ray Spectroscopy (XRS) [Diffraction, Absorption, Fluorescence, Luminescence, Reflectivity, and Scattering]
- Nuclear Magnetic Resonance (NMR)

Other techniques apart from spectroscopy techniques includes,

- Scanning Electron Microscopy (SEM)
- Atomic Force Microscopy (AFM)
- Scanning Tunneling Microscopy (STM)
- Transmission Electron Microscopy (TEM)
- Tomography

2.5 Spectroelectrochemistry

Spectroelectrochemistry is the collaboration of spectroscopy and electrochemistry techniques to characterize materials.

These combined instrumental techniques provide both molecular and kinetic information during electron transfer process with respect to the reactants, products and or intermediate compounds produced. [35]

One of such techniques is the in situ Raman spectroelectrochemistry which can be explained as coupling of Raman spectroscopy to electrochemistry for the characterization of electrochemically active materials [10]. It has the advantage of obtaining single or complementary information about a complex system. Chemical and structural information can be obtained by Raman spectroelectrochemistry. The level of doping of the polymers can be predicted by using Raman spectroelectrochemistry. Vibrational modes of the elements can also be determined by Raman spectroscopy.

2.5.1 Raman Spectroscopy

Raman spectroscopy has been used in various fields of discipline such as investigating the nucleic acid and its biological complexes [11]. UV-Visible-NIR and Raman spectroelectrochemistry has been effectively employed as synthesizing and characterization tool for conducting polymer studies. The application of these conducting polymers has found their purpose in light emitting diodes, sensors and biosensors, solar cells or fuel cells in materials science [12].

Raman spectroscopy is one of the most effective techniques used in carbon-based materials and graphene structures. The C=C and C=C – O bond stretching for electropolymerized PEDOT as an example, can be well explained by Raman spectroscopic technique on the basis of the strongest bands found in the spectra. The shifting of the peaks in Raman spectra can also be ascribed to the interactions of $\pi - \pi^*$ bonds of the conducting polymer and its composites. Conducting polymers with PEDOT as an illustration can also show several weaker bands which come as a result of $C_\beta - C_\beta$ bond stretching and $C_\alpha - C_\alpha$ bond inter-ring stretching in the material [14].

Raman spectroscopic techniques can be used to reveal the identification of unknown structures and polymorphs (structural information) of materials, monitor changes in molecular structure of materials by analyzing the peak position, tracking changes in crystallinity by analyzing the width of the spectra peaks of the material, evaluation of the

magnitude of residual stress in materials by comparing the direction of shift for the peak position of the spectra, to analyze the direction of orientation of the molecules of conducting polymers and its composites, chemical composition and its variations in the material and lastly photoelectric properties of materials [34].

Raman spectroscopy was used to measure the possibilities of chlorine species diffusing into the interstitial spaces of bundled SWNTs and the switching of electrochemical double-layer charging regime to intercalative doping of the SWNT buckypaper. The results explains the feasibility of the electrochemical functionalization of SWNT bundle in aqueous KCl solution [33].

However, one of main challenges during the early stages of the Raman spectroscopy technique was the use of mercury lamp as the standard light source which created improper focusing of light beam on small samples and stray light problems. But these restrictions were overcome by the introduction of laser beams as light source to replace the mercury lamps during the developmental stages of the instrument [35]. Another important challenge that deserves mentioning is the small cross section of Raman scattering which culminates in low sensitivities in the event of Raman spectroscopic measurements and thus becoming very difficult for low concentration samples to be detected [36].

2.5.2 Raman Spectroelectrochemistry Cell Design

One of the major challenges for Raman spectroelectrochemistry is the design of suitable Raman cell that well fit the Raman spectroscopy instrument as well as the electrochemical part and how to integrate an optically transparent window at the same time maintaining an optimal electrochemical cell performance. The cell design comes in various configuration which may include

- Beaker – cell type
- Swagelok – cell type
- Pouch – cell type
- Coin – cell type
- Custom – made cell type

The beaker – cell type is designed in such a way that it can be assembled without any difficulties, diverse electrodes can be employed and reused. The pouch – cell type

components cannot be reused and need to be disposed at the end of every measurement. Alignment difficulties may arise since new components have to be arranged in the cell for every measurement. The coin – cell type and the custom – made type have reusable components and the cell frame is fabricated with precision. The assembly of the electrodes are well fitted thus reducing the problem of misalignment [37].

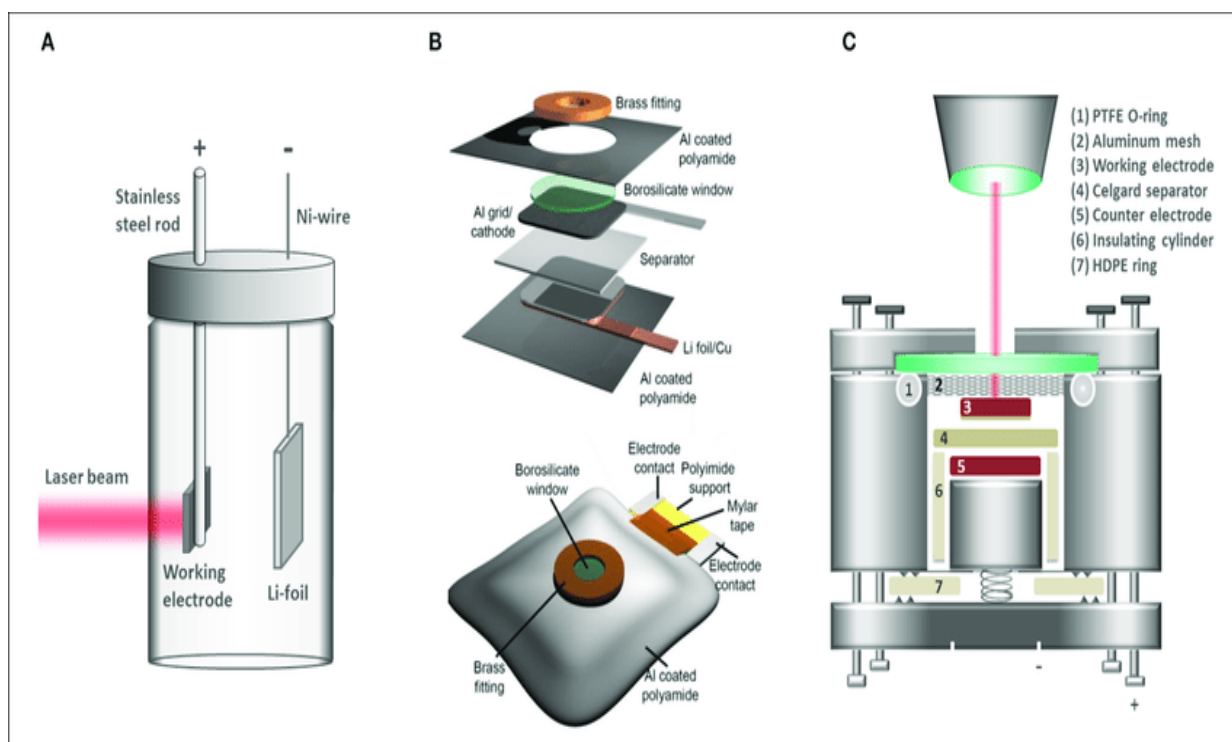


Figure 2.4 Typical cell designs for in situ/operando Raman spectroscopy. (A) Beaker (pyrex) cell design used e.g., by Inaba et al. (1995). (B) Pouch cell from Ghanty et al. [reprinted from reference (Ghanty et al., 2015) with permission of John Wiley and Sons]. (C) Custom-made coin-cell type design developed in our group [37].

Some key parameters for achieving optimal performance for an electrochemical cell include

- **Cell sealing:** The Raman cell is sealed with an “O” rings made from rubber and/or plastic materials. For prevention of contamination of electrolyte solution and corrosion of the objective lens quartz window is employed to form a closed electrochemical system for the Raman setup. Polytetrafluoroethylene (PTFE) and high density polyethylene (HDPE) “O” rings are the commonly used sealant materials in Raman cell fabrication because they are physically and chemically resistance to electrolyte leaking out of the cell and gas leakage into the cell. To prevent poor electrochemical performance and higher risk of side reactions

measurement, constricted cell sealing must be engaged which gives the Raman cell a good chemical stability [37].

- **Electrode pressure:** The electrode must be well compressed into the Raman cell during assembling without any gap to create a good electrochemical polymerization and Raman spectra peaks. Failure to attain a good electrode pressure as an illustration, might lead to incongruous electrical connection between the electrodes and their current collectors resulting in irregular film formation [37].
- **Electrode Size:** The size of the electrode should be of a considerable size to provide appropriate surface area for the electrochemical polymerization reaction and Raman spectroscopy. It is difficult to use electrodes with smaller size (below 2 mm) since it elevates the dangers of electrode misalignment. The issue of low current with low sensitivity can be raised when it comes to small size electrodes [37].
- **Electrolyte Choice:** The type of electrolyte employed can greatly influence the Raman cell construction and thereby having effect on the Raman spectroscopic signals. Organic electrolyte salts for instance are susceptible to the formation fluorescence species during Raman spectroscopic studies. The electrolyte must not react with the Raman cell components to prevent the production of unwanted species during Raman spectro-electrochemical analysis [37].
- **Raman Cell Component Reactivity:** For chemical and electrochemical stability, the reaction between the electrodes, electrolytes and the cell component (cell body, sealing parts and optical window) should be brought to the barest minimum. For an illustration, PEEK is used instead of Teflon since the former is more stable with Li metal than the latter as presented in literature [37].
- **Laser Excitation Wavelength:** The intensity of the Raman spectra can be improved when the excitation wavelength becomes equivalent to the energy of an electronic transition. When the photon energy of the laser is closer to the band gap of the sample being analysed, there is a stronger enhancement of the Raman spectra intensity. Moreover, the effect of fluorescence can be reduced by choosing an appropriate excitation wavelength. The extent of fluorescence emission relies on the closeness of the laser wavelength to the maximum absorption of the fluorescence species. It can be summarised from the above that, there can be a good balance between high Raman scattering power and low background signal a proper adjustment of the laser excitation wavelength. The controlling and improvement of

the spectral acquisition process requires the employment of excitation lasers of different (or tuneable) wavelengths [37] [35].

- **Laser specific Power:** For a better signal-to-noise ratios, there should be enough laser specific power to achieve that. Care must also be taken to prevent the sample from being transformed by the high laser specific power. It can be noted that, since Raman spectro-electrochemistry focuses on very small cross-sectional area, there is high tendency of burning the sample when there is excessive laser specific power. It is recommended that stability test must be conducted to prevent laser induced sample transformation and/ or burning. It has however been reported that the laser specific power ranges from 0.01 to 1.0 mW/ μm^2 for Raman spectro-electrochemistry analysis [37].
- **Working Distance:** The working distance is an important role in improving the signal to noise ratio during Raman measurements and an illustration can be made for 50X long working distance objective with numerical aperture (N.A) of 0.55 could operate with working distance of 10.6 mm. However, other objectives like X100, X50 and X10 coupled with N.A 0.9, 0.75 and 0.25 can have 0.21 mm, 0.38 mm and 10.6 mm as working distance respectively. The working distance of the objective used have significant influence on factors like electrochemical response, detection sensitivity and spatial resolution. The two most used objectives are air objective and water objective with glass cover of different thickness [37].

2.5.3 Surface – Enhanced Raman Spectroscopy (SERS)

SERS is an improved technique of the traditional Raman spectroscopy with the difference arising from the fact that SERS requires the introduction of metal nanostructure or nanoparticles as underlying factor for the signal enhancement. Unlike Raman spectroscopy, SERS gives greater signal enhancement aiding in submonolayer quantity of adsorbates [35][36].

The signal enhancement with enhancement factor (EF) ranging from 10^3 - 10^{10} for SERS can be explained by two mechanisms which are electromagnetic (EM) and chemical (CM) enhancement. The EM enhancement which illustrates the enhanced local electromagnetic fields in the nanomaterial by means of resonant excitation of plasma oscillations is the signal enhancement that can possibly be achieved since it is the most influential of the two mechanisms.

The EM produces a long-range local electromagnetic field enhancement owing to electromagnetic or plasmon resonances from the metal structure. CM produces an electronic interaction between the molecules and metal surface giving rise to polarizability enhancement of the molecule [36][35].

2.5.4 Characterization of PEDOT:PSS/ Graphene

The XRD patterns of PEDOT, PEDOT: PSS, PSS/PEDOT (hybrid film of PEDOT:PSS that is PSS core embedded in PEDOT matrix), PSS/G/PEDOT, graphene films is shown in the figure below with the graphene peak showing a sharp and high intensity at 10.08° as compared to the peaks of CPs. The peak around 39.2° is attributed to the introduction of oxygen-containing functional groups between the graphene layers [9].

The PEDOT spectra in Figure 2.5 (a) showed no significant peak in its pristine form and the blue spectra line with the fading peak in Figure 2.5 (a) explains the dispersion or distribution of graphene in polymer matrix of PSS/G/PEDOT ternary film [9].

The Raman spectroscopy analysis was also shown alongside the XRD pattern for the polymers of PEDOT:PSS, PEDOT:PSS/Graphene and graphene.

In the Raman spectra of PEDOT:PSS and PEDOT:PSS/ graphene, five bands at 1258, 1365, 1438, 1498 and 1557 cm^{-1} are assigned to C–C inter-ring stretching, C–C single bond stretch, C=C symmetric stretch, C=C asymmetric stretch, and C=C anti-symmetric stretch, respectively [13].

The presence of the strong π – π interactions between graphene and PEDOT:PSS explains the small shift of the hybrid polymer PEDOT:PSS/graphene from the PEDOT:PSS spectrum [15].

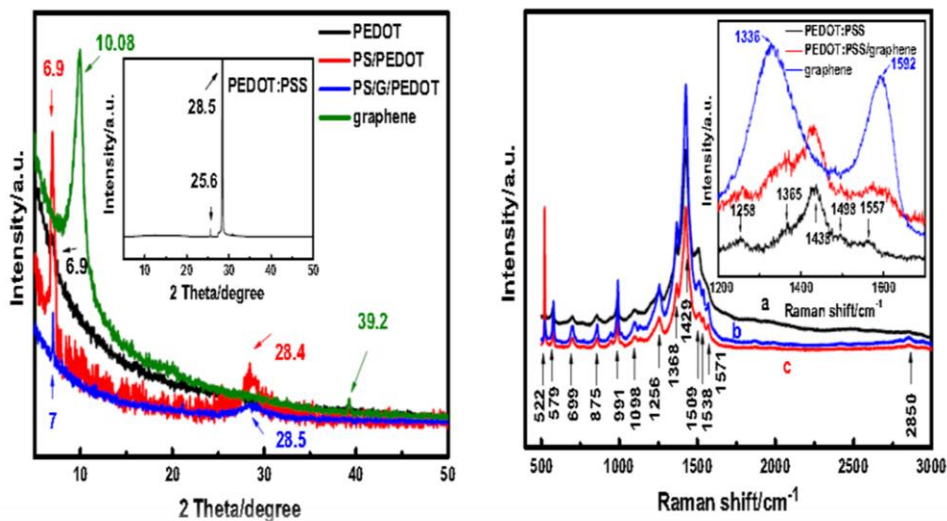


Figure 2.5 (a) XRD patterns of graphene, PEDOT, PS/PEDOT and PS/G/PEDOT; Inset represents the XRD spectrum of PEDOT:PSS and (b) Raman spectra of a PEDOT, b PS/PEDOT, c PS/G/ PEDOT nanocomposites; Inset represents the Raman spectra of graphene, PEDOT:PSS and PEDOT:PSS/graphene hybrid films [9].

Electrosynthesized Pt nanoparticle (PtNP) on PEDOT film used as catalyse for direct methanol fuel cell (DMFC) was characterized spectroelectrochemically and the results deduced was that UV-Vis and NIR spectroscopies does not give clear indication of the modifications or changes of Pt nanoparticle deposition on PEDOT film during electrosynthesis in contrast to Raman spectroscopy where modification was seen in intensity changes. The Working electrode used for this experiment was glassy carbon electrode and the main idea was to reduce Pt in fuel cell to maximize efficiency [12].

However, Raman spectroelectrochemistry of Pt nanoparticle (PtNP) on PEDOT film showed clearly that the deposition was feasible with a 50% intensity reduction for all PEDOT peaks with the greater change occurring between 1400 – 1650 cm⁻¹ which indicates Pt was electrochemically deposited on PEDOT film successfully [12].

Scanning Tunneling Microscope (STM) analysis on PEDOT:PSS showed that the PEDOT:PSS image gave a mixture of conductive regions or domains of PEDOT-rich and non – conductive domains without PEDOT particles but composed of PSS backbone [32].

FTIR in the range 2000–400 cm^{-1} with a resolution of 2 cm^{-1} was performed with the sole intention of measuring molar ratio of the silane coupling agent in the PSS copolymer to enhance the thermal stability and hydrophobicity of the film. NMR at 400-MHz frequency was used to structurally characterize a powder of poly (styrene sulfonate-co-vinyltrimethoxysilane) P(SS-co-VTMS) copolymers with a mixture of KBr powder [figure 2.6(a) and 2.6(b)] and it was elucidated that the absorption spectrum was obtained for the FTIR analysis when a transmittance mode was used. The outcome of the FTIR experiment was that an increase in silane group molar ratio brought about a reduction in peak intensity. However, because of the insolubility nature of the PSS copolymers, the analysis performed by the NMR setup failed [25].

The outcome of the changes in the doping level of PEDOT can be analysed using Raman spectroscopy or UV-VIS-NIR with the Raman spectra remaining constant at various conditions.

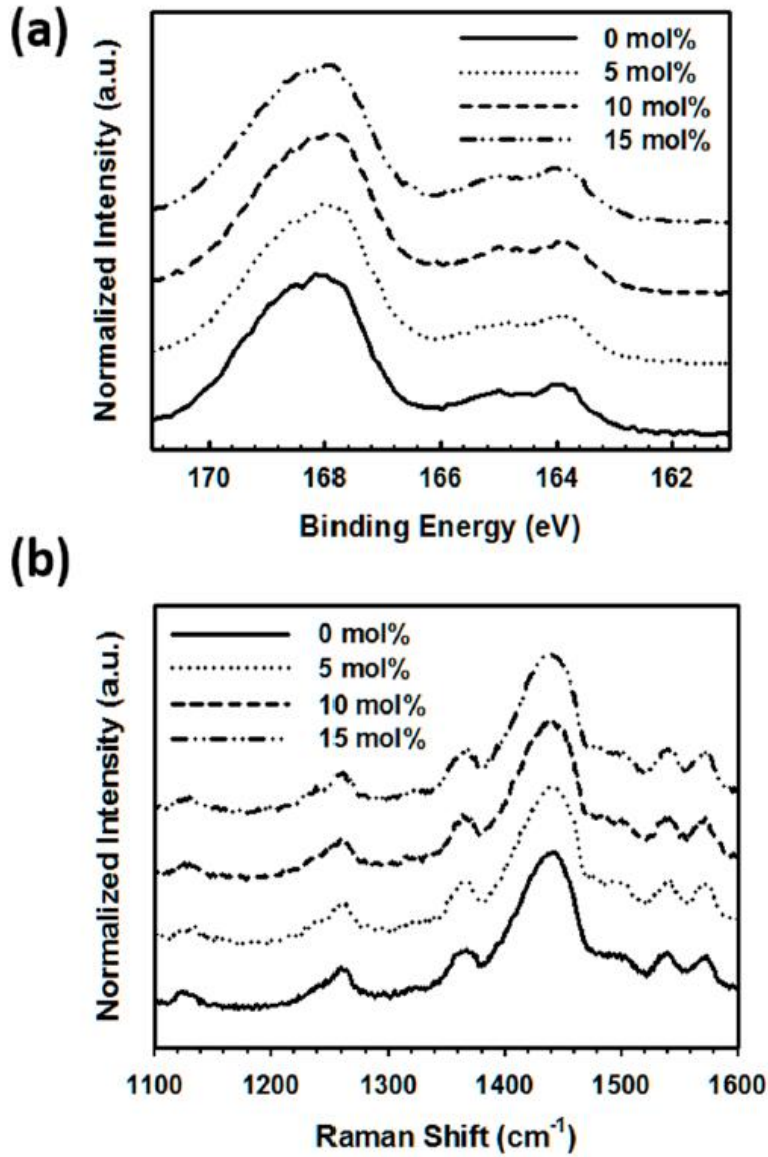


Figure 2.6 XPS spectra (a) and Raman shift spectra (b) of PEDOT:P(SS-co-VTMS) [25].

X-ray photoelectron spectroscopy (XPS) can be used to analyze the elemental composition of both PEDOT:PSS and PEDOT:P(SS-co-VTMS) film surfaces with a monochromated Al $K\alpha$ X-ray radiation.

The phase image of the PEDOT:PSS and PEDOT:P(SS-co-VTMS) films was analyzed with atomic force microscope (AFM) [25].

3. METHODOLOGY

3.1 Materials and Equipment

3.1.1 Materials

3,4-ethylenedioxythiophene (EDOT) monomer used for the experiment was acquired from Sigma-Aldrich with no extra purification process. EDOT monomer was stored in the dark in a refrigerator to prevent monomer degradation and contamination. All aqueous solutions were prepared using deionized water. The electrolytic salts employed for the experiments which includes Potassium Chloride (KCl), Sodium Polystyrene Sulfonate (NaPSS) and Tetrabutylammonium hexafluorophosphate (TBAPF₆) was purchased from Sigma-Aldrich with no extra purification and was tightly sealed to prevent it from reacting with atmospheric moisture. Distilled water was used for the preparation of all aqueous solutions during the experiment except TBAPF₆ electrolyte solution which was prepared by using acetonitrile (ACN) solution.

3.1.2 Equipment

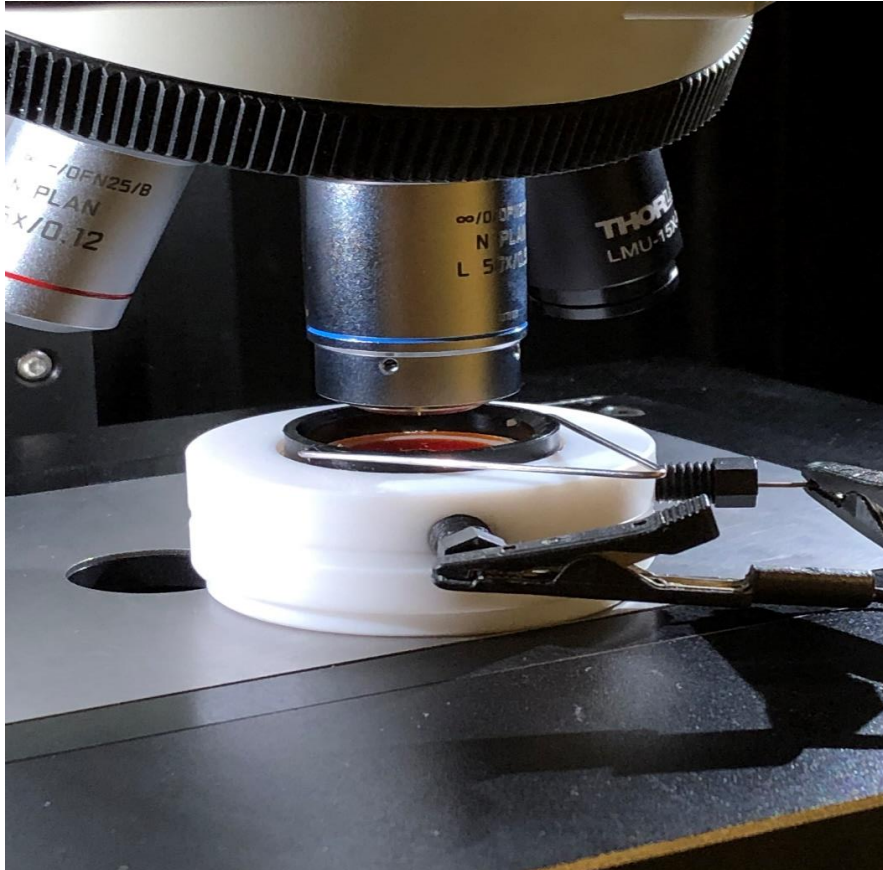
The electrochemical polymerization of EDOT monomer was performed using Fluorinated Tin Oxide (FTO), Gold (Au), Glassy Carbon (GC) and Platinum (Pt) as working electrodes (WE). Ag/AgCl wire and Pt wire were used as reference electrode (RE) and counter electrode (CE) respectively. The electrochemical polymerization EDOT monomer was performed in quartz cuvette, 3-neck electrochemical cell and customized design Raman cell at the lab.

3.1.2.1 Raman Cell Design

The electrochemical/Raman cell was laboratory fabricated and fabricated at the laboratory since there was no readily available cell commercially. The material used for the construction was from polytetrafluoroethylene (PTFE) commonly known as Teflon. A cavity of 1.5ml volume was created to hold up the electrolytic solution. The electrochemical/ Raman cell setup was designed in such a way that the working electrode (WE) was inserted into the cell from the bottom of the cell with the counter electrode (CE) and the reference electrode (RE) inserted at the side of the cell. The slot for the WE were sealed with an “O” ring to prevent leakage of the electrolyte solution.

A quartz window was employed to function as close circuit system for the electrochemical/Raman cell. Another function of the quartz window was to avoid a direct contact of the objective lens and electrolytic solution thereby acting as corrosion and contamination

prevention. The avoidance of evaporation of the electrolyte was an additional reason why the quartz window was used.



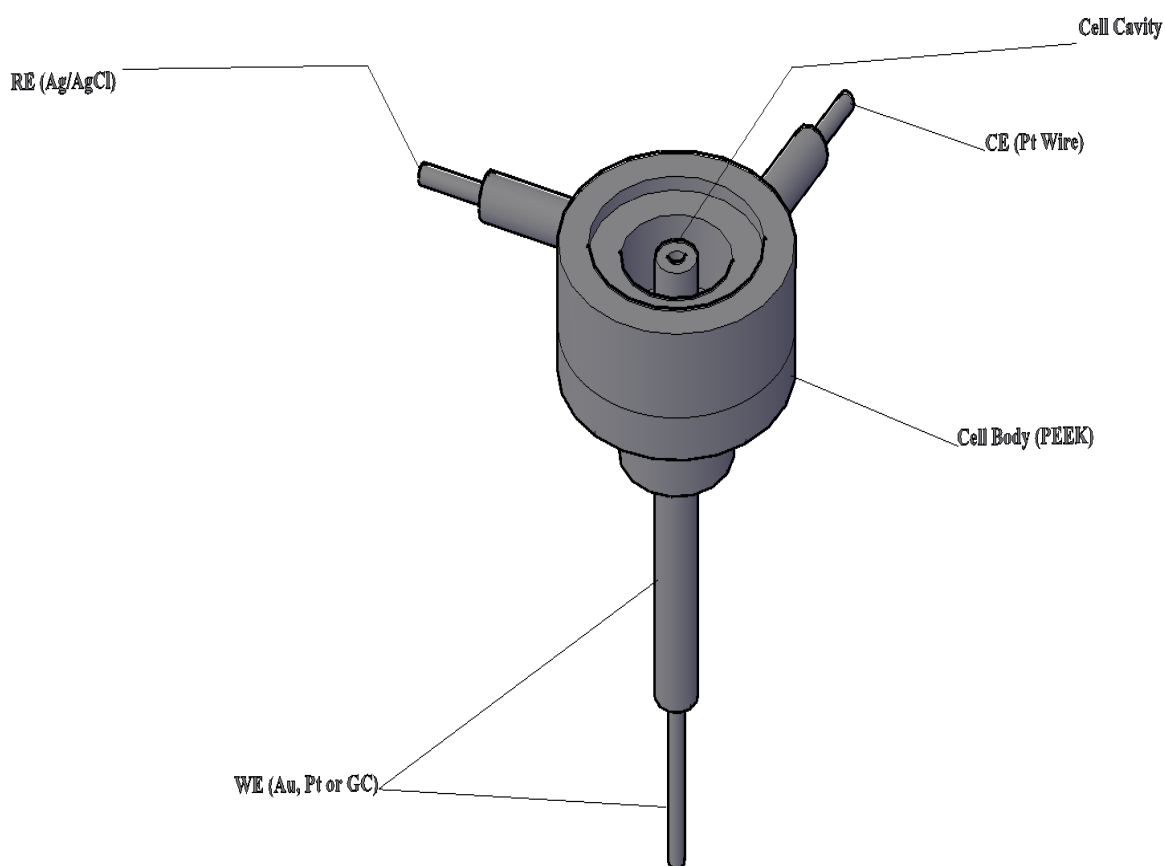


Figure 3.1 (a) Picture of Raman cell setup and (b) Schematic diagram of Raman cell showing all parts.

3.1.3 Preparation of electrolyte solutions

Preparation of saturated KCl solution

A saturated KCl solution was prepared by measuring 9g of KCl salt in 25mL of water and was used for the fabrication of the Ag/AgCl pseudoreference electrode.

Preparation of 0.1 M KCl solution

The concentration of 0.1 M KCl solution with molecular weight of 74.55 g/mol was prepared by measuring 0.19 g KCl salt using electronic balance and transferred into 25 mL volumetric flask and top up to the graduated mark with quartz distilled water.

The concentration of 0.1 M NaPSS solution with a molecular weight of 70 kDa was prepared by measuring 0.175 g of the NaPSS salt into 25 mL volumetric flask and topping it up to the graduated mark with distilled water.

The concentration for 0.1 M TBAPF₆-ACN solution with molecular weight 387.44 g/mol was prepared by measuring 0.387 g of the TBAPF₆ salt into 10 mL volumetric flask and topping it up to the graduated mark with acetonitrile (ACN).

3.1.4 Electrode polishing

The experiment commenced by mechanically polishing the various working electrodes (Au, Pt and GC) in a petri dish using diamond paste and polishing cloth. The polishing was done with diamond paste of coarse size 6 μ m, 3 μ m, 1 μ m and 0.25 μ m. The electrodes surface to be cleaned was rinsed with distilled water and ethanol intermittently during polishing.

The FTO electrodes were carefully cleaned by successive ultrasonication in acetone, followed by ethanol and then deionized water to ensure removal of all traces of acetone and finally dried before use.

3.2 Experimental Procedures

3.2.1 Ag/AgCl Fabrication

The experiment commenced with the preparation of Ag/AgCl reference electrode. The Ag – wire (about 6cm) was rinsed with a distilled water. Pt – wire (about 10cm) was coiled at the end to increase the surface area and burned under a blue flame of Bunsen burner to remove the oxide layers formed on the Pt – wire. A saturated aqueous solution of KCl (9g of KCl in 25ml of H₂O) was prepared for the fabrication of the Ag/AgCl reference electrode. The Ag – wire and the Pt – wire was placed in the electrochemical cell and the saturated KCl solution was poured into the cell as well. The electrochemical cell was connected to a potentiostat (EG&G Princeton Applied Research Potentiostat/ Galvanostat Model 263A). The Ag – wire acted as the working electrode WE and the Pt – wire as the reference electrode/ Auxiliary electrode. A current of 1mA and a time (t) of 7200s (2 hours) was employed and a formation of a black layer electrochemical deposition on the Ag – wire and the graph of voltage against time was obtained. The reference Ag – wire electrode was rinsed with distilled water.

3.2.2 Calibration of Ag/AgCl

The calibration of the Ag/AgCl pseudoreference electrode was performed against a known redox couple. An electrochemical cell was setup with the Pt – wire serving as the counter electrode (CE), glassy carbon (GC) electrode as the working electrode (WE) and the Ag/AgCl – wire acting as the reference electrode was filled with 0.1M aqueous KCl solution as the electrolyte. A small amount of ferrocene [$K_3Fe(CN)_6$] was added to the KCl electrolyte solution to give it a yellow color. Cyclic voltammetry (CV) was used to do the calibration of the Ag/AgCl pseudoreference electrode at a potential range of 0.000V to +0.400V at 100mV/s scan rate over 3 cycles (6 stop crossings).

a.



b.

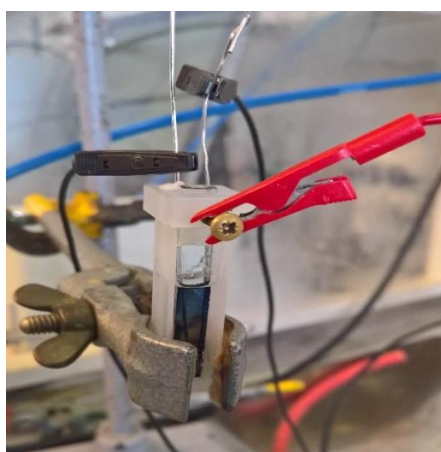


Figure 3.2 images of Electrochemical setup of (a) 3-neck cell and (b) quartz cuvette.

3.2.3 Electrochemical polymerization of EDOT monomer on Fluorinated Tin Oxide (FTO)

The electrochemical deposition of the 0.01M EDOT monomer was performed on Fluorinated Tin Oxide (FTO) glass substrates using KCl, NaPSS, and TBAPF6 as electrolytes with 0.1M concentration. The electrochemical measurements were performed in three-electrode cell made from quartz cuvette using Autolab (PGSTAT101) potentiostat as shown in figure 3.2 (b). The electrodes employed were platinum wire (Pt) as counter electrode (CE), Fluorinated Tin Oxide (FTO) as the working electrode (WE) and Silver wire (Ag) coated with AgCl as the reference electrode (RE).

The applied potential range for the measurements were from 0.5V to 1.0V, at 15 cycles (30 stop crossings) and 20mV/s scan rate. Oxygen was removed from the solution by purging with

dry nitrogen (N_2) gas for 10 min for all three electrolytes (KCl, NaPSS, and TBAPF6) at 0.1M concentration.

The electrochemical polymerization was performed for the PEDOT films in the various electrolytic solutions. Upon continuous sweeping, nucleation and polymer growth of the film were nicely observed on the surface of the FTO substrates.

The polymer films were rinsed with deionized water to remove any remaining electrolytes and EDOT monomer from the film. The polymer films were placed in a monomer free electrolytic solutions (KCl, NaPSS, and TBAPF6) and the redox behavior of the films were studied at a potential range of -1.0V to 1.0V for 5 cycles using four different scan rates of 10mV/s, 20mV/s, 50mV/s and 100mV/s. N_2 gas were bubbled through the electrolyte solutions for 10 minutes to remove oxygen.

3.2.4 Electrochemical polymerization of PEDOT films using 3-neck cell

The 3 – neck cell in figure 3.2 (a) was assembled for the electrochemical polymerization of the EDOT monomer on the WE surface. The Pt- wire (CE), Ag – wire (RE) and the Au electrode (WE) were inserted into the 3-neck cell accordingly. KCl electrolyte solution of 0.1M concentration containing the 0.01M EDOT monomer was poured into the cell for the polymerization and N_2 gas was bubbled through the cell to remove oxygen. A cyclic potential scan setup was run between -0.5V and 1.0V using 15 cycles (30 stop crossings) and 20 mV/s as scan rate. The cell and electrode were rinsed with monomer free electrolyte solution (0.1M KCl) and doping of the thin film deposited on the Au electrode surface was tested using monomer free electrolyte solution (0.1M KCl). N_2 gas was bubbled through the cell to remove oxygen and the scanning parameters used for the CV staircase were -1.0V to 1.0V potential, 3 cycles (6 stop crossings), 100mV/s scan rate.

Characterization of the polymer films in a monomer-free KCl electrolyte of known concentration of 0.1M were conducted to obtain the CV for the doping response for the three WE electrodes (Au, Pt and GC). The applied potential range for the characterization were between -1.0V and 1.0V for 5 cycles using 10mV/s, 20mV/s, 50mVs and 100mV/s as scan rates. The process was deaerated by purging the monomer-free KCl electrolyte with N_2 gas for 10 minutes.

3.2.5 Electrochemical polymerization of PEDOT film using the laboratory fabricated Raman cell

The Au, Pt and GC WE were polished like previously done for the 3-neck cell.

The electrochemical measurement for PEDOT film on Au electrode was performed in the already laboratory fabricated Raman cell coupled to Autolab (PGSTAT101) potentiostat. Au, GC and Pt electrodes were used as the WE and inserted through the bottom of the cell with the electrode surface appearing at the electrolytic cavity of the cell. The platinum wire used as counter electrode (CE) and Ag wire coated with AgCl was used as the reference electrode (RE) were inserted at the sides of the Raman cell as shown in figure 3.1.

A 0.01M EDOT monomer in 0.1M KCl electrolyte solution was poured into the cell cavity of about 1.5ml volume. The cell was closed using the glass quartz window and the oxygen was removed by bubbling N₂ gas through the solution for 10 min. The PEDOT film was polymerized by a potential scan range of -0.5V to 1.0V. A scan rate of 20mVs and the number of cycles used for the CV staircase was 15 cycles (30 stop crossings).

Characterization of the polymer films in a monomer-free KCl electrolyte with known concentration of 0.1M were conducted to obtain the CV for the doping response for the three WE electrodes (Au, Pt and GC). The applied potential range for the characterization were between -1.0V and 1.0V for 5 cycles using 10mV/s, 20mV/s, 50mVs and 100mV/s as scan rates. The process was deaerated by purging the monomer-free 0.1M KCl electrolyte with N₂ gas for 10 minutes.

3.3 Spectroelectrochemistry

The main spectroscopic technique used for the characterization process was Raman spectroscopic measurements using a Renishaw inVia Raman Spectroscopy instrument. Cary 60 UV-VIS Spectroscopic instrument from Agilent technology was employed as auxiliary characterization technique during spectroelectrochemistry process.

During the in situ Raman spectroscopy measurement, the electrochemically polymerized PEDOT on the three different electrodes (Au, Pt, and GC) were studied upon application of seven different constant potentials (-0.8V, -0.5V, -0.1V, 0.3V, 0.5V, 0.6V, 0.7V) taken from a CV conducted during p-doping of a PEDOT film to properly observe all the Raman bands during doping. Two lasers of wavelengths 532nm and 785nm with laser power of 1% were

separately used to record the Raman spectra of the film after the polymerization process has been performed. The waiting time between the potentiostat and the starting of the Raman spectroscopy measurement was 20 seconds. A constant potential was maintained before each measurement at total time of 120 seconds. The magnification of the objective lens used for the measurements at applied potential range was X50.

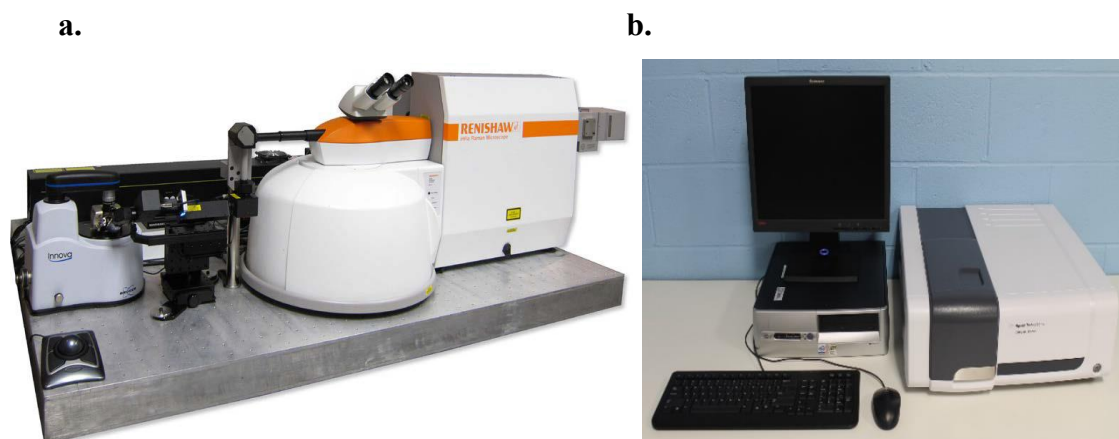


Figure 3.3 Image of (a) Raman spectrometer from Renishaw and (b) UV-vis spectrometer from Agilent Cary 60. [61].

For the UV – Vis measurements, the electrochemical polymerization was performed on an fluorinated tin oxide (FTO) electrode. The scanning electrode potential was cycled between - 0.9V and 0.6V against Ag/AgCl reference electrode and Pt wire CE. The number of scans were 31 times at a scan rate of 2mV/s. The absorbance spectra were recorded at the end of each potential cycle for 31 times. The absorbance spectra were recorded for constant potentials as the current drops to zero.

4. RESULTS AND DISCUSSIONS

4.1 Electrochemical Polymerization of PEDOT film on FTO substrate.

CV shapes observed for all the PEDOT films were different and this can be accredited to the various electrolyte solutions used for the electrochemical polymerization performed. An increase in oxidation and reduction peaks current was observed for three CVs and a steady rise in current density on each potential sweep was noticed signifying polymer film deposition on the FTO substrates.

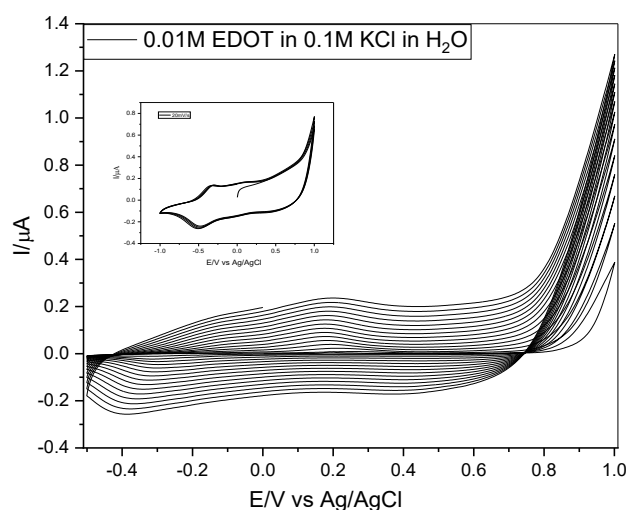


Figure 4.1 Cyclic voltammogram for an electrochemical polymerization of PEDOT film in KCl electrolyte solution. The insert shows characterization CV of the PEDOT film in monomer free 0.1M KCl solution at potential range -1.0V to 1.0V for 5 cycles.

The cyclic voltammogram shown in the figure 4.1 consist of 0.01M EDOT in 0.1M KCl electrolyte solution in aqueous medium. The insert is CV showing the first 5 cycles of the characterization of the PEDOT film in 0.1M KCL monomer-free solution at 20 mV/s scan rate. The CV from the polymerization with monomer in solution showed constant growth of current during scanning as the amount of electrochemically active polymer material is increasing onto the working electrode surface. The CV also showed very broad and smaller oxidation and reduction peaks which indicates movement of charges inside the film and counter ions move from electrolyte solution to compensate the charges. It was observed during scanning that the PEDOT film at oxidized state gave light blue color whiles dark blue color was noticed at the reduced state. A consistent and smooth growth of the polymer film was observed throughout the scanning process. The applied potential of oxidation peak occurs at 0.2V and the reduction peak potentials occurs at -0.4V and 0.45V.

The inserted CV for the above polymer film depicted a slight shift in potential for both the oxidation and reduction peaks in the 0.1M KCl monomer-free electrolyte solution during scanning for the redox response of the polymer film. During doping there is no increase in current during continuous scanning [74][32][13].

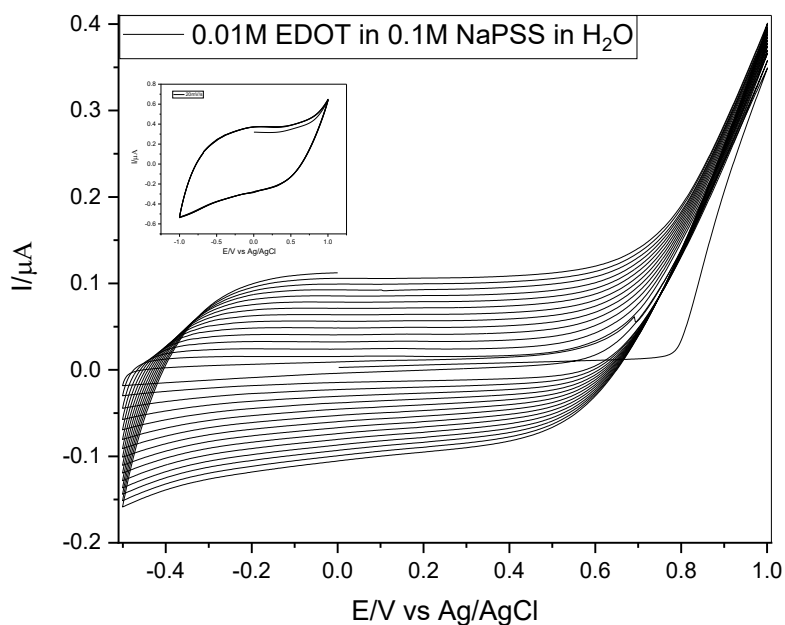


Figure 4.2 Cyclic voltammogram for an electrochemical polymerization of PEDOT film in NaPSS solution. The insert shows characterization CV of the PEDOT film in monomer free 0.1M NaPSS solution at potential range -1.0V to 1.0V for 5 cycles.

The CV in figure 4.2 shows the electropolymerization of PEDOT in 0.1M NaPSS electrolyte solution in aqueous medium. The figure also shows an insert characterization CV for the first 5 cycles of the PEDOT film in 0.1M NaPSS monomer-free electrolyte solution at 20mV/s showing the redox behavior of the film. The oxidation and reduction peaks of the CV were seen at -0.2V and 0.5V respectively even though they are broad and not distinct. The film showed color change from light blue to dark blue during continuous sweeping of the polymerization process for the oxidation/ reduction state respectively. The CV for the NaPSS electrolyte also exhibited consistent and smooth growth polymerized film on the surface of the FTO substrate [13][21][24][74].

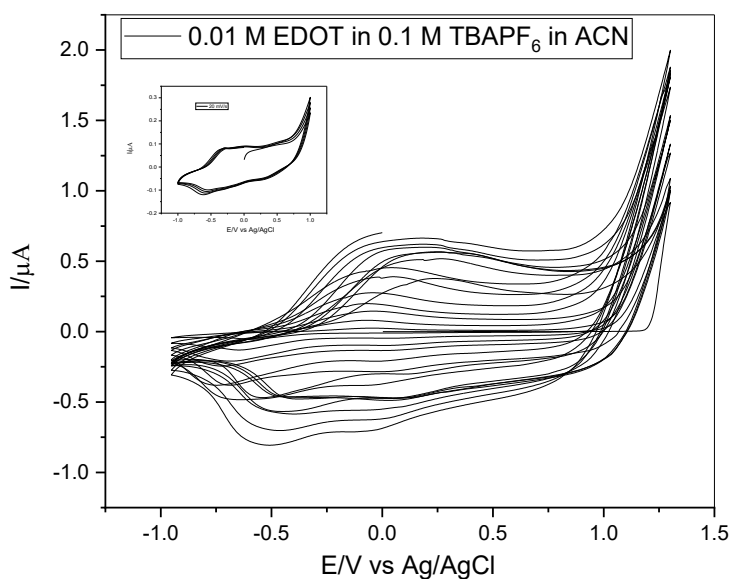


Figure 4.3 Cyclic voltammogram for an electrochemical polymerization of PEDOT film in TBAPF₆-ACN solution. The insert shows characterization CV of the PEDOT film in monomer free 0.1M TBAPF₆-ACN solution at potential range -1.0V to 1.0V for 5 cycles.

The figure 4.3 above represents the CV for electrochemically polymerized film of 0.1M EDOT monomer in 0.1M TBAPF₆ in Acetonitrile (ACN) at 20mV/s scan rate and an applied potential range of -1.0V to 1.25V for 15 cycles.

The CV showed broad oxidation peak which occurred at 0.1V and two reduction peaks at -0.5V and -0.1V potentials respectively. Unlike the CV films in the aqueous medium electrolytes discussed earlier, the CV of TBAPF₆ in ACN as organic medium electrolytes gave fibrous (rough) film on the FTO substrate. The poor stability or adherence of the film on the FTO surface might be due to higher potential greater than 0.8V which leads to formation of overoxidized film after electropolymerization [74]. It can also be attributed to low solubility EDOT monomer in the electrolyte solution [74]. The color change of the film presented light blue for the oxidation potential and dark blue for reduction potential on continuous sweeping for the polymerization process. The CV insertion presented the redox response of the first 5 cycles of the film in 0.1M TBAPF₆ in ACN monomer-free electrolyte solution [52].

4.1.1 Electrochemical Characterization of FTO polymer films.

Characterization of films deposited on the FTO polymer films were performed in a monomer-free electrolyte solution of concentration 0.1M for KCl, NaPSS and TBAPF6 accordingly. The applied potential range for the characterization was -1.0V to 1.0V for 5 cycles. The different scan rates used for the characterization were 10mV/s, 20mV/s, 50mV/s and 100mV/s for polymer films.

Cyclic voltammograms of polymer films in the presence of monomer-free electrolyte exhibited an increase in the oxidation and reduction peak potentials. It was observed from the CV that increasing the scan rate caused small shift in the peak potentials for the polymer films. The CVs of the films show one oxidation peak and two reduction peaks for all the electrolyte solutions. The changes observed in the CVs resulting from different scan rates gives an indication of the influence of the electrolyte solutions. The characterization CVs also displayed behavior comparable to the CVs of their corresponding electrochemical polymerization on the FTO substrates.

The oxidation and the reduction peaks shown in characterization CVs below were broad which implies slow redox response and ion movements in the polymer film at the elevated scan rates for the electrolyte solutions.

From the CVs, current densities of the films increase with increasing scan rates suggesting that conductivity of the film is high [6][13][25][32][74].

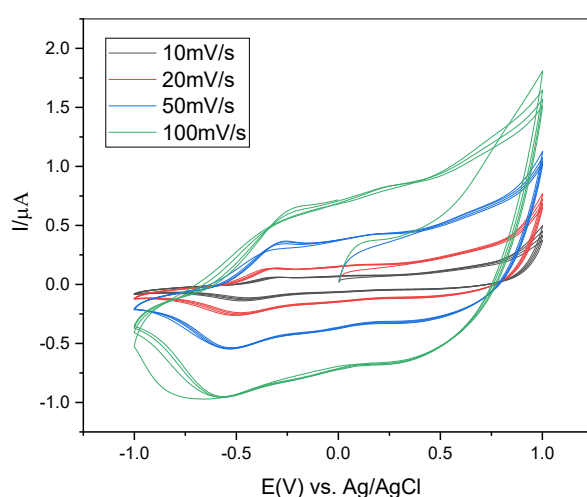


Figure 4.4 Cyclic voltammogram of PEDOT film in KCl monomer free solution showing different scan rates.

Furthermore, in comparing the CVs obtained for the three electrolyte solutions it can be noticed that the peaks for the KCl electrolyte film looked more pronounced unlike the NaPSS and TBAPF6 electrolyte solutions. The oxidation and reduction peak currents increases linearly with increasing scan rates for the polymer film characterized in KCl film fig 4.4. The oxidation and reduction peaks for the polymer films of NaPSS and TBAPF6 electrolyte solutions are not well defined and seems to disappear. The broader peaks seen in the CVs of the redox cycle is an indicative of slow diffusion of ions from the respective electrolytic solutions into the polymer films. From the CVs above, it can be predicted that there is linear dependence between oxidation/reduction peaks and scan rate. Even though peaks of CVs were not too prominent the films showed some form of activeness electrochemically [22][25][31][32][74].

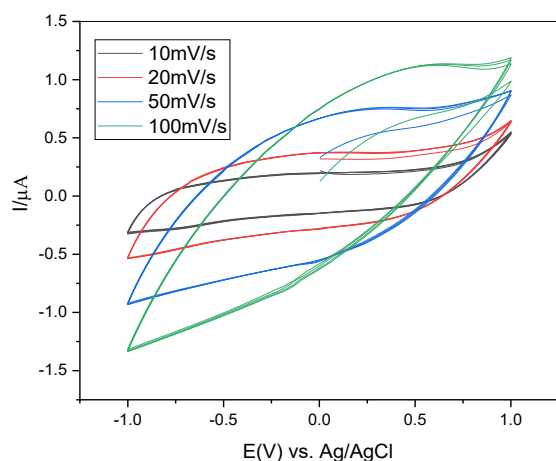


Figure 4.5 Cyclic voltammogram of PEDOT film in NaPSS monomer free solution showing different scan rates.

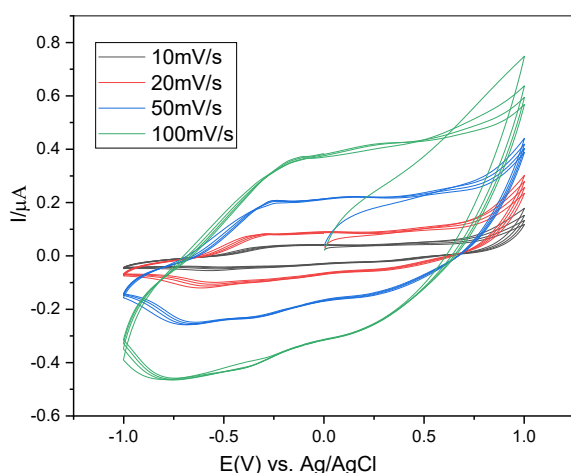


Figure 4.6 Cyclic voltammogram of PEDOT film in TBAPF6-ACN monomer free solution showing different scan rates.

4.2 Electrochemical Polymerization of PEDOT film using 3-neck cell.

The cyclic voltammograms using the 3-neck cell with the potential range -0.5V to 1.0V, 15 cycles and scan rate 20mV/s are shown in the figures 4.7 (a), (c) and (e) below. The concentrations of PEDOT: PSS EDOT monomer and KCl electrolyte was 0.01M and 0.1M respectively for the three different WE (Au, GC and Pt). The comparison of the polymerization film shown in figures 4.7 (a), (c) and (e) below indicated similar responses for all the WE (Au, GC and Pt) showing small and broader oxidation peak at potential of 0.1V for all three electrodes and likewise reduction peak for all three WE at reduction potential of -0.4V. Even though similar potential ranges -0.5V to 1.0V can be seen for all the WE (Au, GC and Pt) yet they have different intensities. On the other hand, there is sharp peak depicted for the Au electrode in CVs for the polymerization and characterization in Fig. 4.7 (a)-(b) which cannot be seen for the Pt in fig. 4.7 (c)-(d) and GC in fig. 4.7 (e)-(f) electrodes during the reverse scan. This sharp and well-defined peak might be due to impurities from the electrolyte solution and or inadequate preparation of the Au WE surface [2][22][74].

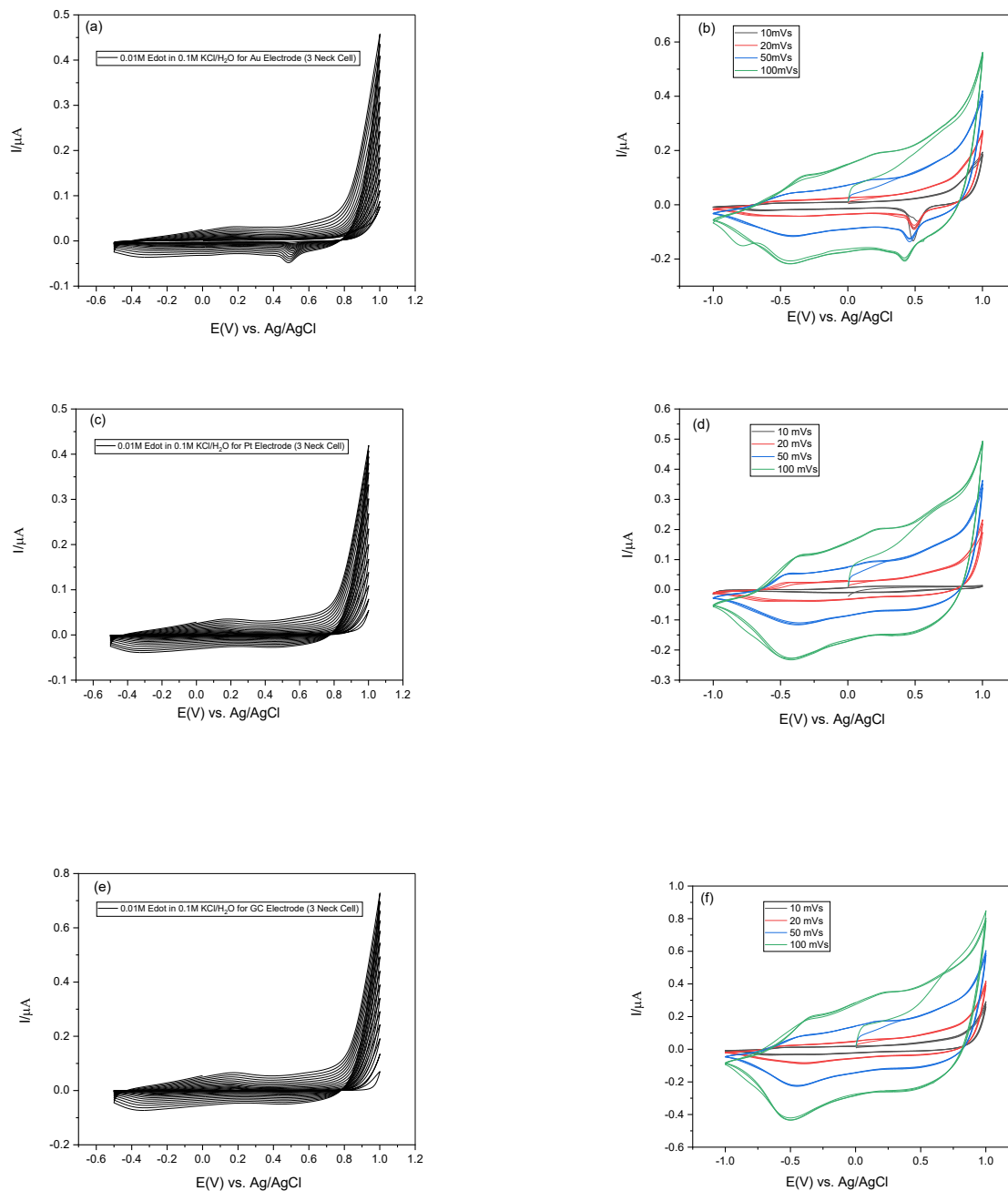


Figure 4.7 Electrochemical polymerization of PEDOT film and the corresponding CV in monomer free KCl electrolyte solution. (a-b) for Au electrode, (c-d) for Pt electrode, (e-f) for GC electrode, at different scan rates for 3-neck cell.

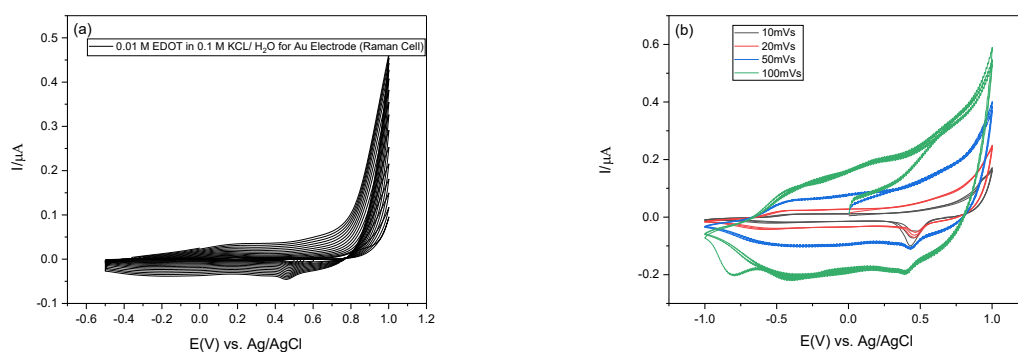
Moreover, there are no clear distinction between the CVs for the WE (Au, Pt, & GC) for the 3-neck cell (above) and that of the CVs of the Raman cell. The cathodic and anodic peaks for both 3 neck cell and Raman cell shows the same potentials (0.25V, -0.4V for oxidation peaks and 0.45V, -0.4V for reduction peaks) at 20mV/s scan rate during polymerization in the electrolyte solution. The oxidation/reduction potential peaks produced from the

characterization of the film were broad with low current intensities. The reason that can be assigned to these broad peaks is slow diffusion of the KCl electrolyte to the film.

4.3 Electrochemical Polymerization for laboratory fabricated Raman cell

This section brings out the redox response for the PEDOT polymerized film on the WE (Au, Pt & GC) during doping (p and n – doping). It can be noticed from the CVs above and below that as the scan rate increases from 10mVs to 100mVs there is also an increase in the oxidation/reduction peak potential for all the WE (Au, Pt & GC) used. The CVs also shows swelling of the film as the scan rate increases from 10mVs to 100mVs [2]. The applied potentials are similar for all the WE, but variations are seen in the current intensities. It can also be seen that there are slight variations between the CVs above (3 neck cell) and that below (Raman cell).

From the CVs representing the laboratory fabricated Raman cell below, the electrochemical polymerization of the WE electrodes and their corresponding redox characterizations voltammograms were measured under similar conditions to the 3-neck cell used. The characterization CVs were measured using an applied potential range of -1.0V to 1.0V, 5 cycles (10 stop crossings) and scan rates 10 mV/s, 20 mV/s, 50 mV/s and 100mV/s in succession. From the CVs, slight shift in oxidation/reduction peaks could be observed for all the electrodes used akin to the CVs for the 3-neck cell. The oxidation peaks potentials were seen at -0.45V and 0.2V whereas the reduction peaks potentials were found at -0.5V and 0.4V. The oxidation /reduction peaks increase along with increasing scan rate showing linear dependence in terms of relationship [52][74][77].



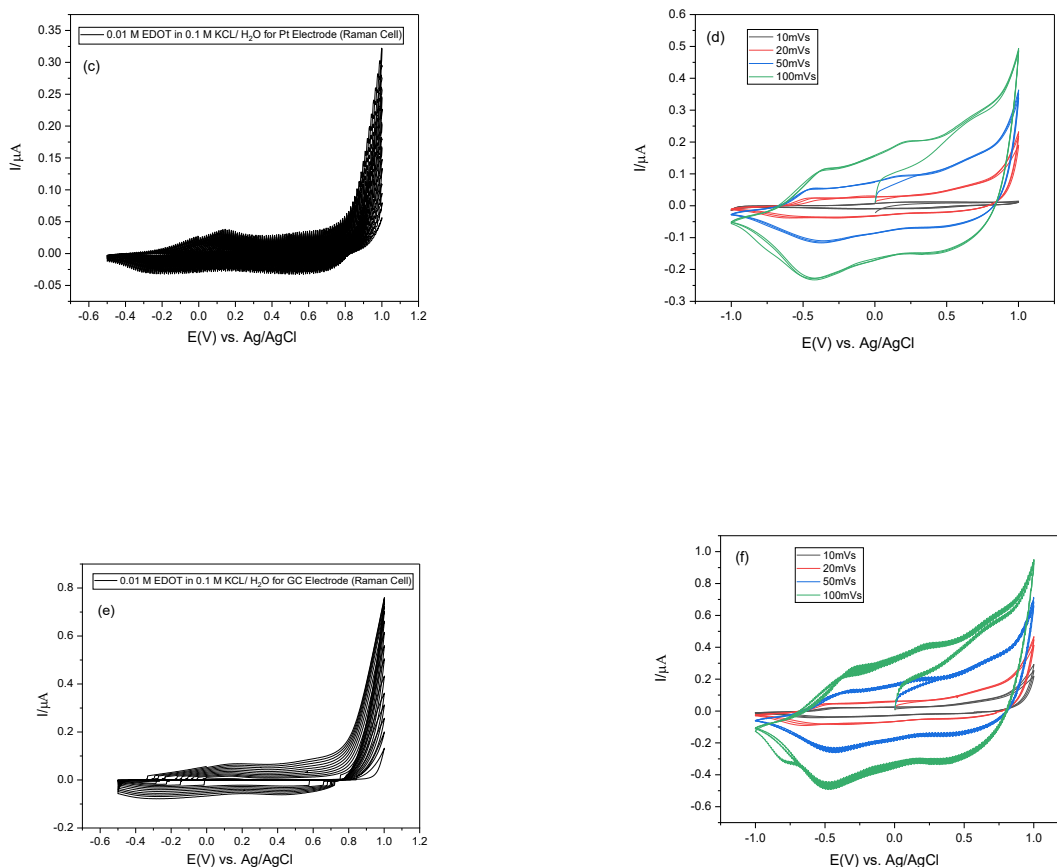


Figure 4.8 Electrochemical polymerization of PEDOT film and the corresponding CV in monomer free KCl electrolyte solution. (a-b) for Au electrode, (c-d) for Pt electrode, (e-f) for GC electrode, at different scan rates for Raman cell.

4.4 In situ UV-Vis Spectroscopy

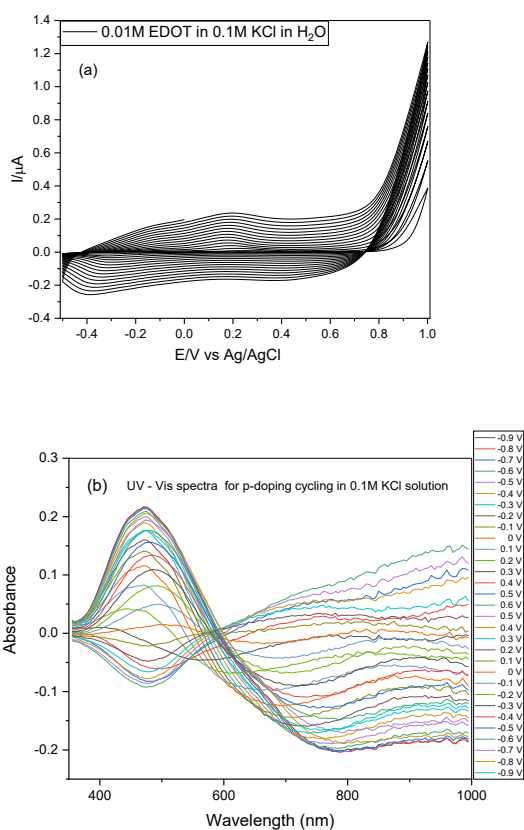
In situ UV-Vis spectroelectrochemistry was used to study the doping (p- and n-doping) characteristics and to indicate the various vibrational modes of the PEDOT film. It is a useful tool for studying the structural and optical properties of the conducting polymers. The EDOT monomer with 0.01M concentration was electrochemically polymerized on glass substrate coated with FTO in three different electrolytic medium. The electrolyte used are 0.1M KCl solution, 0.1M NaPSS solution and 0.1M TBAPF₆ in ACN solution. The in situ UV-Vis was used to characterize the changes in the absorption spectra and obtain optical properties information of the PEDOT film.

The in situ UV-Vis measurement of the already electrochemically polymerized film of 0.01M EDOT monomer was carried out in 0.1M monomer-free electrolyte where a series of oxidized

and reduced form spectra was observed and recorded at different potentials during doping of the films.

The parameters used for the UV-Vis measurements includes applied potentials from 0.6V down to -0.9V, 2mV/s scan rate per each potential was used given a total scan rate of 100mV/s. The total time for the entire measurements was 1500 sec with 50 sec intervals between the applied potentials for 31 cycles or spectra. An electrochemically polymerized PEDOT film on FTO electrode in quartz cuvette using a monomer-free solution of 0.1M (KCl, NaPSS and TBAPF6-ACN) was cycled through potential of 0.6 V to -0.9 V for 31 scans during which spectra was recorded after each scan.

It was worth mentioning that the above parameters were used to record the UV-Vis spectra of the PEDOT film in three different monomer-free electrolytic solutions during doping. The 0.1M KCl solution and 0.1M NaPSS represents aqueous medium electrolytes whereas organic medium electrolyte is 0.1M TBAPF6-ACN solution.



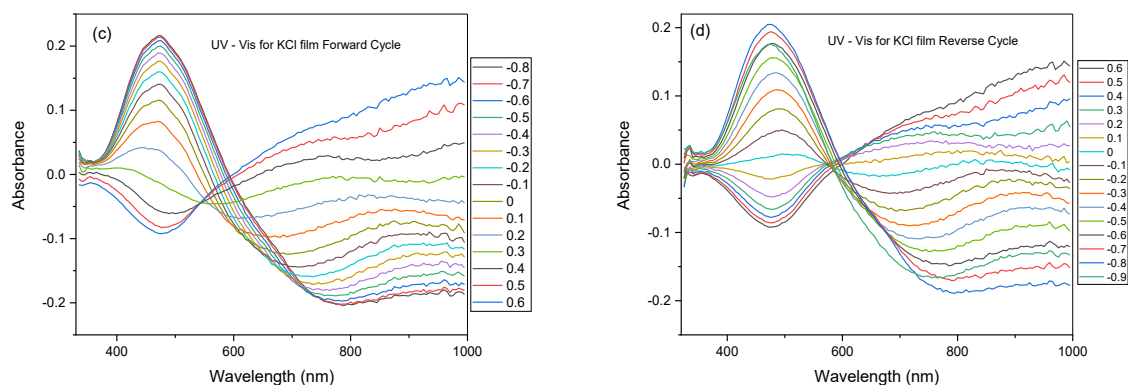


Figure 4.9 (a) CV for film growth of electrochemically polymerized PEDOT film on FTO in 0.1M KCl solution and UV-VIS absorption spectra measurement of the film (b) spectra of complete cycle for p-doping (c) forward cycle (d) reverse cycle. The cycling potential employed was between 0.6nV and -0.9 V for 31 scans in monomer-free solution of 0.1M KCl.

From figure 4.9 (b) to (d), absorbance increases as the wavelength of the visible range increases for p-doping of the PEDOT film in 0.1M KCl electrolyte solution. The highest absorbance for the p-doping can be seen at 0.23 and 460 nm wavelength with oxidation potential 0.6V down to -0.9V reduction potential for both forward and reverse cycle.

The highest absorption peak which occurred at 460 nm for p-doping illustrates $\pi - \pi^*$ transition absorption of the conjugated PEDOT main chain.

Moreover, at applied negative potentials the absorbance peak was realize at 460 nm wavelength for the reduced (n-doping) state. Nothing much can be seen at the neutral state since no significant absorption peaks corresponding to polarons formation and bipolarons are present.

It can be noticed that the forward and the reverse cycles have little or no difference in terms of absorbance and wavelengths.

Figure 4.9 (b) shows a complete cycle of the spectra obtained for p-doping when the film was cycled through -0.8 V to 0.6 V. The forward and reverse cycles of the p-doping is also shown in figures 4.9 (c) and (d) respectively. The n-doping of the film from -0.9 V to -2.0 V could not be performed since PEDOT often breaks down during n-doping and again the potential limit of water system makes n-doping difficult in aqueous electrolyte medium.

Electrochromic properties of the PEDOT polymer was observed as spectra changes color from the oxidation potential of 0.6V to the reduction potential of -0.9V. The change in color of the

polymer is the underlying factor for display properties in PEDOT material. It was illustrated in both spectra cycles that electrochromic switching properties of the PEDOT film showed constant and reversible change in absorbance [74].

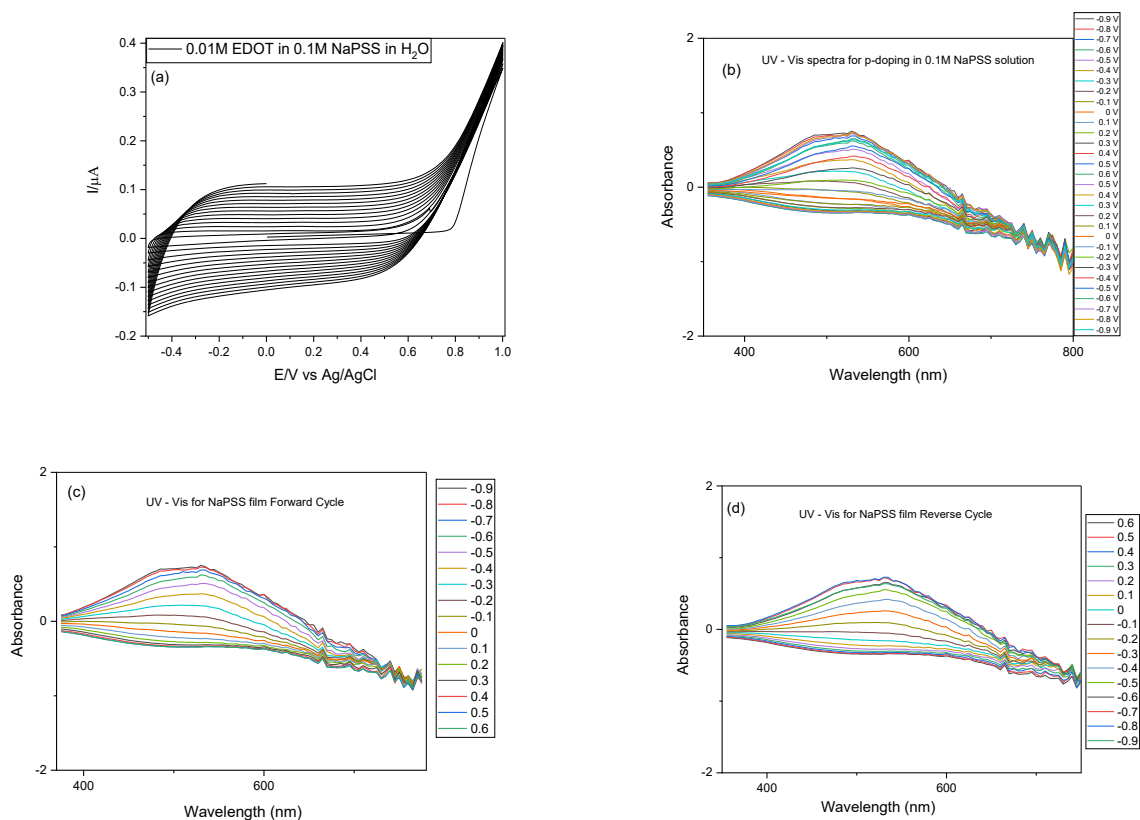


Figure 4.10 (a) CV for film growth of electrochemically polymerized PEDOT film on FTO in 0.1M NaPSS solution and UV-VIS absorption spectra measurement of the film (b) spectra of complete cycle for p-doping (c) forward cycle (d) reverse cycle. The cycling potential employed was between 0.6V and -0.9 V for 31 scans in monomer-free solution of 0.1M NaPSS.

From the figures 4.10 (c) and (d) above, only p-doping can be realized for the PEDOT film in 0.1M NaPSS monomer free electrolyte solution and broad absorbance peak was 540 nm wavelength which explains $\pi - \pi^*$ transition absorption for the conjugated polymer main chain. The applied potential for forward and reverse cycle measurements ranges from -0.9V to 0.6V representing 31 cycles in total. It can be observed that n-doping state absorption was very weak and thus vanishes as the PEDOT film reduces to intrinsic conjugated state.

In like manner to the spectra in figure 4.9, the figure 4.10 (b) also shows complete cycle of the spectra obtained for p-doping when the film was cycled through -0.8 V to 0.6 V. The forward and reverse cycles of the p-doping is also shown in figures 4.10 (c) and (d) respectively. The n-doping of the film from -0.9 V to -2.0 V could not be performed since PEDOT often breaks down during n-doping and again the potential limit of water system makes n-doping difficult in aqueous electrolyte medium.

From the graphs, the wavelength for the spectra lines of the PEDOT film in 0.1M NaPSS was truncated at 750 nm since noisy signal was produced beyond this wavelength. The formation of polarons and bipolarons was difficult to detect unlike the 0.1M KCl electrolyte solution. Similarly, the spectra of 0.1M KCl electrolyte figure 4.10, the 0.1M NaPSS electrolyte solution also showed some electrochromic properties since there was color change over the applied potential range [58][59][74].

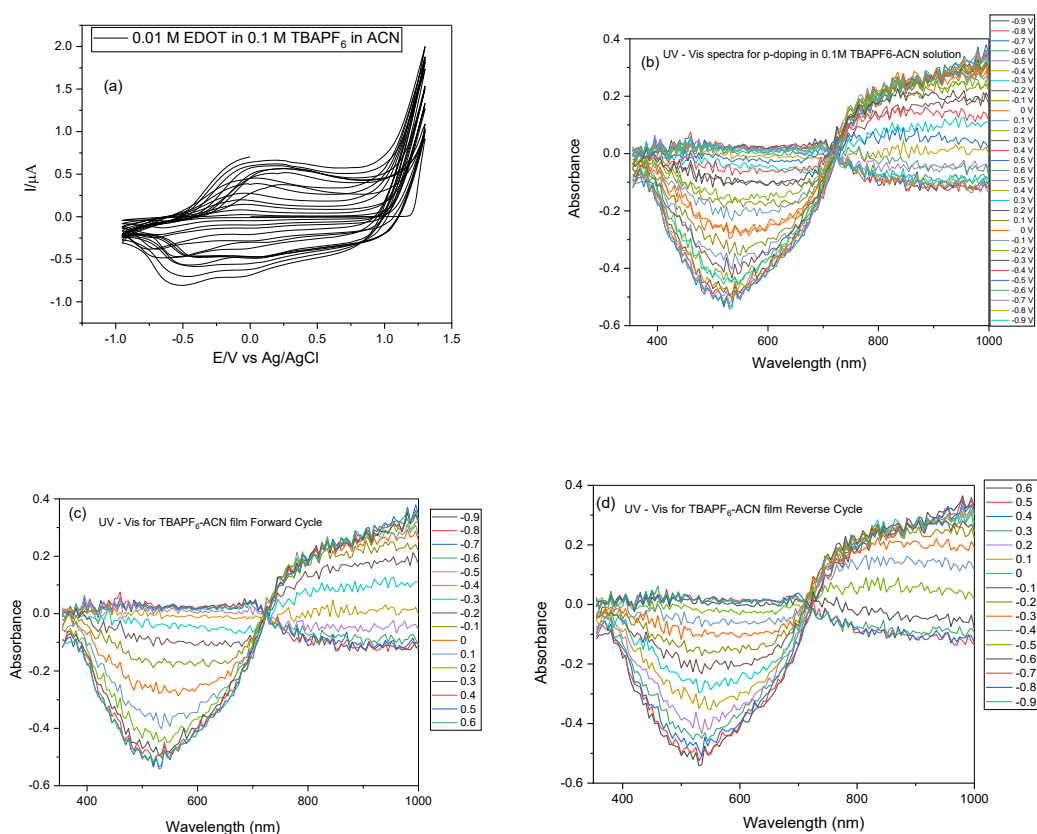


Figure 4.11 (a) CV for film growth of electrochemically polymerized PEDOT film on FTO in 0.1M TBAPF6-ACN solution and UV-VIS absorption spectra measurement of the film (b) spectra of complete cycle for p-doping (c) forward cycle (d) reverse cycle. . The cycling potential employed was between 0.6V and -0.9 V for 31 scans in monomer-free solution of 0.1M TBAPF6-ACN.

Contrary to the 0.1M KCl and 0.1M NaPSS UV-Vis spectra for the aqueous medium, the UV-Vis spectra for the 0.1M TBAPF6 in ACN representing organic medium electrolyte was fibrous in nature and it is evident from the electropolymerized PEDOT film produced on the FTO glass substrate.

The p-doping spectra for the 0.1M TBAPF6-ACN monomer free electrolyte showed negative absorbance present for both forward and reverse cycles. From the figures 4.11 (b) to (d), absorption for the spectral peaks were seen at 520nm wavelength which corresponds to the p-doping state of the polymer main chain. There is the formation of polarons and bipolarons for the during doping of the PEDOT film. Electrochromic properties for display applications of the PEDOT film in 0.1M TBAPF6-ACN monomer free electrolyte looked promising as spectra measurement across -0.9V to 0.6V potential range was applied [58][59][74].

4.5 Raman spectroscopy

The electrochemically polymerized film on the electrodes were studied by using in situ Raman spectroelectrochemistry. Applied potentials of -0.8V to 0.7V was employed for all the Raman measurements. Two different lasers were used to record the spectra and these are 532nm and 785nm with laser power of 1%. The time taken to record each Raman spectra was 20s. It is worth noticing that the tables 4.1 and 4.2 below show the various vibrational assignments associated with PEDOT main peaks and other bands in the Raman spectra were observed after electropolymerization and during electrochemical doping of the PEDOT film.

Wavenumber (cm ⁻¹)	Assignments
1563	PSS
1532	PEDOT C α = C β (intra-chain)
1425	PEDOT C α = C β (-O) (intra-chain)
1367	PEDOT C β - C β ' (inter-chain)
1256	PEDOT C α - C α ' (inter-ring)
1136	PEDOT C-O-C (intra-ring)
1093	PSS

989	PSS
701	PSS
577	PEDOT C-S-C (intra-ring)
522	PEDOT
437	PEDOT S-S (inter-ring)

Table 4.1 The main Raman peaks and their vibrational or functional group assignment for the PEDOT-PSS films [57].

Wavenumber (cm ⁻¹)	Assignments
1509	Asymmetric $\nu(\text{C}_\alpha = \text{C}_\beta)$
1432	Symmetric $\nu\text{C}_\alpha = \text{C}_\beta$ (-O)
1366	$\nu(\text{C}_\beta\text{-C}_\beta)$
1266	Inter-ring $\nu(\text{C}_\alpha\text{-C}_\alpha)$
1096	$\nu(\text{C-O-C})$
990, 573	Oxyethylene ring deformation
699	Symmetric $\nu(\text{C-S-C})$
439	$\delta(\text{SO}_2)$

Table 4.2 Observed frequencies of doped poly(3,4-ethylenedioxythiophene) with assignment of principal bands [53].

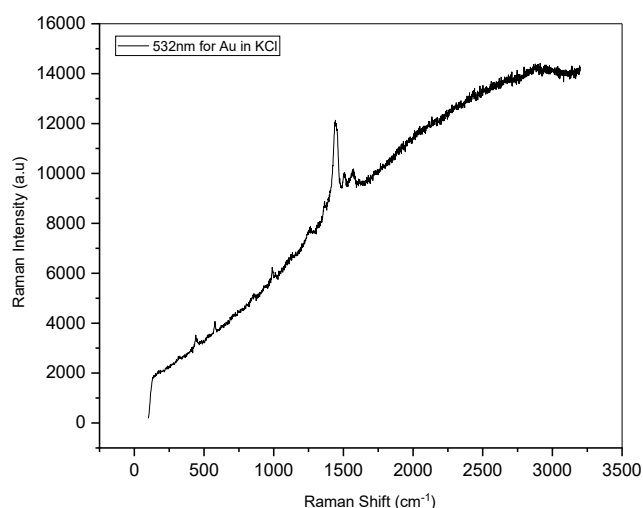


Figure 4.12 Raman spectra for PEDOT film on Au electrode in KCl solution using 532 nm excitation wavelength.

The figure above shows the Raman peaks of Au electrode in KCl electrolyte solution for 0.5V applied potential using 532nm laser at 1% laser power for 20s. The recorded spectra showed very weak peaks at high intensity. The most prominent peak was recorded at Raman shift 1460 cm^{-1} at the disorder induced mode (D mode) region is assigned to $C_{\alpha}=C_{\beta}$ intra-chain symmetric stretching of the PEDOT film with medium intensity. However, very small peaks were found to emerge at the RBM (radial breathing mode) region 450 cm^{-1} and 1000 cm^{-1} with very weak intensity which is ascribed to δSO_2 and Oxyethylene ring deformation respectively [37][52][53][74].

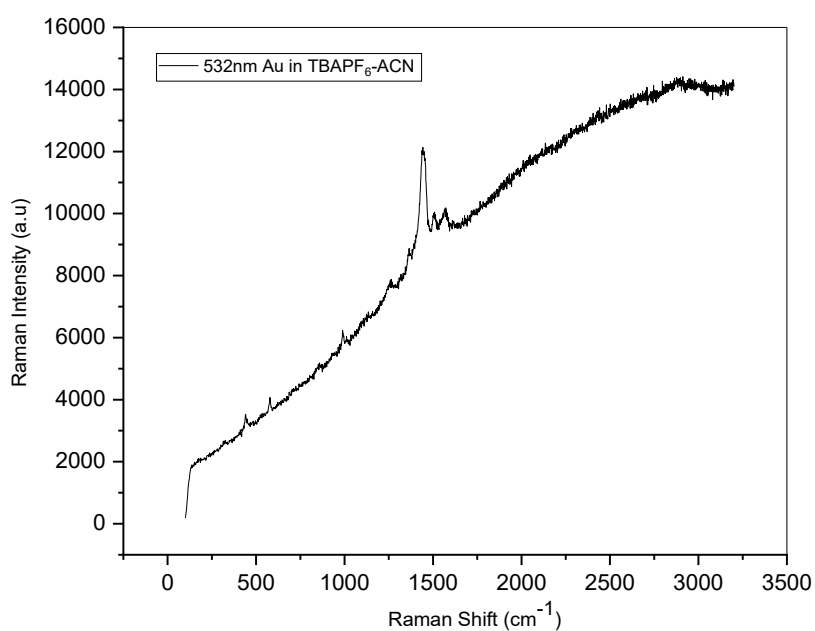


Figure 4.13 Raman spectra for PEDOT film on Au electrode in TBAPF6-ACN solution using 532 nm excitation wavelength.

The figure above shows the Raman peaks of Au electrode in TBAPF6-ACN electrolyte solution for 0.5V applied potential using 532nm laser at 1% laser power for 20s. The recorded spectra showed very weak peaks at high intensity. The most prominent peak was recorded at Raman shift 1460 cm^{-1} at the disorder induced mode (D mode) region is assigned to $C_{\alpha}=C_{\beta}$ intra-chain symmetric stretching of the PEDOT film with medium intensity. However, very small peaks were found to emerge at the RBM (radial breathing mode) region 450 cm^{-1} and 1000 cm^{-1} with very weak intensity which is ascribed to δSO_2 and Oxyethylene ring deformation respectively [52][53][74].

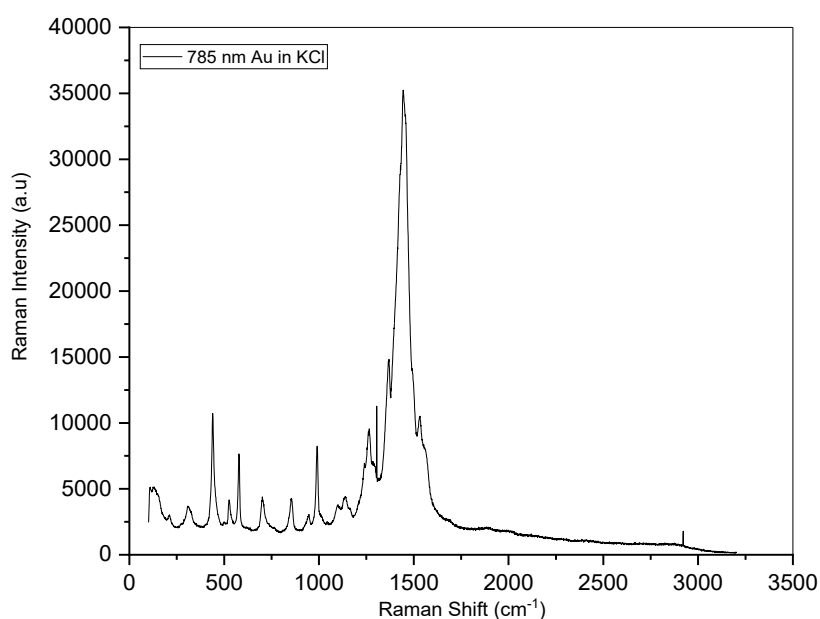


Figure 4.14 Raman spectra for PEDOT film on Au electrode in KCl solution using 785 nm excitation wavelength.

The above figure shows spectra of Au electrode in KCl electrolyte solution for 785nm excitation laser at 0.5V applied potential, 1% laser power and measuring time of 20s were employed. The most distinct peak for the spectra was measured at 1460cm^{-1} indicating the highest intensity for the disorder induced mode (D Mode) region was attributed to $C_{\alpha} = C_{\beta}$ intra-chain asymmetric stretching of the backbone PEDOT film. However, an auxiliary peak was also realized at 1250 cm^{-1} representing $C_{\alpha} - C_{\alpha}$ inter-ring PEDOT chain film. Several peaks were observed at 1100 cm^{-1} for C-O-C ring deformation, 1000 cm^{-1} for Oxyethylene ring deformation, 850 cm^{-1} for Oxyethylene ring deformation, 680 cm^{-1} for $C_{\alpha}\text{-S-}C_{\alpha}$ ring deformation, 520 cm^{-1} for Oxyethylene ring deformation, whereas 470 cm^{-1} , 356 cm^{-1} and 236 cm^{-1} denotes δSO_2 around the Radial Breathing Mode (RBM) and D mode region of the spectra. The peaks at this region showed insignificant intensities. It can be seen from the spectra that an emerging peak at Raman shift of 1560cm^{-1} representing the G Mode (high frequency two phonon) region where charge transfer related to intermediate doping is observed as well [50][52][53][74].

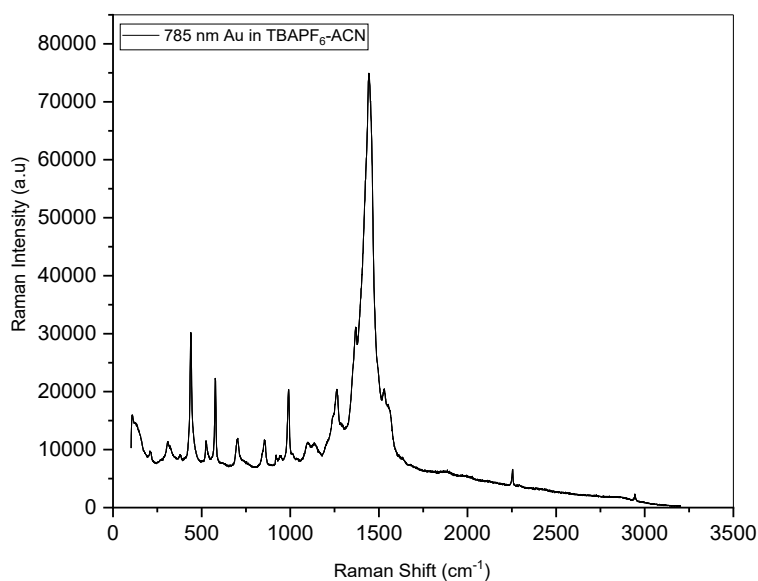


Figure 4.15 Raman spectra for PEDOT film on Au electrode in TBAPF6-ACN solution using 785 nm excitation wavelength.

The Raman spectra above was recorded for Au electrode in ACN electrolyte solution for excitation wavelength of 785nm at 0.5V applied potential. Similarly, 1% laser power was used and the measuring time for recording the spectra was 20s.

The most prominent peak can be noticed at Raman shift 1460cm^{-1} was assigned to D Mode region for the PEDOT film belonging to $C_{\alpha}=C_{\beta}$ intra-chain asymmetric stretching functional group. The emerging peak closer to the main peak at Raman shift 1250cm^{-1} can be attributed to $C_{\alpha}-C_{\alpha}$ inter-ring PEDOT chain film. In like manner, the RBM region of the spectra was realised cluster of peaks which was assigned to $\delta(\text{C-C})$ aliphatic chains and $\nu(\text{C-Cl})$ functional groups. The peaks gave similar Raman shift as the Au in KCl in the above with the peak positions being found at 1100cm^{-1} for C-O-C ring deformation, 1000cm^{-1} for Oxyethylene ring deformation, 850cm^{-1} for Oxyethylene ring deformation, 680cm^{-1} for $C_{\alpha}\text{-S-C}_{\alpha}$ ring deformation, 520cm^{-1} for Oxyethylene ring deformation, 470cm^{-1} , 356cm^{-1} and 236cm^{-1} for δSO_2 . However, there were massive increase in intensities of the peaks (peak height) that is about twice as much as the intensities of that of Au in KCl spectra. An evolving peak at 1560cm^{-1} for the G Mode (high frequency two phonon) region like previously, explains the charge transfer activities related to intermediate doping of the PEDOT film [44][52][54][69][74].

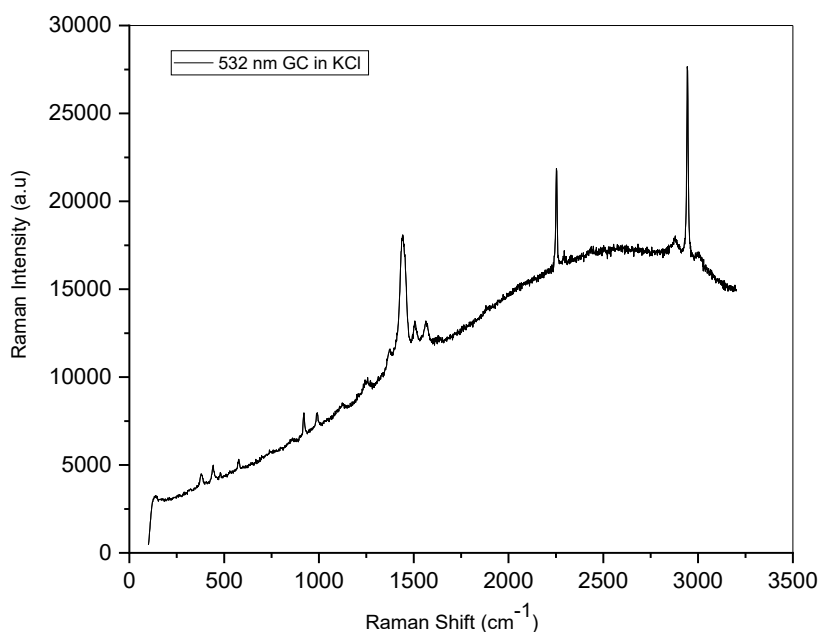


Figure 4.16 Raman spectra for PEDOT film on GC electrode in KCl solution using 532 nm excitation wavelength.

The spectra above was recorded for GC electrode in KCl electrolyte using 532nm excitation wavelength, and laser power of 1%, at 0.5V applied potential at 20s recording time.

The most significant peak occurred at 1460cm^{-1} at the D mode being assigned to Symmetric $\nu_{C\alpha} = C\beta$ (-O) stretching of the main PEDOT backbone chain with two emerging peaks at the shoulder of the main peak at Raman shift of 1520 cm^{-1} and 1560 cm^{-1} which are doping induced and intermediate doping respectively gives an indication of changes in the polymer chain film during doping. Two prominent bands are seen at 2200cm^{-1} and 2910cm^{-1} beyond the G mode region (2D mode) representing C=C asymmetrical stretching of the PEDOT chain. The bands found at 1300 cm^{-1} is ascribed C-C vibrational group, 1050 cm^{-1} represents C-O-C stretching of PEDOT film, 980 cm^{-1} could be assigned to C-S-C deformation, 560 cm^{-1} are assigned to Oxyethylene ring deformation, 420 cm^{-1} , 380 cm^{-1} extending from the D mode region to the RBM region representing $\delta(\text{S-S})$ inter-ring PEDOT [52][53][57][74].

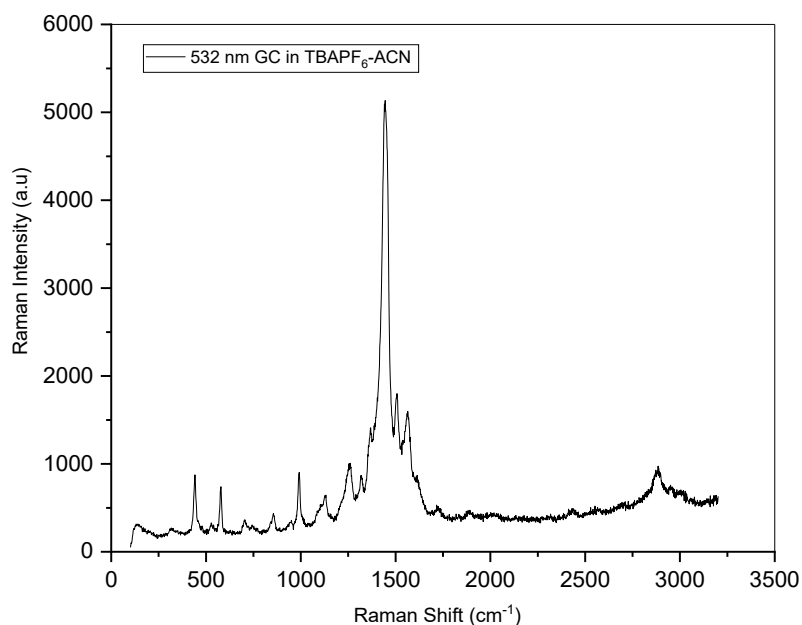


Figure 4.17 Raman spectra for PEDOT film on GC electrode in TBAPF6-ACN solution using 532 nm excitation wavelength.

The figure above shows the spectra recorded for PEDOT film on GC electrode in 0.1M TBAPF6 (ACN) electrolyte solutions at 532 nm laser excitation wavelength, 0.5V potential, 20s measuring time and 1% laser power. The conspicuous peak for the spectra was observed at 1460 cm^{-1} was attributed to asymmetric C-C stretching. The main peak was accompanied by two shoulder peaks at 1405 cm^{-1} and 1520 cm^{-1} represent C=C symmetrical and asymmetrical vibrations respectively. A broader and emerging peak was noticed at 2875 cm^{-1} which indicated $\nu(\text{C-H})$ i.e. CH_2 stretching vibrations. Several doping induced bands were recognized at 1260 cm^{-1} for Inter-ring $\nu(\text{C}\alpha\text{-C}\alpha)$, 1140 cm^{-1} for ethylenedioxy group deformation, 992 cm^{-1} for Oxyethylene ring bending, 792 cm^{-1} , 680 cm^{-1} , 520 cm^{-1} representing Oxyethylene ring deformation and 470 cm^{-1} assigned to $\delta(\text{S-S})$ inter-ring PEDOT vibrations. The Raman intensities observed were low for all the peaks in the spectra [52][53][57][74].

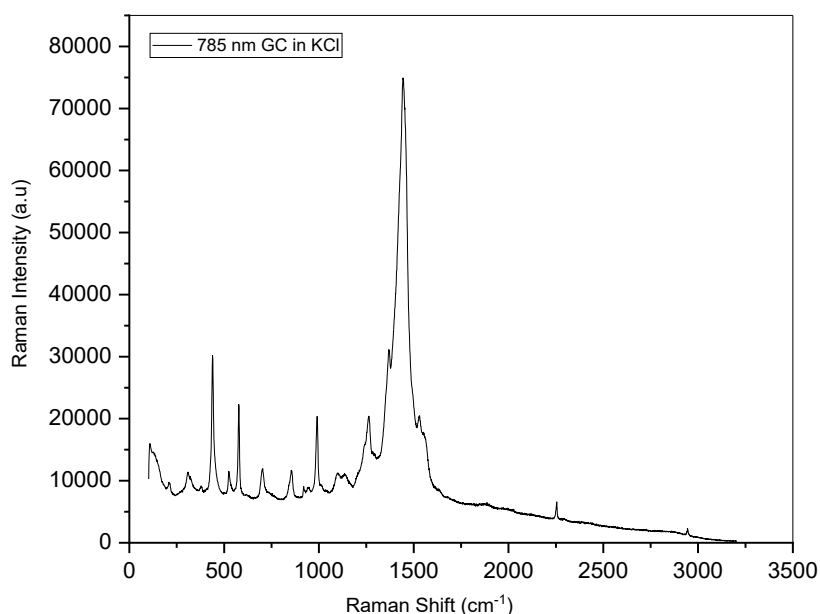


Figure 4.18 Raman spectra for PEDOT film on GC electrode in KCl solution using 785 nm excitation wavelength.

The Raman spectrum above shows electropolymerized PEDOT film on GC electrode in 0.1 M KCl solvent using 785 nm excitation laser for 0.5 V applied potential.

The main peak located at Raman shift 1460 cm^{-1} gives an indication of C-C stretching of the main PEDOT chain. Other peaks observed at 1250 cm^{-1} for 1260 cm^{-1} for Inter-ring $\nu(\text{C}\alpha\text{-C}\alpha)$, 1100 cm^{-1} for C-O-C ring deformation, 1000 cm^{-1} for C-O-C stretching, 875 cm^{-1} for Oxyethylene ring deformation, 705 cm^{-1} for C-S-C deformation, 548 cm^{-1} and 510 cm^{-1} for Oxyethylene ring deformation, 487 cm^{-1} and 360 cm^{-1} for PEDOT $\delta(\text{S-S})$ inter-ring vibrations. An emerging peak was observed at 1520 cm^{-1} which was attributed to Asymmetric $\text{C}\alpha=\text{C}\beta$ stretching of the PEDOT accordingly. However, much higher intensities were portrayed by the various peaks in the spectrum in comparison to other spectra [53][57][69][74].

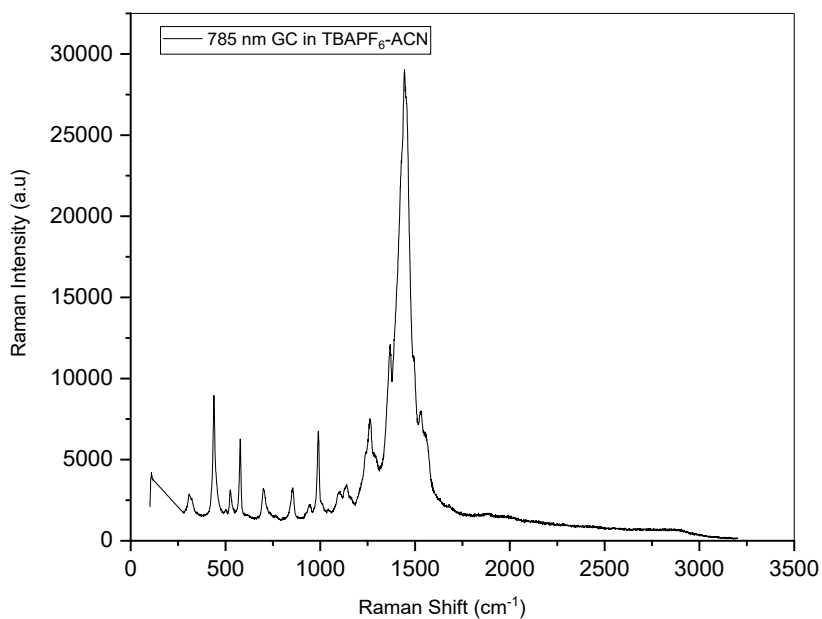


Figure 4.19 Raman spectra for PEDOT film on GC electrode in TBAPF6-ACN solution using 785 nm excitation wavelength.

The above spectra represent PEDOT film on GC electrode in 0.1M TBAPF6 (ACN) for 785 nm laser excitation wavelength, 1% laser power and 0.5V applied potential for 20s measuring time. The most noticeable peaks like the previous spectra was found at 1460 cm^{-1} assigned to asymmetric C-C stretching. A shoulder band at 1515 cm^{-1} was attributed Asymmetric $C\alpha=C\beta$ stretching vibrations beyond which no peak is found. Numerous bands at 1250 cm^{-1} for PEDOT $C\alpha - C\alpha$ inter-ring stretching, 1125 cm^{-1} for PEDOT C-O-C intra-ring deformation, 997 cm^{-1} , 820 cm^{-1} , 512 cm^{-1} , 500 cm^{-1} was ascribed to oxyethylene ring deformation, 685 cm^{-1} attributed to symmetric $\nu(\text{C-S-C})$, 486 cm^{-1} and 310 cm^{-1} could be connected to PEDOT $\delta(\text{S-S})$ inter-ring vibrational group [52][53][57][74].

4.5.1 In situ Raman Spectroscopy

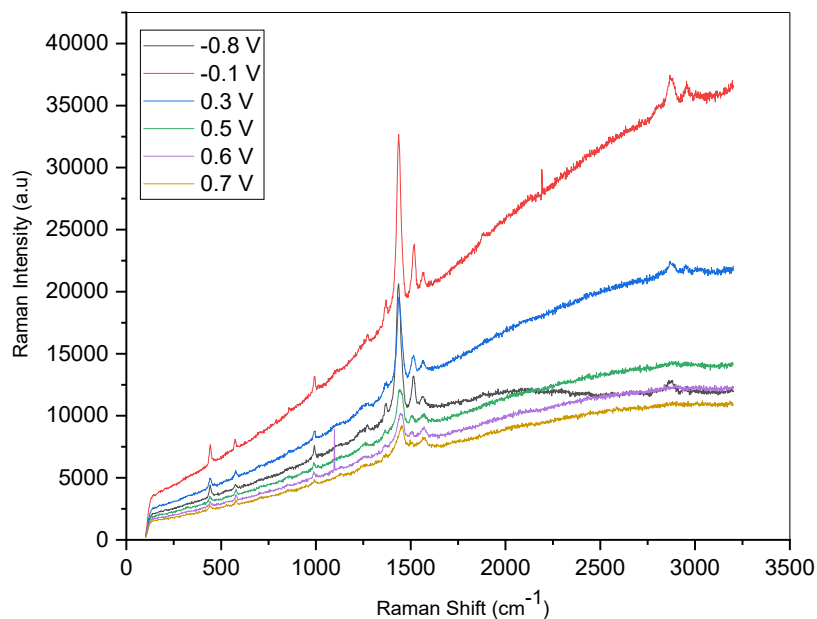


Figure 4.20 In situ Raman spectra recorded for electrochemically polymerized PEDOT film on Au electrode in 0.1M KCl solution using 532 nm excitation wavelength at -0.8 V to 0.7 V scanning potential for p- and n-doping.

The figure above shows Raman spectra recorded for PEDOT film on Au electrodes in 0.1 M KCl with a scanning potential range of -0.8 V to 0.7 V using excitation laser with wavelength of 532 nm. The main peak for the spectra was observed at 1460 cm^{-1} corresponding to Symmetric $C\alpha = C\beta$ ($-O$) stretching vibration of the PEDOT main chain for all the scanning potentials with shoulder peaks seen at 1410 cm^{-1} and 1520 cm^{-1} which can be assigned to symmetrical and asymmetrical $C\alpha=C\beta$ stretching vibrations respectively. There is slight shift of the main peaks together with the shoulder peaks and other peaks for all the scanning potentials and spectra upshift could also be observed which might results from higher laser power used. Bands found at 2850 cm^{-1} and 2910 cm^{-1} were assigned to $\nu(C-H)$ vibrations for both n-doping and p-doping and these bands looked more prominent for the negative scanning potentials than the positive potentials. Higher and much stronger intensities were observed for the n-doping spectrum compared to the p-doping [53][57][68][74].

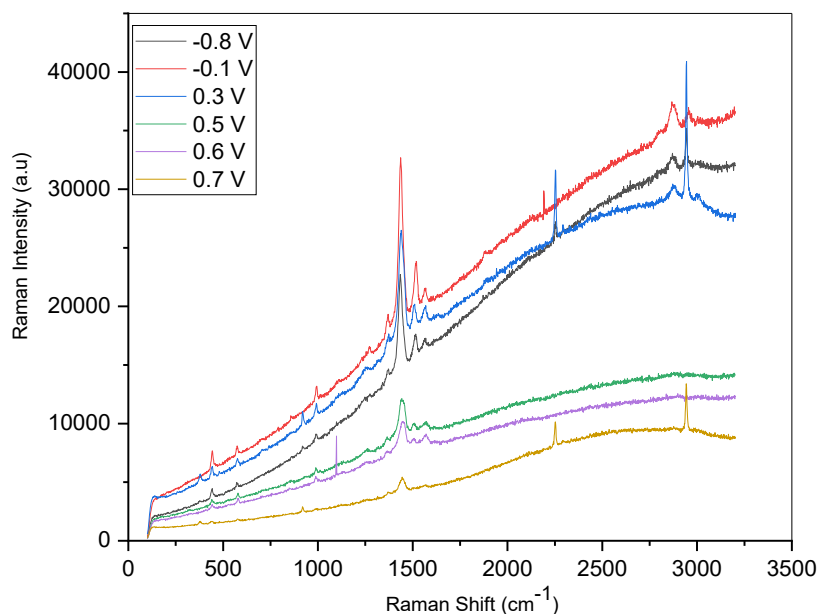


Figure 4.21 In situ Raman spectra recorded for electrochemically polymerized PEDOT film on Au electrode in 0.1M TBAPF6-ACN solution using 532 nm excitation wavelength at -0.8 V to 0.7 V scanning potential for p- and n-doping.

The above figure represents Raman Spectra recorded for PEDOT film polymerized on Au electrode in 0.1 M TBAPF6-ACN electrolyte with scanning potential ranging from -0.8 V to 0.7 V using 532 nm excitation wavelength laser. The most significant peaks for the spectra were observed at 1460 cm^{-1} and attributed to $C\alpha=C\beta$ symmetric stretch of intra-chain vibration of the PEDOT film backbone for all scanning potentials. It also showed shoulder peaks at 1410 cm^{-1} and 1520 cm^{-1} was accounted for as $C\alpha=C\beta$ symmetrical and asymmetrical vibrational groups which also denotes induced and intermediate doping respectively. Bands found at 2250 cm^{-1} and 2270 cm^{-1} were assigned to $\nu(C\equiv C)$ vibrational group for -0.8 V, 0.3 V and 0.7 V potentials and other bands could be seen further beyond these bands at 2820 cm^{-1} , 2850 cm^{-1} and 2910 cm^{-1} accredited to strong Raman intensity of $\nu(C-H)$ functional group. Several fading bands were seen at the RBM region which are representation of Oxyethylene ring deformation, $C\alpha-S-C\alpha$ ring deformation and C-O-C ring deformation for the polymerized PEDOT film. As stated earlier on, stronger and much higher intensities were observed for n-doping as compared to the p-doping that is doping increases with negative potentials [52][54][59][71][74].

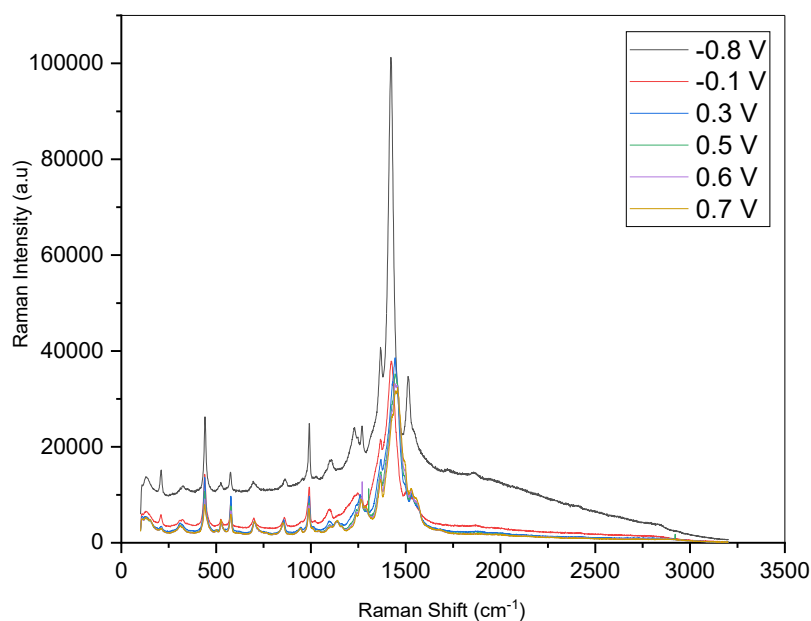


Figure 4.22 In situ Raman spectra recorded for electrochemically polymerized PEDOT film on Au electrode in 0.1M KCl solution using 785 nm excitation wavelength at -0.8 V to 0.7 V scanning potential for p- and n-doping.

The above figure is recorded Raman spectra for 785 nm excitation laser of PEDOT film on Au electrode in KCl solvent for scanning potential range of -0.8 V to 0.7 V.

The obvious peaks were found at 1460 cm^{-1} assigned to $C\alpha=C\beta$ symmetric stretch of intra-chain PEDOT chain vibrations for all scanning potentials. A small shift was realized for the peaks and particularly more pronounced for the main peaks at 1460 cm^{-1} for the PEDOT film which is an indicating of doping of the PEDOT film. The Raman spectra for the PEDOT film also exhibited several weaker bands at 1360 cm^{-1} and 1320 cm^{-1} for $\nu(C\beta-C\beta)$, 1100 cm^{-1} for C-O-C ring deformation, 1000 cm^{-1} for $\nu(C-O-C)$, 820 cm^{-1} , 710 cm^{-1} and 560 cm^{-1} for Oxyethylene ring deformation, 460 cm^{-1} and 320 cm^{-1} which is representation of $\delta(\text{SO})_2$. The spectra showed much higher intensity for the spectrum with -0.8 V scanning potential and no bands were noticed beyond the G (high frequency two phonon mode) [52][53][74]. The shoulder peaks observed at 1360 cm^{-1} and 1510 cm^{-1} were accredited to inter-chain PEDOT $C\beta-C\beta$ stretching and Asymmetric $\nu(C\alpha = C\beta)$ respectively. Furthermore, these bands are representation of induced and intermediate doping respectively [50][52][57][59].

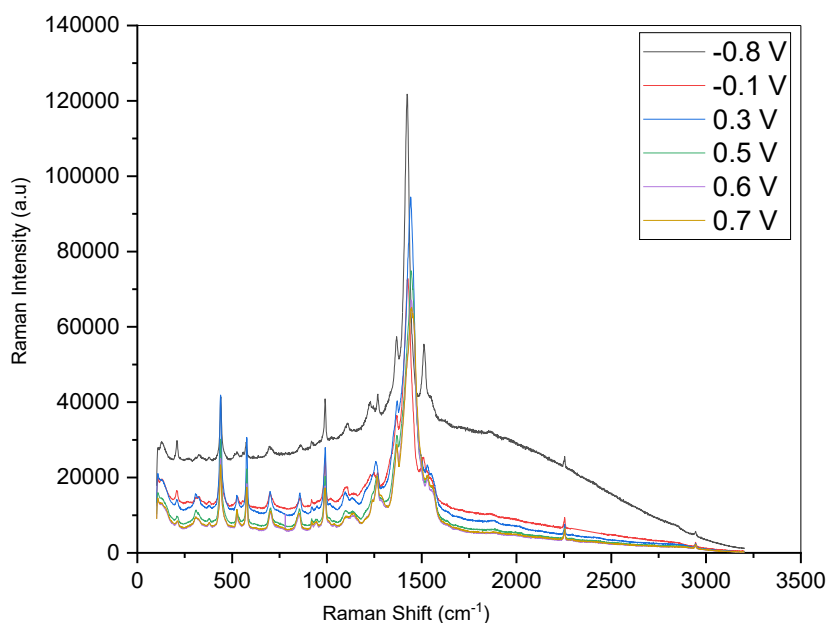


Figure 4.23 In situ Raman spectra recorded for electrochemically polymerized PEDOT film on Au electrode in 0.1M TBAPF6-ACN solution using 785 nm excitation wavelength at -0.8 V to 0.7 V scanning potential for p- and n-doping.

The figure above represents recorded Raman spectra of electrochemically polymerized PEDOT on Au electrode in 0.1M TBAPF6-ACN solvent using 785 nm excitation laser for an applied scanning potential range of -0.8 V to 0.7 V.

The principal bands for these spectra was noticed at 1460 cm^{-1} like the previous spectra was ascribed to intra-chain $C\alpha=C\beta$ symmetric stretch of PEDOT chain vibrations for all scanning potentials. A slight shift in bands for the applied potentials was seen for the main peaks of the spectra and it also exhibited more pronounce shoulder peaks besides the principal at 1364 cm^{-1} and 1526 cm^{-1} which were recognized as $\nu(C\beta-C\beta)$ and asymmetric $\nu(C\alpha = C\beta)$ respectively. The numerous bands realized at 1250 cm^{-1} for Inter-ring $\nu(C\alpha-C\alpha)$, 1115 cm^{-1} for C-O-C ring deformation, 1000 cm^{-1} for $\nu(C-O-C)$, 840 cm^{-1} for oxyethylene ring deformation, 680 cm^{-1} for symmetric $\nu(C-S-C)$, 540 cm^{-1} are associated to oxyethylene ring deformation, 470 cm^{-1} and 324 cm^{-1} for $\delta(SO_2)$. However, no bands were observed beyond the G mode region and more intense peaks are shown in the spectra. Doping of the spectra is characterized by shift in bands and broadening of the peaks [52][53][66][74].

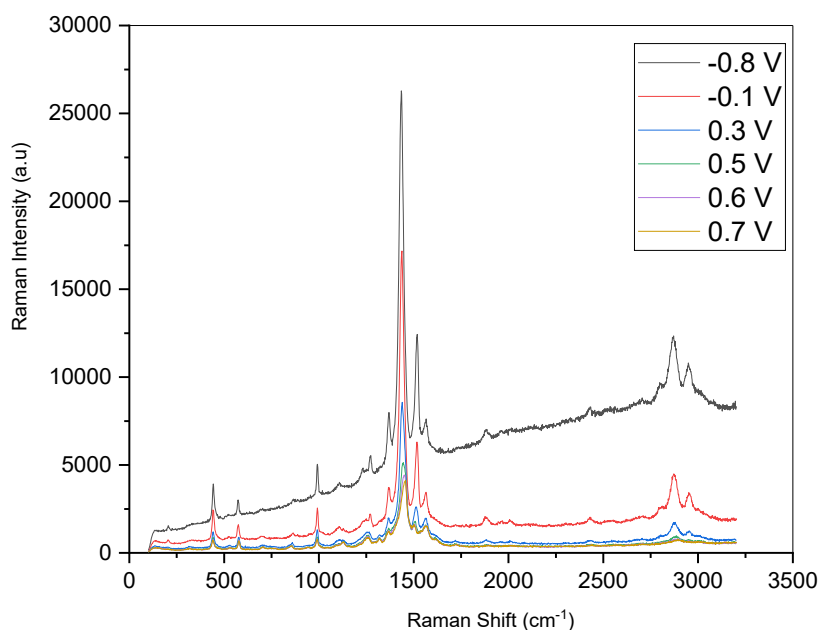


Figure 4.24 In situ Raman spectra recorded for electrochemically polymerized PEDOT film on GC electrode in 0.1M KCl solution using 532 nm excitation wavelength at -0.8 V to 0.7 V scanning potential for p- and n-doping.

The Raman spectra shown in figure above is resulted from electrochemically polymerized PEDOT on GC electrode in KCl solvent using 532 nm excitation laser and applied potential range -0.8 V to 0.7 V.

The major bands for the spectra at 1460 cm^{-1} were assigned to symmetric $\nu\text{C}\alpha = \text{C}\beta$ ($-\text{O}$) stretching of intra-chain PEDOT chain vibrational mode. Two strong shoulder bands found at 1360 cm^{-1} and 1505 cm^{-1} are ascribed to $\text{C}\beta - \text{C}\beta'$ (inter-chain) stretching of PEDOT and asymmetric $\nu(\text{C}\alpha = \text{C}\beta)$ respectively. Raman bands found at 1250 cm^{-1} for $\text{C}\alpha - \text{C}\alpha'$ inter-ring stretching of PEDOT, 1125 cm^{-1} for C-O-C intra-ring deformation of PEDOT, 1000 cm^{-1} for $\nu(\text{C-O-C})$, 696 cm^{-1} for symmetric $\nu(\text{C-S-C})$ and 480 cm^{-1} for $\delta(\text{SO}_2)$ [52][53][74]. However, the medium and strong intensity Raman bands witnessed at 2850 cm^{-1} and 2910 cm^{-1} might possibly be aligned to symmetric and asymmetric stretching of CH_2 respectively. The spectra also showed that the bands in the negative potentials (n-doping) are more explicit as compared to its corresponding positive potential (p-doping) [50][54][59].

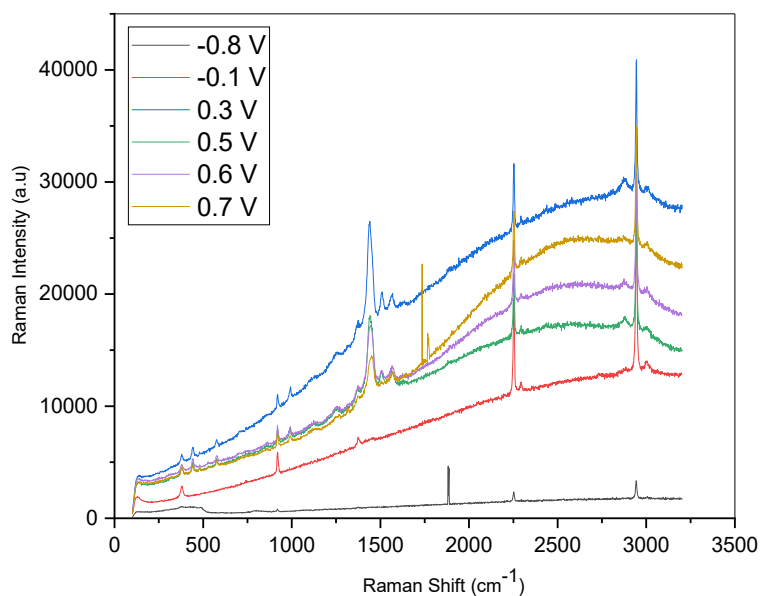


Figure 4.25 In situ Raman spectra recorded for electrochemically polymerized PEDOT film on GC electrode in 0.1M TBAPF6-ACN solution using 532 nm excitation wavelength at -0.8 V to 0.7 V scanning potential for p- and n-doping.

The Raman spectra shown in figure above represents PEDOT film electrochemically polymerized on GC electrode in 0.1 M TBAPF6-ACN in the potential range -0.8 V to 0.7 V for 532 nm excitation laser.

It can be noticed that the main PEDOT peaks found at 1460 cm^{-1} are assigned to intra-chain symmetric $\nu\text{C}\alpha = \text{C}\beta(-\text{O})$ stretching vibrational mode of the PEDOT polymer chain. However, the shoulder peaks which are observed at 1509 cm^{-1} asymmetric $\nu(\text{C}\alpha = \text{C}\beta)$ akin to the main peaks are not precise and seems to be disappearing at more negative potentials gives an indication that charge transfers related to the doping and intermediate doping of the PEDOT film are not effective. The bands found at 2250 cm^{-1} and 2910 cm^{-1} are assigned to $\nu(\text{C}\equiv\text{C})$ and asymmetric stretching of $\nu(\text{C}-\text{H})$ respectively. The bands found noticed at 1250 cm^{-1} , 1000 cm^{-1} , 950 cm^{-1} and 420 cm^{-1} which are ascribed to $\text{C}\alpha - \text{C}\alpha$ inter-ring stretching of PEDOT, $\nu(\text{C}-\text{O}-\text{C})$, Oxyethylene ring deformation and $\delta(\text{SO}_2)$ respectively [52][53][74].

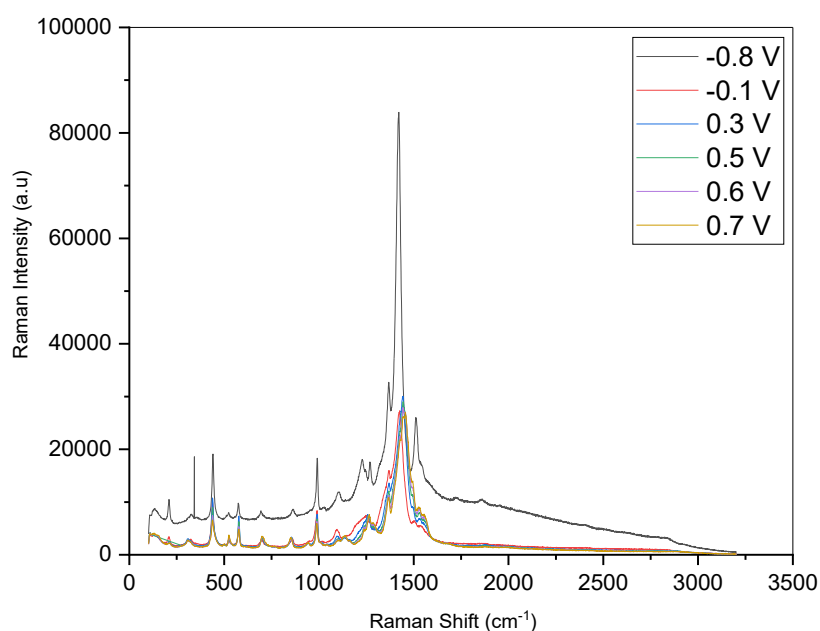


Figure 4.26 In situ Raman spectra recorded for electrochemically polymerized PEDOT film on GC electrode in 0.1M KCl solution using 785 nm excitation wavelength at -0.8 V to 0.7 V scanning potential for p- and n-doping.

The above figure is recorded spectra of electropolymerized PEDOT film on GC electrode in 0.1 M KCl solvent using 785 nm excitation laser for -0.8 V to 0.7 V potential range. The most significant Raman bands for these spectra were observed at 1460 cm^{-1} ascribed to symmetric $\nu\text{C}\alpha = \text{C}\beta$ ($-\text{O}$) stretching for intra-chain vibration mode of the PEDOT polymer chain film with an indication of slight shift in the bands of -0.8 V spectrum from other spectra. The shoulder peaks associated with the main peaks were noticed at 1250 cm^{-1} and 1505 cm^{-1} accredited to inter-ring $\text{C}\alpha - \text{C}\alpha$ PEDOT and intra-chain PEDOT $\text{C}\alpha = \text{C}\beta$. The various bands found at 1115 cm^{-1} for C-O-C ring deformation, 995 cm^{-1} oxyethylene ring deformation, 820 cm^{-1} for oxyethylene ring deformation, 700 cm^{-1} for symmetric $\nu(\text{C-S-C})$, 587 cm^{-1} for oxyethylene ring deformation, 460 cm^{-1} and 320 cm^{-1} for δSO_2 [52][53][74].

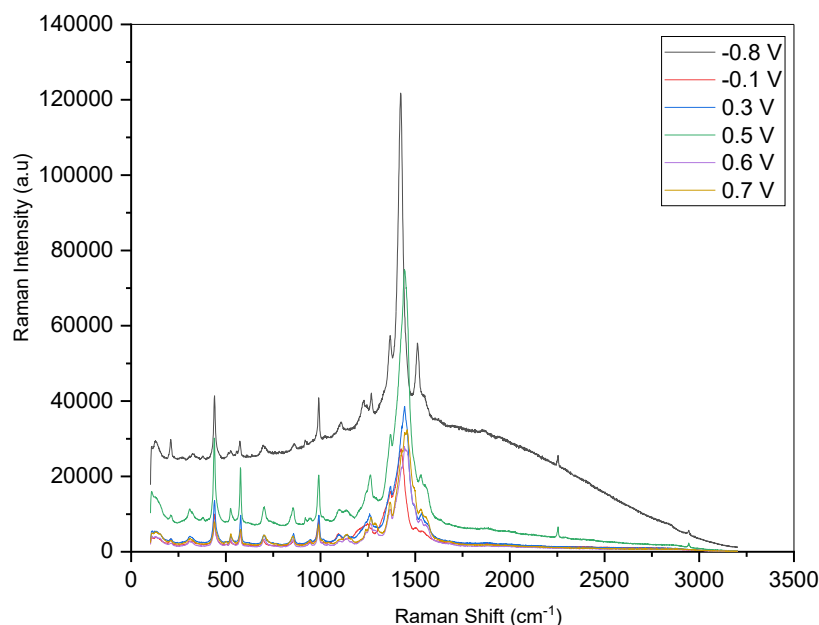


Figure 4.27 In situ Raman spectra recorded for electrochemically polymerized PEDOT film on GC electrode in 0.1M TBAPF6-ACN solution using 785 nm excitation wavelength at -0.8 V to 0.7 V scanning potential for p- and n-doping.

The above Raman spectra denotes electrochemically polymerized PEDOT film on GC electrode in 0.1 M TBAPF6-ACN solvent using 785 nm laser for -0.8 V to 0.7 V potential range. The most distinct peaks for the spectra are located at 1460 cm^{-1} symbolizing an intra-chain symmetric $\nu C\alpha = C\beta$ ($-O$) stretching of the PEDOT backbone polymer chain rings. The main peaks were seen to be shouldered at either side with other peaks at 1410 cm^{-1} and 1512 cm^{-1} corresponding to symmetric $C\alpha=C\beta$ stretching PEDOT film and symmetrical $C=C$ of PEDOT respectively. The various bands recognized at 1250 cm^{-1} for inter-ring $C\alpha - C\alpha$, 1125 cm^{-1} for $C-O-C$ intra-ring PEDOT, 1000 cm^{-1} for Oxyethylene ring deformation, 868 cm^{-1} for oxyethylene ring deformation, 745 cm^{-1} for $C-S-C$ deformation, 573 cm^{-1} for oxyethylene ring deformation, 520 cm^{-1} for oxyethylene ring deformation, 478 cm^{-1} and 340 cm^{-1} for δSO_2 . A slight shift was realized for -0.8 V and 0.5 V potentials which are very obvious looking at the main peaks [52][53][74].

4.5.2 Comparison of various in situ Raman spectra

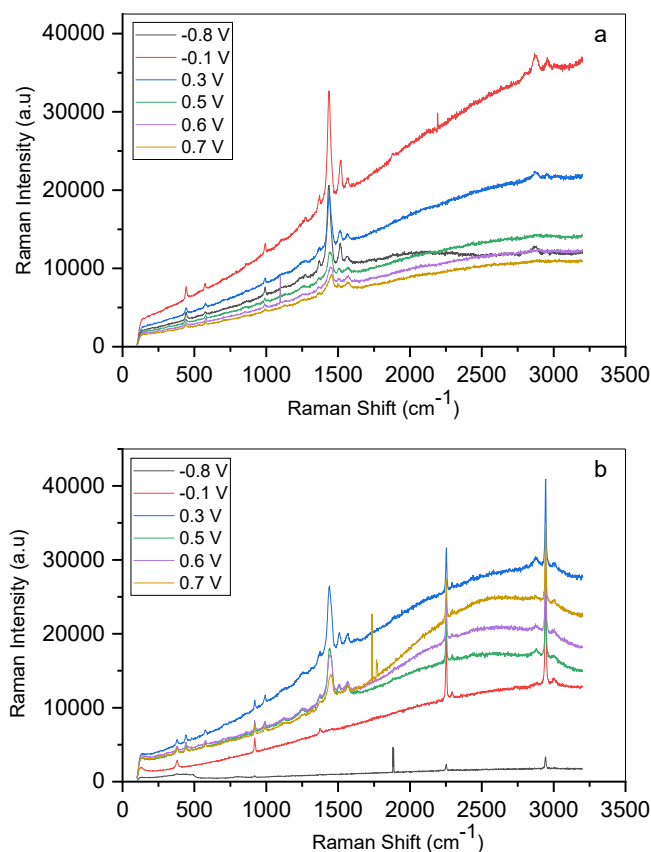


Figure 4.28 Comparison of in situ Raman spectra of PEDOT film polymerized on (a) Au electrode and (b) GC electrode both in 0.1 M KCl using 532 nm excitation wavelength ($\lambda_L=532$ nm).

The figure above shows the spectra of electrochemically polymerized PEDOT on Au electrode versus GC electrode in KCl solvent using 532 nm excitation wavelength. This shows how PEDOT film behaves when polymerized on different electrodes using the same solvent. The main peaks at 1460 cm^{-1} for GC electrode in KCl solvent at -0.8 V and -0.1 V seems to have disappeared compared to the Au electrode in KCl. The GC electrode in KCl also showed other sharp and strong intense bands beyond the main peaks even though -0.8 V spectrum showed no peaks compared to the Au electrode in KCl spectra which showed weak intense broader bands at 2910 cm^{-1} for -0.8 V, -0.1 V and 0.3V spectra. The difference in spectra comes as a result of different electrodes used even though the same electrolytic solvent was employed [28][51][55][69][76].

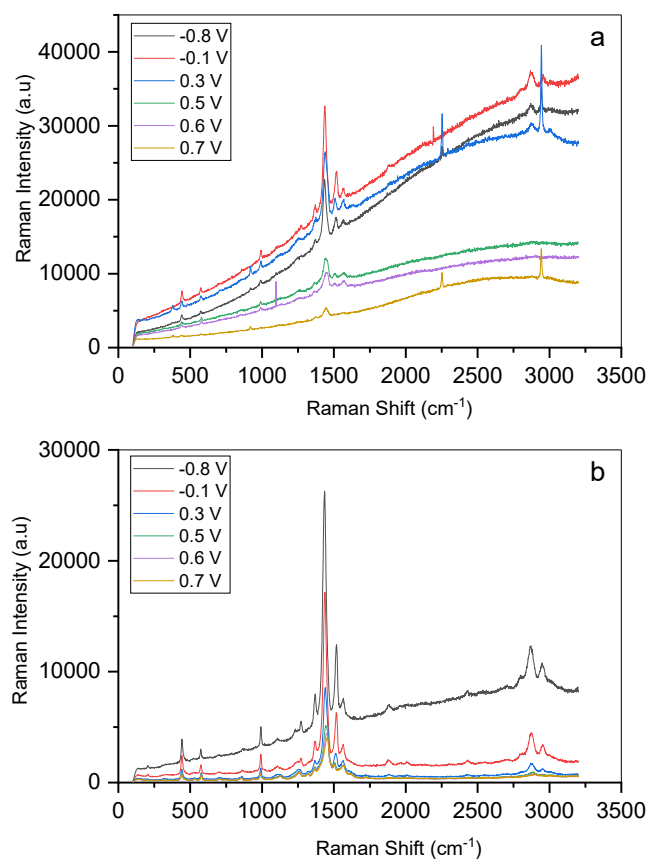


Figure 4.29 Comparison of PEDOT film on (a) Au electrode in 0.1 M TBAPF6-ACN and (b) GC electrode in 0.1 M KCl both in using 532 nm excitation wavelength ($\lambda_L=532$ nm).

The figure above shows the comparison of electrochemically polymerized PEDOT film on Au electrode in 0.1 M TBAPF6-ACN and GC electrode in 0.1 M KCl using 532 nm excitation wavelength. The latter spectra of GC electrode in 0.1 M KCl showed more intense and sharp peaks in comparison to Au electrode in TBAPF6-ACN except for the peaks found at 2850 cm^{-1} and 2910 cm^{-1} which are broad. It is obvious that the n-doping potentials were more intense than the corresponding p-doping for both spectra. It is also worth mentioning that the above spectra employed different electrode (Au & GC) but same electrolyte solvent [33][42][50][51].

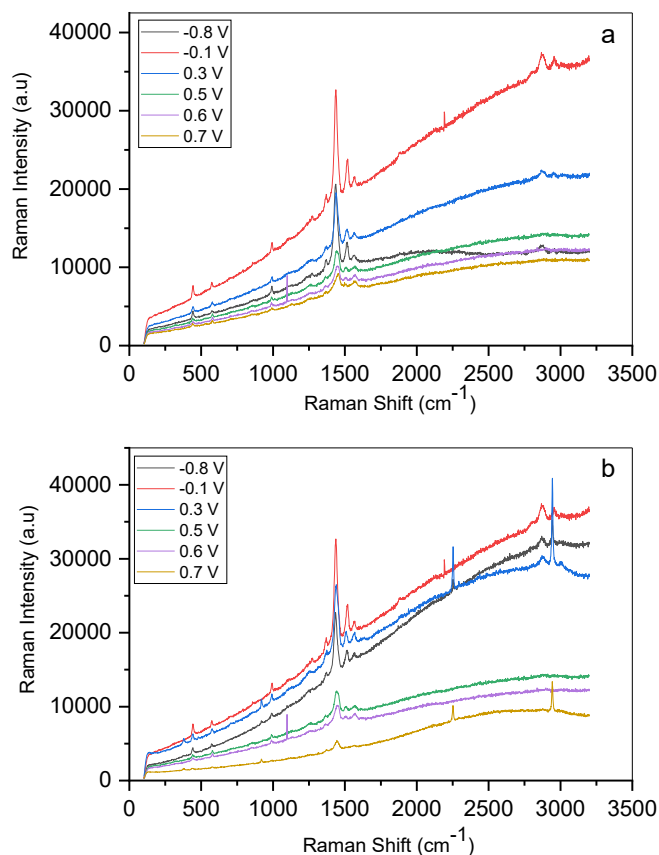


Figure 4.30 Comparison of PEDOT film on Au electrode in both (a) 0.1 M KCl and (b) 0.1 M TBAPF6-ACN solvents using 532 nm excitation wavelength ($\lambda_L=532$ nm).

The above figures are the representation of PEDOT film on Au electrode in both KCl and TBAPF6-ACN electrolyte solvents for 532 nm excitation wavelength. The two spectra look similar in nature but there are more bands for Au electrode in TBAPF6-ACN spectra. However, the bands found in Au electrode TBAPF6-ACN spectra are not distinct compared to Au electrode in KCl spectra. It was also noticed that the p-doping potentials showed more weaker bands especially Au electrode in TBAPF6-ACN spectra in contrast to corresponding n-doping potentials [39][42][50][51].

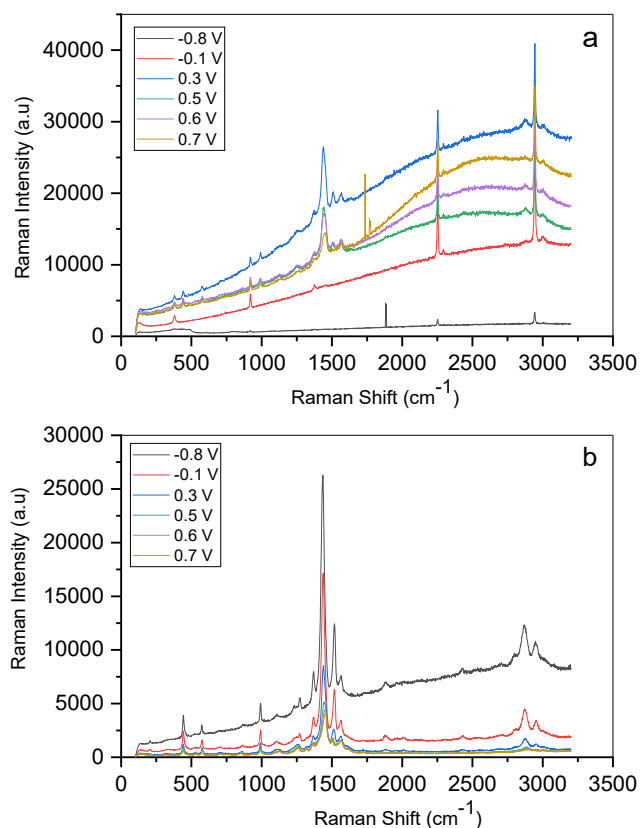


Figure 4.31 Comparison of PEDOT film on GC electrode in both (a) KCl and (b) TBAPF6-ACN solvents using 532 nm excitation wavelength ($\lambda_L=532$ nm).

The above spectra are representation of PEDOT film polymerized on GC electrode in KCl against GC electrode in TBAPF6-ACN using 532 nm excitation wavelength that is the same electrode used but different solvents. The latter portrayed much stronger peaks for the main PEDOT chain compared to preceding spectra which has rather weak peaks for the main PEDOT chain. Unlike the second spectra where the main peaks for the -0.8 V and -0.1 V potentials are more profound, the first spectra showed no peaks for the main PEDOT chain. However, the peaks related to doping are more prominent with higher intensities for GC electrode in KCl in contrast to GC electrode in TBAPF6-ACN spectra [39][42][50][51].

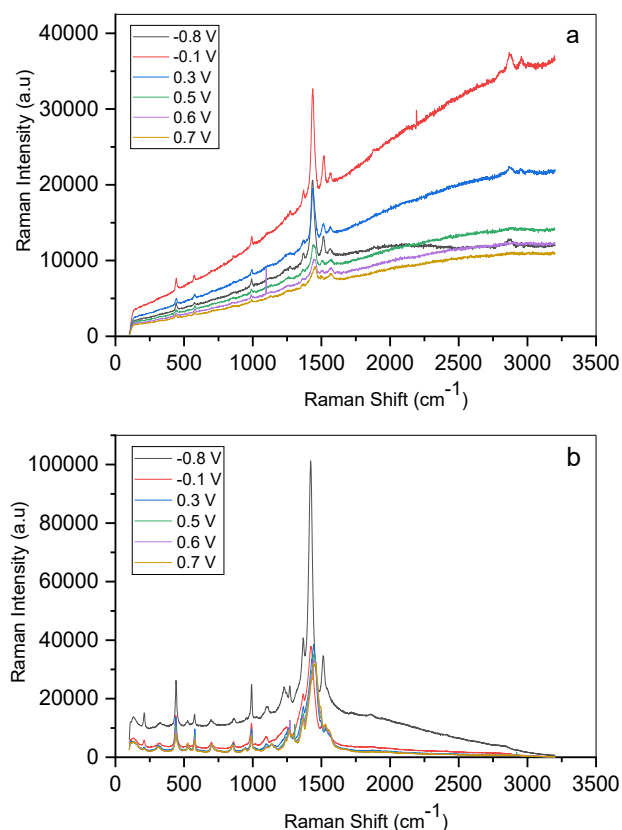


Figure 4.32 Comparison of the Raman spectra of PEDOT films using (a) 532 nm on Au electrode and (b) 785 nm Au electrode both in 0.1 M KCl solvent.

The figure above denotes two spectra of an electropolymerized PEDOT film on Au electrode in KCl for both 532 nm and 785 nm excitation wavelength. The Major peaks for the second spectra ($\lambda = 785$ nm) have much higher intensity compared to the first spectra ($\lambda = 532$ nm) which gave much lower intensities. The G mode region of the $\lambda = 785$ nm spectra showed no peaks in contrast to the $\lambda = 532$ nm spectra which showed some peaks for at 2850 cm^{-1} and 2910 cm^{-1} for -0.8 V , -0.1 v and 0.3 v potentials. Another noticeable thing is that the peaks found in $\lambda = 785$ nm spectra were more profound than the peaks in $\lambda = 532$ nm spectra which were observed to be disappearing [39][40][51].

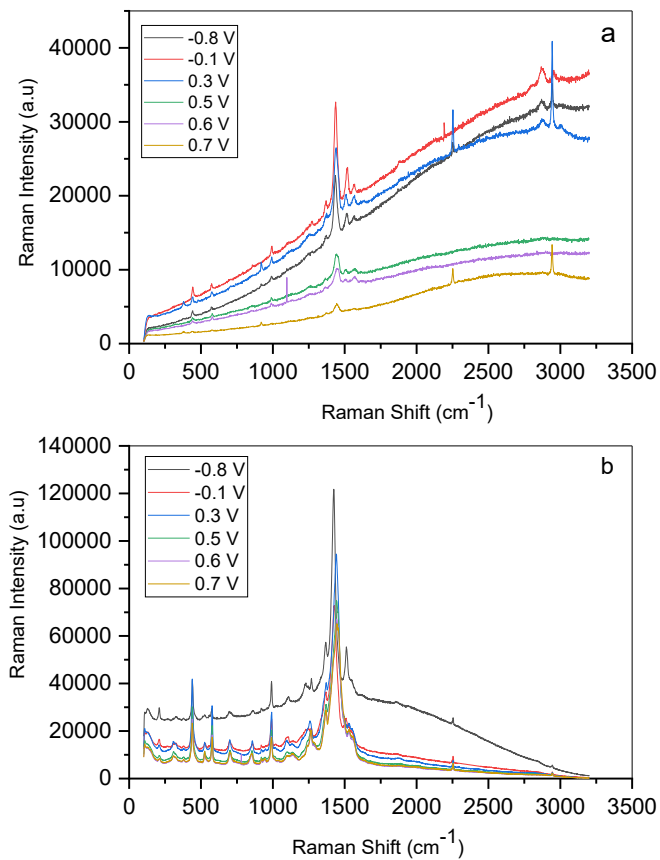


Figure 4.33 Comparison of the Raman spectra of PEDOT films using (a) 532 nm on Au electrode and (b) 785 nm Au electrode both in 0.1 M TBAPF6-ACN solvent.

The figures above represent the spectra of electrochemically polymerized PEDOT film on Au electrode in TBAPF6-ACN using both 532 nm and 785 nm excitation wavelengths respectively. The main PEDOT peaks of the spectra for $\lambda = 785$ nm bands were observed to have higher intensities than the bands found in $\lambda = 532$ nm spectra. The $\lambda = 785$ nm spectra also showed much well-defined bands in the D mode and RBM regions than the $\lambda = 532$ nm spectra which showed very feeble bands. However, there were bands noticed beyond the G mode regions of the $\lambda = 532$ nm spectra unlike the $\lambda = 785$ nm spectra where no bands were found [39][40][51].

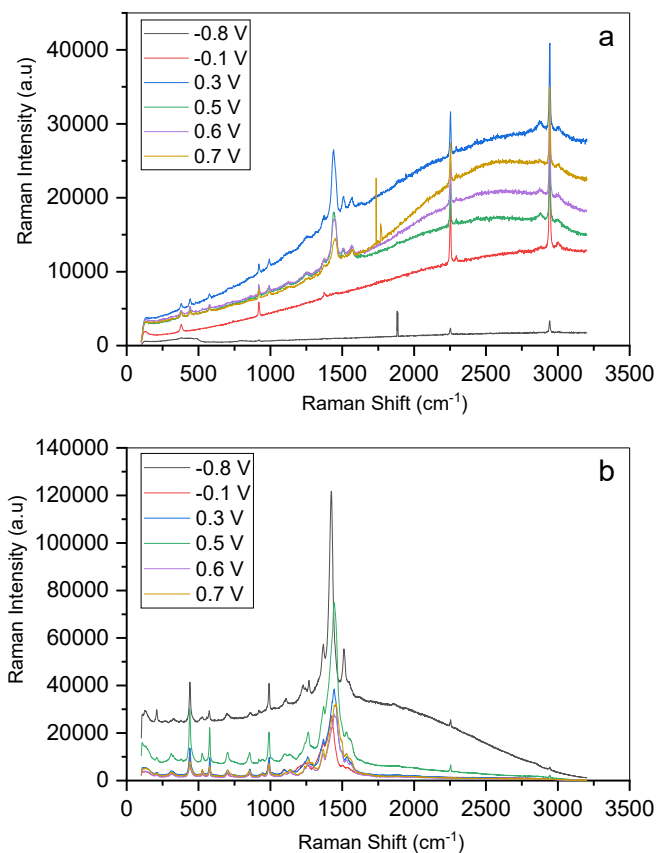


Figure 4.34 Comparison of the Raman spectra of PEDOT films using (a) 532 nm on GC electrode and (b) 785 nm GC electrode both in 0.1 M KCl solvent.

The above figures denote electrochemically polymerized PEDOT of GC electrode in KCl using both 532 nm and 785 nm excitation wavelength. It can be observed that there was shift of the main peaks both the $\lambda = 532$ nm and $\lambda = 785$ nm spectra. The $\lambda = 785$ nm spectra also showed peaks in the D mode and RBM region whereas bands showed in the same region in the $\lambda = 532$ nm spectra are weak. Furthermore, the $\lambda = 532$ nm spectra showed number of bands beyond the G mode region (2D mode) but no bands were noticed in that region in the case of the $\lambda = 785$ nm spectra. The main PEDOT peaks shown in $\lambda = 785$ nm spectra were stronger and highly intense than corresponding $\lambda = 532$ nm spectra which rather showed very weak intensities [39][42][50][51].

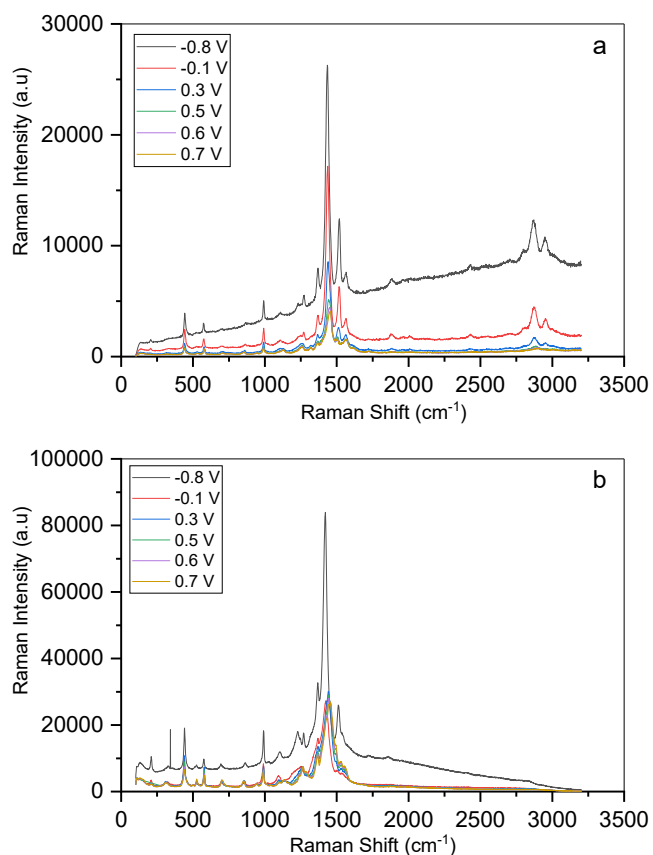


Figure 4.35 Comparison of the Raman spectra of PEDOT films using (a) 532 nm on GC electrode and (b) 785 nm GC electrode both in 0.1 M TBAPF6-ACN solvent.

The figures shown above symbolize the electrochemically polymerized PEDOT film on GC electrodes in TBAPF6-ACN solvents for the excitation wavelengths of $\lambda = 532$ nm and $\lambda = 785$ nm respectively. The major PEDOT peaks observed in both spectra were strong and highly intense. Both spectra showed medium and weak intensities bands in the D mode and RBM regions. Some few bands at 2850 cm^{-1} and 2910 cm^{-1} were detected for the $\lambda = 532$ nm spectra but no bands were noticed for the $\lambda = 785$ nm spectra beyond the G mode region (2D mode) [42][44][50][51].

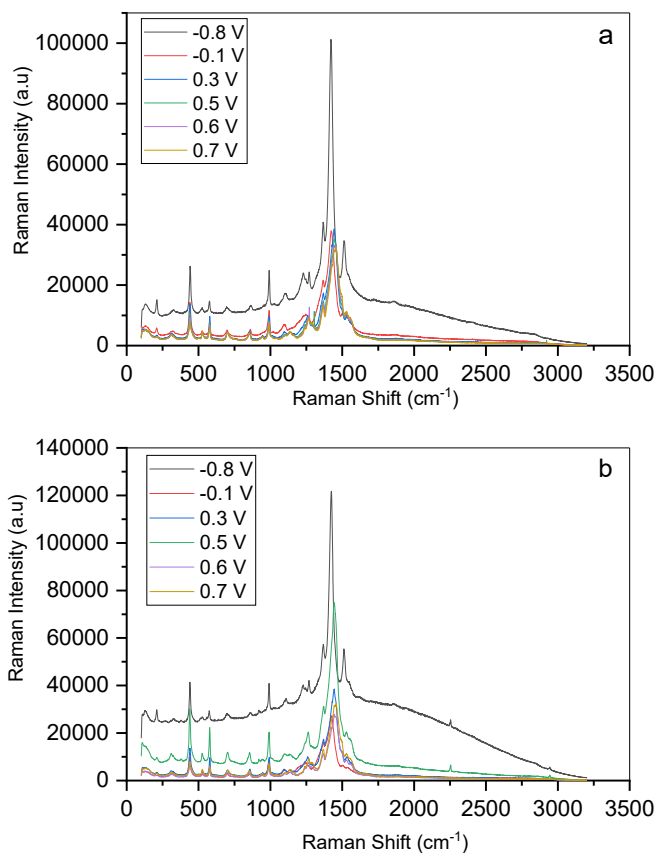


Figure 4.36 Comparison of Raman spectra of the PEDOT films polymerized on (a) Au electrode and (b) GC electrode in 0.1 M KCl using 785 nm excitation wavelength ($\lambda_L = 785$ nm).

The above figures show the spectra of an electropolymerized PEDOT of Au and GC electrodes in KCl solvent using 785 nm excitation wavelength. There are shift in both cases which indicates process of doping in the PEDOT film. The disparities between the two spectra were observed in the intensities with the GC electrode spectra been higher in intensity than the Au electrode spectra. It can however be emphasized that doping is higher in the GC electrode spectra compared the Au electrode spectra since intensities have influence on doping of the material. Moreover, the shift in peaks coupled with changes in wavenumber contributes to the doping process since greater shift denotes higher doping and thus GC electrode spectra shows higher doping level than the Au electrode spectra [39][42][50][51].

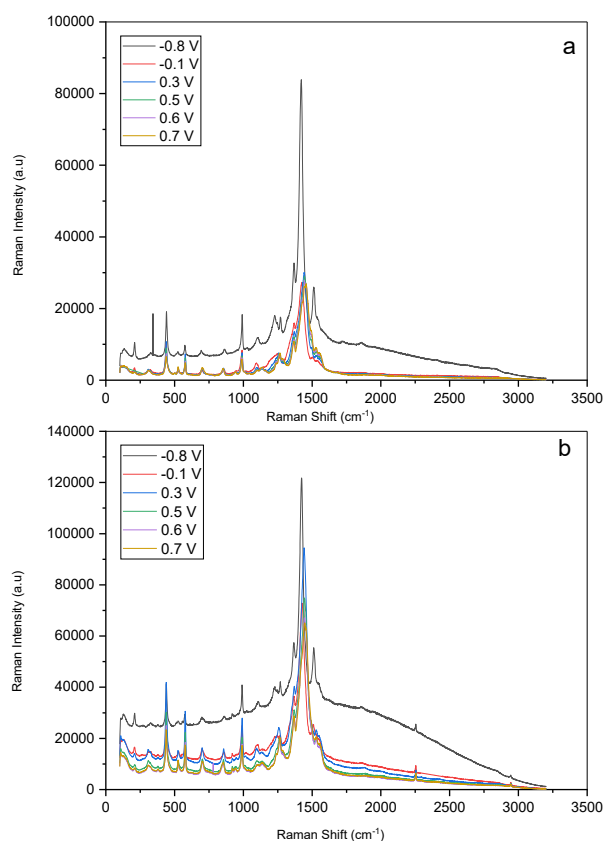


Figure 4.37 Comparison of Raman spectra of PEDOT films polymerized on (a) Au electrode and (b) GC electrode in 0.1 M TBAPF6-ACN using 785 nm excitation wavelength ($\lambda_L = 785$ nm).

The above figures signify spectra of electrochemically polymerized PEDOT film on Au electrode and GC electrode in TBAPF6-ACN solvent using 785 nm excitation wavelength. A shift was realized for the peaks and wavenumbers of both spectra even though Au electrode spectra showed greater shift than GC electrode spectra. The shifting of bands and changes in wavenumbers indicates the extent or degree of doping in the material. The intensities of the GC electrode spectra was observed to be higher than Au electrode spectra which explains how the magnitude of the intensities could have impact on the doping process [50][51].

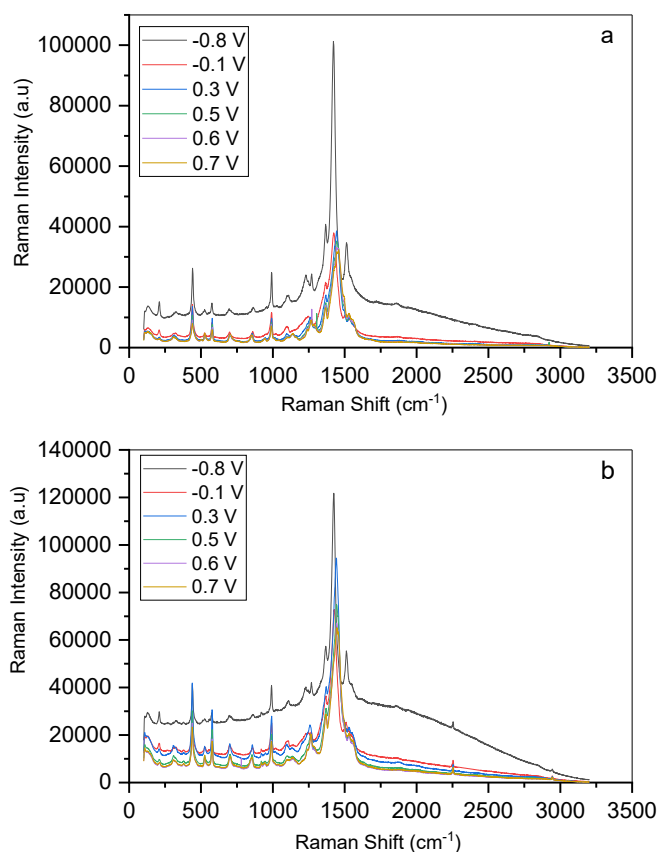


Figure 4.38 Comparison of in situ Raman spectra of PEDOT film polymerized on Au electrode in (a) 0.1 M KCl and (b) 0.1 M TBAPF6-ACN using 785 nm excitation wavelength ($\lambda_L = 785$ nm).

The figures above symbolize spectra of electropolymerized PEDOT films on Au electrode in both KCl and TBAPF6-ACN solvents. It can be noticed that KCl spectra exhibited greater shift in peaks and changes in wavenumber than TBAPF6-ACN. However, greater peak intensities were observed in TBAPF6-ACN as compared to KCl. Furthermore, it can be explained the peak shifting, changes in wavenumbers and level of intensities has effect on the doping of the polymer film. It can also be deduced from the spectra that different solvents used has influence on the doping process of the PEDOT film and the intensities as well [42][44][50][51].

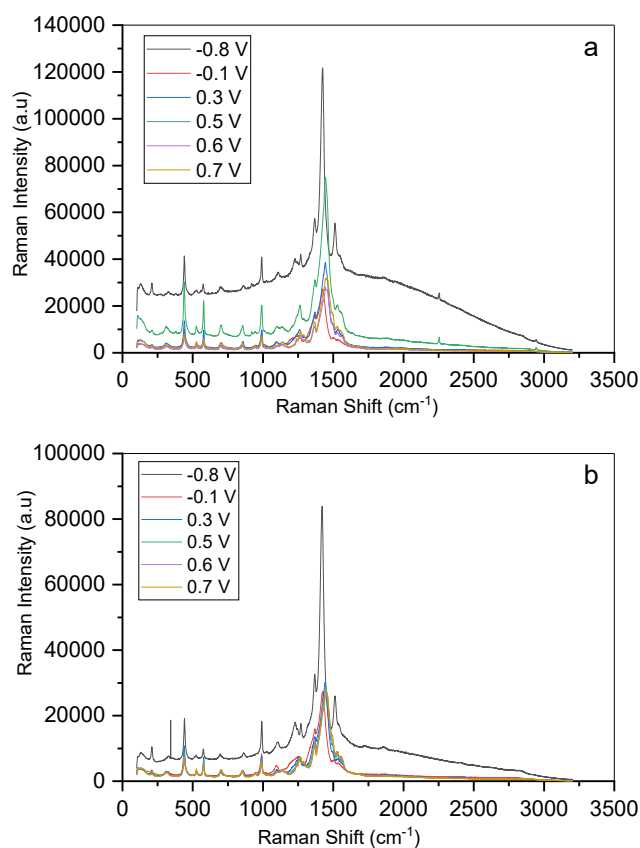
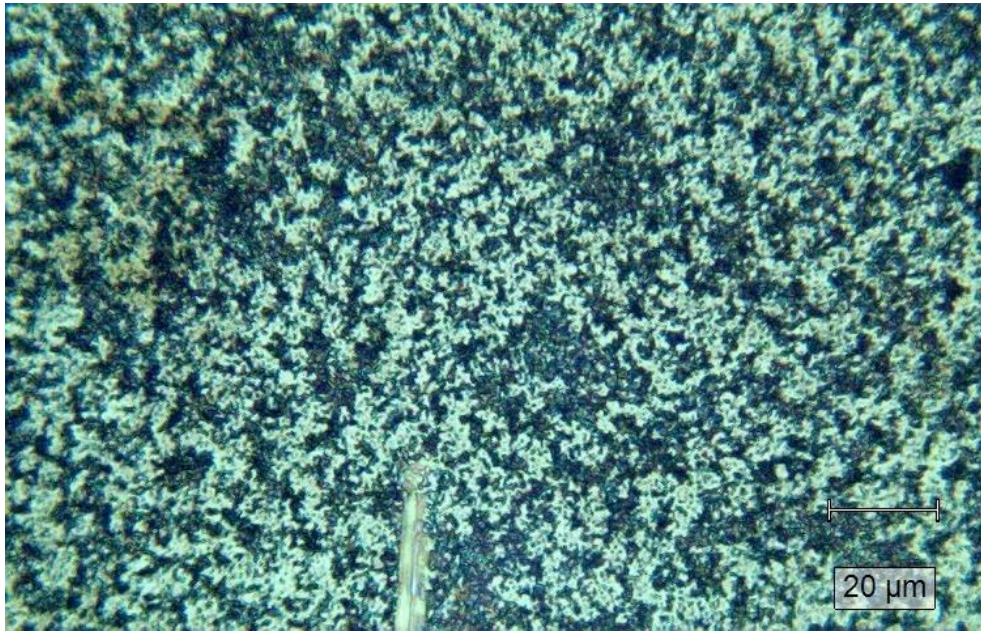


Figure 4.39 Comparison of in situ Raman spectra of PEDOT film polymerized on GC electrode in (a) 0.1 M TBAPF6-ACN and (b) 0.1 M KCl using 785 nm excitation wavelength ($\lambda_L = 785$ nm).

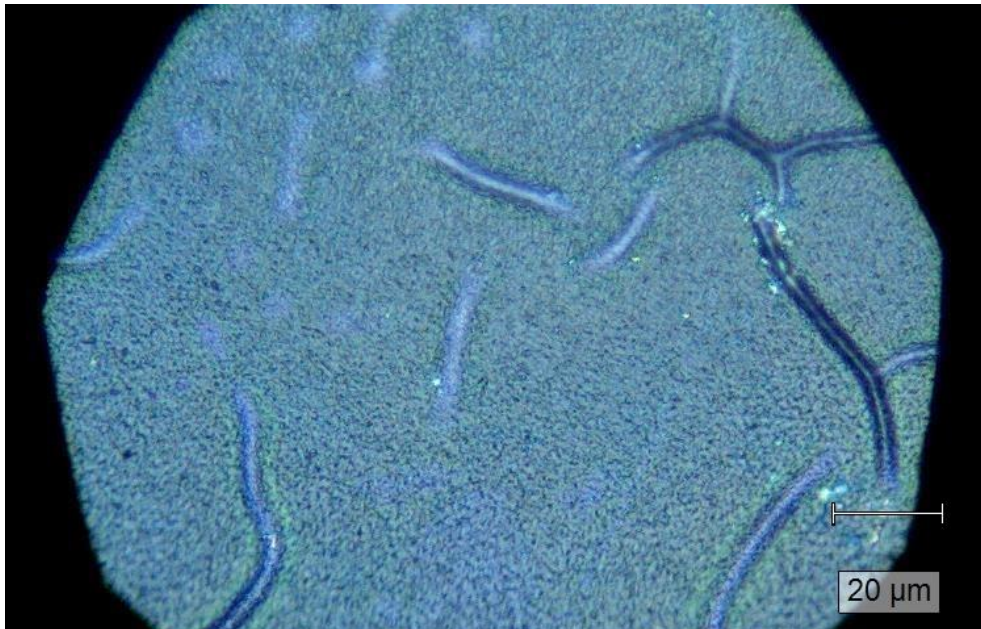
The above figures are representation of electrochemically polymerized PEDOT film on GC electrode using KCl and TBAPF6-ACN electrolyte solvents. Doping of the films were observed through shifting of the spectra peaks coupled with changes in wavenumbers as well as difference in intensities. It can be realized from the above that the spectra with KCl solvent displays much higher intensities for all the peaks than the TBAPF6-ACN spectra. It can be reiterated that the significance of the electrolytic solvents in the doping process of the spectra are clearly seen from the figures above [42][44][50].

4.5.3 Raman Images

a.



b.



c.

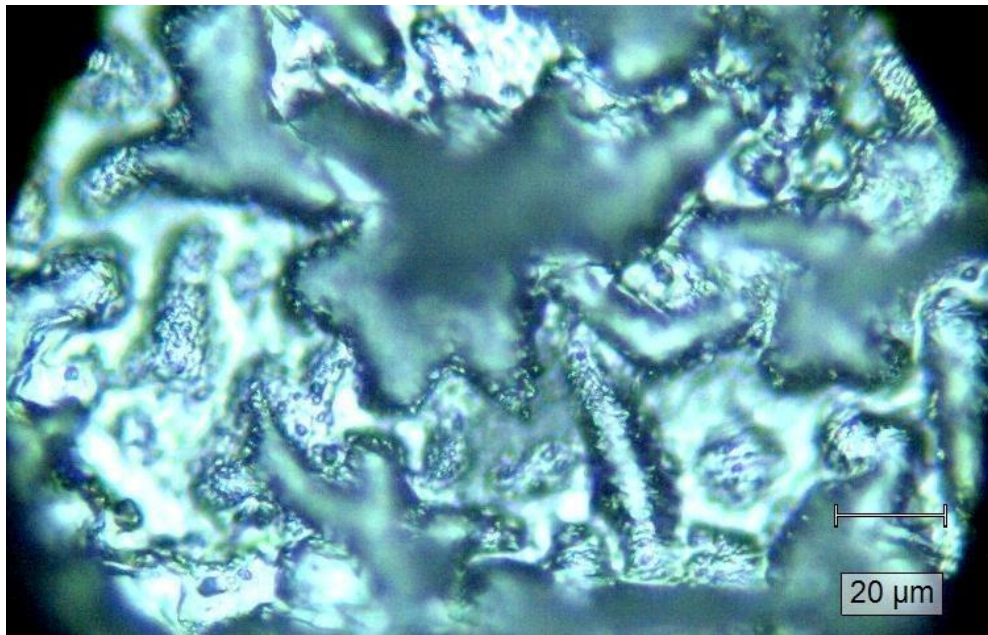


Figure 4.40. Different Raman images showing the morphologies of electropolymerized PEDOT film in (a) 0.1M KCl solution (b) 0.1M NaPSS solution (c) 0.1M TBAPF6-ACN solution.

Figure 4.40 shows Raman images for the PEDOT films produced on FTO substrates were taken during spectral analysis for the KCl, NaPSS and TBAPF6-ACN electrolyte solvents. The 3 images showed different morphologies which indicate the influence of the electrolyte solutions used for the electrochemical polymerization. The image for the KCl film shows granular flakes with pores that permits movements of ions in and out the film. The image for the NaPSS film shows more refined grains with smaller pores indicates that movements of ions is slower than that of the PEDOT film made from KCl electrolyte since the pores are small. The image for PEDOT film made from TBAPF6-ACN can be predicted to have high permeability for the movement of ions in and out of the film owing to its coarser grains and highly porous nature. The movement of ions in and out of the PEDOT film could suggest the effectiveness of doping process of the polymer and hence higher doping could be associated to the TBAPF6-ACN, KCl and NaPSS PEDOT films in that order.

5. CONCLUSION AND RECOMMENDATION

CONCLUSIONS

The concept behind this work was to investigate the possibility of synthesizing PEDOT films in aqueous medium of KCl and NaPSS electrolyte solutions as against PEDOT films synthesized in organic medium of TBAPF₆-ACN electrolyte solution by electrochemical polymerization. The electrochemical polymerization of the PEDOT films were achieved successfully by employing different working electrodes. The WE used which included Au, Pt, GC and FTO electrodes. The PEDOT film also exhibited good adherence to the surface of the electrodes.

The CVs for the PEDOT films polymerized on the WEs were observed to have smooth and consistent growth. The CVs also showed good response in terms of the redox behavior when the films were cycled through different scan rates in monomer-free electrolyte solutions. The CVs from the experiment showed that the PEDOT film was electrochemically active when doping was conducted in the monomer-free electrolyte solutions.

The PEDOT films were studied using in situ Raman spectroscopy and in situ UV-Vis spectroscopy and the outcome gave good behavior for p- and n-doping. During UV-Vis spectroscopy, the polymer films studied changed from neutral to doped form and this was observed by shift in the absorbance maximum of the spectra. Moreover, the Raman spectroscopy measurement of the PEDOT films were successfully studied for both p- and n-doping. Doping of the PEDOT films using Raman spectroscopy were noticed by peak shifting and changes in intensities of the peaks.

More importantly, there is relationship between the Raman laser wavelength and the UV-Vis results obtained during characterization. It can be deduced that the wavelength of the absorbance maximum of the UV-Vis can influence the choice of the laser wavelength used in the measurement of Raman spectra such that the neutral form of the polymer films are enhanced and strong Raman bands observed. The laser excitation wavelengths of 532nm and 785nm chosen for the Raman spectra measurement were in close proximity to the absorbance maximum wavelengths of 460nm, 750 nm and 520nm of the UV-Vis measurement of the polymer film in KCl, NaPSS and TBAPF₆-ACN monomer-free electrolyte solutions [4][37].

Finally, the morphologies of the various PEDOT films gave clues to how doping of the film will be with TBAPF₆-ACN PEDOT film predicted to show higher doping than the corresponding PEDOT film from KCl solution. The former is more porous than the latter and hence can allow easy movement of dopant ions in and out of the structure.

RECOMMENDATIONS

During the experiment, the electrochemically polymerized PEDOT film on the Pt electrode was not stable enough and got deteriorated in the monomer-free electrolyte when subjected to redox response during doping. This might be due to inadequate surface preparation of the Pt working electrode.

In view of this situation, it is recommended that the Pt working electrode and all other WE surfaces should be adequately prepared to prevent dissolution of the PEDOT films in any future work.

References

1. Rivnay J. and Inal S, Structural control of mixed ionic and electronic transport in conducting polymers. *Nature Communications*, (2016) pp.1-7.
2. Le, T., Kim, Y. and Yoon, H. Electrical and Electrochemical Properties of Conducting Polymers. *Polymers*, 9(4), (2017) pp.1-32.
3. Mantione, D., del Agua, I., Sanchez-Sanchez, A. and Mecerreyes, D. Poly(3,4-ethylenedioxythiophene) (PEDOT) Derivatives: Innovative Conductive Polymers for Bioelectronics. *Polymers*, 9(8), 354 (2017) pp.1-21.
4. Damlin, P., Kvarnström, C., Petr, A., Ek, P., Dunsch, L. and Ivaska, A. In situ resonant Raman and ESR spectroelectrochemical study of electrochemically synthesized poly(p-phenylenevinylene). *J Solid State Electrochem* (2002) 6: pp. 291–301.
5. Lehtimäki, S., Suominen, M., Damlin, P., Tuukkanen, S., Kvarnström, C. and Lupo, D. Preparation of SupercapacFTOrs on Flexible Substrates with Electrodeposited PEDOT/Graphene Composites. *ACS Appl. Mater. Interfaces*, 7, 40, (2015), pp.22137–22147.

6. Mao, H., Lu, Y., Lin, J., Zhong, S., Wee, A. and Chen, W. Manipulating the electronic and chemical properties of graphene via molecular functionalization. *Progress in Surface Science*, 88(2), (2013) pp.132-159.
7. Novoselov, K. Electric Field Effect in Atomically Thin Carbon Films. *Science*, 306(5696), (2004) pp.666-669.
8. Land, T., Michely, T., Behm, R., Hemminger, J. and Comsa, G. STM investigation of single layer graphite structures produced on Pt (111) by hydrocarbon decomposition. *Surface Science*, 264(3), (1992) pp.261-270.
9. Chen, Y., Xu, J., Yang, Y., Li, S., Yang, W., Peng, T., Mao, X. and Zhao, Y. PEDOT:PSS/graphene/PEDOT ternary film for high performance electrochemical electrode. *Journal of Materials Science: Materials in Electronics*, 26(11), (2015) pp.8292-8300.
10. Itoh, T. and McCreery, R. In situ Raman spectroelectrochemistry of azobenzene monolayers on glassy carbon. *Analytical and Bioanalytical Chemistry*, 388(1), (2007) pp.131-134.
11. Benevides, J., Overman, S. and Thomas, G. Raman, polarized Raman and ultraviolet resonance Raman spectroscopy of nucleic acids and their complexes. *Journal of Raman Spectroscopy*, 36(4), (2005) pp.279-299.
12. Fernandez-Blanco, C., Ibañez, D., Colina, A., Ruiz, V. and Heras, A. Spectroelectrochemical study of the electrosynthesis of Pt nanoparticles/poly(3,4-ethylenedioxythiophene) composite. *Electrochimica Acta*, 145, (2014) pp.139-147.
13. Wang, X. and Wong, K. Effects of a base coating used for electropolymerization of poly(3,4-ethylenedioxythiophene) on fluorinated tin oxide electrode. *Thin Solid Films*, 515(4), (2006) pp.1573-1578.
14. Damlin, P., Suominen, M., Heinonen, M., and Kvarnström, C. Non-covalent modification of graphene sheets in PEDOT composite materials by ionic liquids. *ScienceDirect*, carbon 93, (2015) pp.533-543
15. Zhang, J. and Zhao, X. Conducting Polymers Directly Coated on Reduced Graphene Oxide Sheets as High-Performance Supercapacitor Electrodes. *The Journal of Physical Chemistry C*, 116(9), (2012) pp.5420-5426.
16. McGarry, S. and Tarr, N. Fabrication and modelling of screen-printed active electrolytic polymer devices. *Semiconductor Science and Technology*, 23(5), (2008) p.055009.

17. Mortimer, R., Dyer, A. and Reynolds, J. Electrochromic organic and polymeric materials for display applications. *Displays*, 27(1), (2006) pp.2-18.
18. Siegmund Roth. Conducting polymers-physical concepts and practical applications. *Indian Journal of Chemistry*, vol 33A, (1994) pp. 453-460,
19. Daniel L. Gochbauer and T. H. Gilani*. Conduction Mechanism in Electrically Conducting Polymers. *American Journal of Undergraduate Research*, Vol 14, Issue 4, (2018) pp. 49-56.
20. Damlin* P., Kvarnström C., Nybäck A., Käldestrom M., Ivaska A. Electrochemical and spectroelectrochemical study on bilayer films composed of C₆₀ and poly(3,4-ethylenedioxythiophene) PEDOT. *Electrochimica Acta*, 51(27), (2006) pp. 6060-6068.
21. Fadi Alakhras. Conductivity Measurements of Electrochemically Synthesized Selenophene–Thiophene Conducting Materials: Effect of Temperature and Polymerization Solution. *Arab J Sci Eng*, 40: (2014) pp. 2913–2918
22. Li Y., Conducting Polymers. Organic Optoelectronic Materials. *Springer*, (2015) pp. 23-50
23. Saha U., Control of Pore Characteristics of Porous Silicon Using Non-toxic Electrochemical Etching for Photovoltaics and Supercapacitor Applications. *Theses and Dissertations*. 1676, (2017) pp 1-82.
24. Österholm A., Electronic and structural properties of polyazulene materials: an in situ spectroelectrochemical investigation. *Laboratory of Analytical Chemistry Process Chemistry Centre Department of Natural Sciences Åbo Akademi University*. (2011) pp. 1-59.
25. Cho, Wonseok; Im, Soeun; Kim, Seyul; Kim, Soyeon; Kim, Jung H. Synthesis and Characterization of PEDOT:P(SS-co-VTMS) with Hydrophobic Properties and Excellent Thermal Stability. *Mdpi Journal, Polymers* 8, no. 5: 189. (2016) pp. 1-11.
26. Alcácer, L., Electronic structure of Organic Semiconductors: Small Molecules and Polymers. *Organic Electronics Group*. <http://www.lx.it.pt/~alcacer/OrganicS.pdf>. (2014) pp. 1-44.
27. Huang S., EkWeis J., Costa S., Kalbac M. and Dresselhaus M.S. Properties of Carbon: An Overview., *Electrochemistry of Carbon Electrodes, First Edition*. (2015) pp. 1-29.
28. Kalbáček* M, Kavana L, Dunsch L. An in situ Raman spectroelectrochemical study of the controlled doping of semiconducting single walled carbon nanotubes in a conducting polymer matrix. *Elsevier B. V., Synthetic Metals* 159. (2009) pp. 2245–2248.

29. Bakhshi, A.K.*, Bhalla, G., Electrically Conducting polymers: Materials of the twentyfirst century. *Journal of Scientific & Industrial Research, Vol 63.* (2004) pp. 715-728.
30. Mayuri R., Electrochemical and Surface Compositional Studies on Uranium Dioxide. *Electronic Thesis and Dissertation ReposFTOry. The University of Western Ontario.* 1740. (2013) pp. 67-282.
31. Salaneck*, W.R., Friend R.H., Bredas J.L., Electronic structure of conjugated polymers: consequences of electron-lattice coupling. *Elsevier Science B.V. Physics Reports 319.* (1999) pp. 231-251.
32. Ramirez E.B., Eng B., Characterization of a PEDOT:PSS Electrolytic Device Using an in situ Spectroelectrochemical Technique. *Ottawa-Carleton Institute for Electrical and Computer Engineering Department of Electronics Carleton University Ottawa, Ontario, Canada.* (2013) pp. 12-87.
33. Rafailov* P. M, Thomsen C, Dettlaf-Weglikowska U, Hornbostel B, and Roth S, Raman spectroelectrochemistry on SWNTs at higher doping levels: Evidence for a transition to intercalative doping. *phys. stat. sol. (b) 244, No. 11,* (2007) pp. 4060–4063 / DOI 10.1002/pssb.200776134.
34. Lahiri A., Behrens N., Pulletikurthi G., Yochelis A., Kroke E., Cui T., Endres F., Electrochemically induced phase separation and in situ formation of mesoporous structures in ionic liquid mixtures. *Sci. Adv.* **4**, (2018) eaau9663.
35. Martínez D. I., Development of New Devices for Time-Resolved Raman Spectroelectrochemistry. *Universidad De Burgos Departamento De Química Área De Química Analítica.* (2015) pp. 3-129.
36. Länger M., Application note: SERS study of EMImTFSI on gold surfaces. *rhd instruments GmbH & Co. KG, flexible cell solutions.* (2013-2018) pp. 1-7.
37. Flores E, Novák P and Berg EJ In situ and Operando Raman Spectroscopy of Layered Transition Metal Oxides for Li-ion Battery Cathodes. *Front. Energy Res.* **6**:82. (2018) pp. 1-13. doi: 10.3389/fenrg.2018.00082.
38. Zhang L., Hou B., Lang Q., *In Situ UV–Vis Spectroelectrochemical Studies on the Copolymerization of Diphenylamine and o-Phenylenediamine. American Journal of Analytical Chemistry,* **2011, 2.** (2011) pp. 182-193. doi:10.4236/ajac.2011.22021.
39. van den Beld, W. T. E. *et al.* In-situ Raman spectroscopy to elucidate the influence of adsorption in graphene electrochemistry. *Sci. Rep.* **7**, 45080; doi: 10.1038/srep45080. (2017) pp. 1 – 8.

40. Prudkovskiy V., *et al.* Electronic coupling in fullerene-doped semiconducting carbon nanotubes probed by Raman spectroscopy and electronic transport. *Elsevier Science report, carbon* 57. (2013) pp. 498 – 506.
41. Melendres C.A., And McMahon J.J., * And Ruther W., High-Temperature “In-Situ” Surface Raman Spectroelectrochemistry In Aqueous Solutions. *J. Electroanal. Chem.*, 208 (1986). (1986) pp. 175-178.
42. Kavan L.*, Raptá P., and Dunsch L., In situ Raman and Vis-NIR spectroelectrochemistry at single-walled carbon nanotubes. *Chemical Physics Letters* 328 (2000). (2000) pp. 363 – 368.
43. Dittmer S., *et al.* In situ Raman studies of single-walled carbon nanotubes grown by local catalyst heating. *Chemical Physics Letters* 457 (2008). (2008) pp. 206 – 210.
44. Pons S., In Situ Vibrational Spectroelectrochemistry. *Journal of Electron Spectroscopy and Related Phenomena*, 45 (1987). (1987) pp. 303-322.
45. Chaunchaiyakul S., *et al.* Nanoscale analysis of multiwalled carbon nanotube by tip-enhanced Raman spectroscopy. *Science Direct, Carbon* 99 (2016). (2015) pp. 642 – 648.
46. Zhang L., Liao V., and Yu Z*., Raman spectroelectrochemistry of a single-wall carbon nanotube bundle. *Science Direct, Carbon* 48 (2010). (2010) pp. 2582 – 2589.
47. Mortimer R.J., (2017). Spectroelectrochemistry, Applications. *Encyclopedia of Spectroscopy and Spectrometry, Third Edition, Elsevier Ltd.* pp. 160 – 171.
48. Xie Y. and Dong S., Theory of analytical spectroelectrochemistry Catalytic process. *J. Electroanal. Chem.*, 291 (1990), Elsevier Sequoia S.A., Lausanne. (1990) pp. 1 – 10.
49. Viinikanoja A., Kauppila J., Damlin P., Suominen M and Kvarnström C., In situ FTIR and Raman spectroelectrochemical characterization of graphene oxide upon electrochemical reduction in organic solvents. *Royal Society of Chemistry, Phys.Chem.Chem.Phys.*, 2015, 17. (2015) pp. 12115 – 12123.
50. Itoh T. and McCreery R.L., In Situ Raman Spectroelectrochemistry of Electron Transfer between Glassy Carbon and a Chemisorbed Nitroazobenzene Monolayer. *J. Am. Chem. Soc.* 9 Vol. 124, No. 36. (2002) pp. 10894 – 10902.
51. Grzeszczuk* M., Grańska A., Szostak R., Raman Spectroelectrochemistry of Polyaniline Synthesized Using Different Electrolytic Regimes – Multivariate Analysis. *Int. J. Electrochem. Sci.*, 8 (2013). (2013) pp. 8951 – 8965.
52. Kulandaivalu S, Zainal Z, Sulaiman Y., Influence of Monomer Concentration on the Morphologies and Electrochemical Properties of PEDOT, PANI, and PPy Prepared

- from Aqueous Solution. *International Journal of Polymer Science Volume 2016*, Article ID 8518293, (2016) pp. 1 – 12.
53. Pistillo B. R, Menguelti K, Arl D, Leturcq R and Lenoble R., PRAP-CVD: A Novel Technique to Deposit Intrinsically Conductive Polymers. *Recent Research in Polymerization, Intech Open Science* (2018) pp. 139-154.
 54. Nallasamy P, Anbarasan P. M, Mohan S., Vibrational Spectra and Assignments of cis- and Trans-1,4-Polybutadiene*. *Turk J Chem*, (2002) pp. 105-111.
 55. Almeida P. V, Izumi C. M. S, Santos H. F. D, and Sant'Ana A. C, Spectroscopic Characterization Of Pedot:Pss Conducting Polymer By Resonance Raman And Serr's Spectroscopies. *Quim. Nova, Vol. 42, No. 9*, (2019) pp.1073-1080.
 56. Forsberg V, * Maslik J and Norgren M, Electronic performance of printed PEDOT:PSS lines correlated to the physical and chemical properties of coated inkjet papers. *RSC Adv.*, 2019, 9, pp. 23925–23938.
 57. O. Brîncoveanu, A. Ioanid, S. Iftimie, J. Al-Zanganawee, M. Enachescu, S. Antohe*, Study Of Physical Properties Of Bsa:Pedot-Pss Thin Film Obtained By Spin-Coating. *Digest Journal of Nanomaterials and Biostructures Vol. 11, No. 3*, (2016) pp. 833 – 843.
 58. Jae Hoon Bong J.H, Sul O, Yoon A, Choi SY and Cho* B.J, Facile graphene n-doping by wet chemical treatment for electronic applications. *Royal society of Chemistry, Nanoscale*, 2014, 6, (2014) pp. 8503–8508.
 59. Kunz T, Hessmann M.T, Seren S, Meidel B, Terheiden B, and Brabec C.J, Dopant mapping in highly p-doped silicon by micro-Raman spectroscopy at various injection levels. *J. Appl. Phys.* 113, 023514 (2013); pp.1-8 doi:10.1063/1.4773110.
 60. HORIBA Jobin Yvon, Raman Data and Analysis: Raman Spectroscopy for Analysis and MonFTOring. *HORIBA*, pp. 1-2.
 61. Raman spectroscopy explained Handbook. *Renishaw plc* (2015) pp. 1-44.
 62. Wang W, Zhao J, Short M and Zeng*, H, Real-time in vivo cancer diagnosis using Raman spectroscopy. *J. Biophotonics* 8, No. 7, (2015) pp. 527–545 / DOI 10.1002/jbio.201400026.
 63. Materny A, Popp J, Schmitt M, Schro"tter H. W and Zheltikov A. M., Wolfgang Kiefer. *J. Raman Spectrosc.* (2006); 37: pp. 1–19.
 64. Doty K. C, Muro C. K, Bueno J, Halámková L and Lednev* I. K. What can Raman spectroscopy do for criminalistics? *J. Raman Spectrosc.* (2016), 47, pp. 39–50.

65. Puviarasan N, Arjunan V and Mohan S. FT-IR and FT-Raman Studies on 3-Aminophthalhydrazide and N-Aminophthalimide*. *Turk J Chem.* 26 (2002) pp. 323-333.
66. Kochan K, Maslak E, Krafft C, Kostogrys R, Chlopicki S and Baranska* M. Raman spectroscopy analysis of lipid droplets content, distribution and saturation level in Non-Alcoholic Fatty Liver Disease in mice. *J. Biophotonics* 8, No. 7, (2015) pp. 597–609 / DOI 10.1002/jbio.201400077.
67. Materny A, Chen T, Vierheilig A and Kiefer* W. A review on linear and non-linear resonance Raman spectroscopy of the conjugated system polydiacetylene. *J. Raman Spectrosc.* (2001); 32: pp. 425–445.
68. Prinsloo* L. C, Colombari P, Brink J. D and Meiklejohn I. A Raman spectroscopic study of the igneous rocks on Marion Island: a possible terrestrial analogue for the geology on Mars. *J. Raman Spectrosc.* (2011), 42, pp. 626–632.
69. Stöckel S, Kirchhoff J, Neugebauer U, Rösch P and Popp J. The application of Raman spectroscopy for the detection and identification of microorganisms. *J. Raman Spectrosc.*, 47, (2016) pp. 89–109.
70. Sonmez G, Shen C. K. F, Rubin Y and Wudl* F. A Red, Green, and Blue (RGB) Polymeric Electrochromic Device (PECD): The Dawning of the PECD Era**. *Angew. Chem. Int. Ed.*, 43, (2004) pp. 1498 –1502.
71. Eghbalnia M. Electrochemical and Raman Investigation of Pyrite and Chalcopyrite Oxidation. *The University of British Columbia (Vancouver)*, (2012) pp. 1-201.
72. Hyeonseok Yoon. Current Trends in Sensors Based on Conducting Polymer Nanomaterials. *Nanomaterials*, 3, (2013) pp. 524-549.
73. Tehrani P. Electrochemical Switching in Conducting Polymers – Printing Paper Electronics. *Linköping Studies in Science and Technology. Dissertations, no.1212 Norrköping* (2008) pp. 1-37.
74. Astratine L. (2012). *Preparation and Characterization of Conducting Polymer Materials for Electrochromic Devices*. Doctoral Thesis. Dublin Institute of Technology. (2012) pp. 1-154.
75. Wain A. J and O’Connell M. A. Advances in surface-enhanced vibrational spectroscopy at electrochemical interfaces, *Advances in Physics: X*, 2:1, (2017) pp. 188-209, DOI:10.1080/23746149.2016.1268931.
76. Binder*J, Urban J. M, Stepniewski R, Strupinski W. and Wyszomolek A. In-situ Raman spectroscopy of the graphene/water interface of a solution-gated field effect transistor:

electron-phonon coupling and spectroelectrochemistry. *Institute of Physical Chemistry, University of Freiburg, Albertstraße 23a, 79104 Freiburg, Germany*, pp. 1-32.

77. Hutchison G. R et al. Electronic structure of conducting polymers: Limitations of oligomer extrapolation approximations and effects of heteroatoms. *Physical Review B* 68, (2003) pp. 035204-1-13.